General Disclaimer

One or more of the Following Statements may affect this Document

- This document has been reproduced from the best copy furnished by the organizational source. It is being released in the interest of making available as much information as possible.

- This document may contain data, which exceeds the sheet parameters. It was furnished in this condition by the organizational source and is the best copy available.

- This document may contain tone-on-tone or color graphs, charts and/or pictures, which have been reproduced in black and white.

- This document is paginated as submitted by the original source.

- Portions of this document are not fully legible due to the historical nature of some of the material. However, it is the best reproduction available from the original submission.

Produced by the NASA Center for Aerospace Information (CASI)

AD-783 915

RESEARCH INVESTIGATION DIRECTED TOWARD EXTENDING THE USEFUL RANGE OF THE ELECTROMAGNETIC SPECTRUM

Sven R. Hartmann, et al

Columbia Radiation Laboratory

DOCUMENT CONTROL DATA · R&D

(Security classification of title, body of abstract and indexing annotation must be entered when the overall report is classified)

1. ORIGINATING ACTIVITY *(Corporate author)*	2a. REPORT SECURITY CLASSIFICATION
COLUMBIA UNIVERSITY, Dept. of Physics Columbia Radiation Laboratory New York, New York 10027	Unclassified
	2b. GROUP

3. REPORT TITLE

RESEARCH INVESTIGATION DIRECTED TOWARD EXTENDING THE USEFUL RANGE OF THE ELECTROMAGNETIC SPECTRUM

4. DESCRIPTIVE NOTES *(Type of report and inclusive dates)*

Progress Report, 1 July 1973 - 30 June 1974

5. AUTHOR(S) *(Last name, first name, initial)*

Hartmann, Sven R. and Happer, William, Co-Directors, CRL

6. REPORT DATE	7a. TOTAL NO. OF PAGES	7b. NO. OF REFS
30 June 1974	xi + 151	115

8a. CONTRACT OR GRANT NO.	9a. ORIGINATOR'S REPORT NUMBER(S)
DAAB07-69-C-0383	
b. PROJECT NO.	Progress Report No. 24
DA 200 61102 B31F	
c.	9b. OTHER REPORT NO(S) *(Any other numbers that may be assigned this report)*
d.	CU-6-74-0383 Physics

10. AVAILABILITY/LIMITATION NOTICES

This document has been approved for public release and sale; its distribution is unlimited.

11. SUPPLEMENTARY NOTES	12. SPONSORING MILITARY ACTIVITY Joint Services Electronics Program through (Administering Service-Office of Naval Research, Air Force Office of Scientific Research, or U.S. Army Electronics Command)

13. ABSTRACT

A powerful new spectroscopic technique, cascade level anticrossing spectroscopy, has been developed and used to determine the complete hyperfine Hamiltonian of the ^4D state of rubidium. The anomalous magnetic hyperfine structure of this state is due to an anisotropic core polarization which has both a contact and a spin-dipole component. The spin-dipole component is so large that the sign of the net spin-dipole interaction is reversed with respect to the sign expected for the direct interaction between the nucleus and the valence electron. This is the first instance of a negative spin-dipole interaction ever discovered, and it may help in the formation of a satisfactory theory for the anomalous magnetic interactions in the D states of alkali atoms.

A number of new hyperfine interaction constants have been measured for S, P, D, and F states of the alkali atoms.

We have succeeded in obtaining narrow optical pumping signals in alkali vapors at vapor densities much higher than those previously attained, demonstrating the existence of a hitherto unsuspected high density optical pumping regime in which the Zeeman resonance frequency is shifted downward by a large factor and spin-exchange broadening vanishes. This new regime opens the way to miniature

I

14. KEY WORDS	LINK A		LINK B		LINK C	
	ROLE	WT	ROLE	WT	ROLE	WT
Metastable atoms and ions						
Metastable autoionizing atoms						
Level-crossing spectroscopy						
Optical double-resonance spectroscopy						
Collision phenomena						
Electron-impact excitation of atoms						
Atomic frequency standards						
Intensity modulation of light						
Molecular beam maser spectroscopy						
Hyperfine spectroscopy						
Carbon monoxide Galaxy survey						
Millimeter-wave radio astronomy						
Photon-echo resonance						
Echo behavior in ruby						
Raman echoes						
Rotation detection						
Two-photon radiation						
Frequency shifts						
Nuclear magnetic resonance						
Magnetometers						
Superfluidity						
Quantum fluids						

INSTRUCTIONS

1. **ORIGINATING ACTIVITY:** Enter the name and address of the contractor, subcontractor, grantee, Department of Defense activity or other organization (corporate author) issuing the report.

2a. **REPORT SECURITY CLASSIFICATION:** Enter the overall security classification of the report. Indicate whether "Restricted Data" is included. Marking is to be in accordance with appropriate security regulations.

2b. **GROUP:** Automatic downgrading is specified in DoD Directive 5200.10 and Armed Forces Industrial Manual. Enter the group number. Also, when applicable, show that optional markings have been used for Group 3 and Group 4 as authorized.

3. **REPORT TITLE:** Enter the complete report title in all capital letters. Titles in all cases should be unclassified. If a meaningful title cannot be selected without classification, show title classification in all capitals in parenthesis immediately following the title.

4. **DESCRIPTIVE NOTES:** If appropriate, enter the type of report, e.g., interim, progress, summary, annual, or final. Give the inclusive dates when a specific reporting period is covered.

5. **AUTHOR(S):** Enter the name(s) of author(s) as shown on or in the report. Enter last name, first name, middle initial. If military, show rank and branch of service. The name of the principal author is an absolute minimum requirement.

6. **REPORT DATE:** Enter the date of the report as day, month, year; or month, year. If more than one date appears on the report, use date of publication.

7a. **TOTAL NUMBER OF PAGES:** The total page count should follow normal pagination procedures, i.e., enter the number of pages containing information.

7b. **NUMBER OF REFERENCES:** Enter the total number of references cited in the report.

8a. **CONTRACT OR GRANT NUMBER:** If appropriate, enter the applicable number of the contract or grant under which the report was written.

8b, 8c, & 8d. **PROJECT NUMBER:** Enter the appropriate military department identification, such as project number, subproject number, system numbers, task number, etc.

9a. **ORIGINATOR'S REPORT NUMBER(S):** Enter the official report number by which the document will be identified and controlled by the originating activity. This number must be unique to this report.

9b. **OTHER REPORT NUMBER(S):** If the report has been assigned any other report numbers (either by the originator or by the sponsor), also enter this number(s).

10. **AVAILABILITY/LIMITATION NOTICES:** Enter any limitations on further dissemination of the report, other than those imposed by security classification, using standard statements such as:

(1) "Qualified requesters may obtain copies of this report from DDC."

(2) "Foreign announcement and dissemination of this report by DDC is not authorized."

(3) "U. S. Government agencies may obtain copies of this report directly from DDC. Other qualified DDC users shall request through
_____."

(4) "U. S. military agencies may obtain copies of this report directly from DDC. Other qualified users shall request through
_____."

(5) "All distribution of this report is controlled. Qualified DDC users shall request through
_____."

If the report has been furnished to the Office of Technical Services, Department of Commerce, for sale to the public, indicate this fact and enter the price, if known.

11. **SUPPLEMENTARY NOTES:** Use for additional explanatory notes.

12. **SPONSORING MILITARY ACTIVITY:** Enter the name of the departmental project office or laboratory sponsoring (paying for) the research and development. Include address.

13. **ABSTRACT:** Enter an abstract giving a brief and factual summary of the document indicative of the report, even though it may also appear elsewhere in the body of the technical report. If additional space is required, a continuation sheet shall be attached.

It is highly desirable that the abstract of classified reports be unclassified. Each paragraph of the abstract shall end with an indication of the military security classification of the information in the paragraph, represented as (TS), (S), (C), or (U).

There is no limitation on the length of the abstract. However, the suggested length is from 150 to 225 words.

14. **KEY WORDS:** Key words are technically meaningful terms or short phrases that characterize a report and may be used as index entries for cataloging the report. Key words must be selected so that no security classification is required. Identifiers, such as equipment model designation, trade name, military project code name, geographic location, may be used as key words but will be followed by an indication of technical context. The assignment of links, rules, and weights is optional.

GPO 886-551

II

13. ABSTRACT (cont'd)

optically pumped devices, such as magnetometers, and affords important new possibilities for investigating basic interactions in dense alkali vapors.

Nuclear magnetic resonance signals from diatomic alkali molecules have been observed in optically pumped cesium and rubidium vapors. Some important rate constants have been deduced from the observed widths of these signals.

Hyperfine structure in the rotational spectrum of the heterocyclic rings pyrrole and pyridine has been resolved with a molecular beam maser. Pressure broadening of millimeter-wave lines of CO and HCN is being investigated as a function of temperature (down to dry ice temperature for HCN, and liquid nitrogen temperature for CO).

A quartet of new interstellar millimeter-wave lines has been discovered, and identified as the ethynyl radical C_2H, a molecule which has never previously been observed in the gas phase, even in the terrestrial laboratory. A radio telescope equipped with spectral line receivers for a sky survey of the carbon monoxide molecule has been completed, and is currently being installed on the roof of the Pupin Physics Laboratory.

We have detected photon echoes in $LaF_3:Nd^{3+}$ and $YAG:Nd^{3+}$ with amplitudes two to three orders of magnitude smaller than in $CaWO_4:Nd^{3+}$. We have observed a temperature-dependent decay which we attribute to photon-induced relaxation of the Orbach and Raman type. Magnetic field dependence results were also studied. For both crystals we observed modulation effects.

Using the Cr-Al interaction parameters determined from PENDOR studies and those determined from spin-echo ENDOR experiments, we have calculated photon-echo modulation behavior in ruby. The results compare favorably with our experimental data taken with an automated, gated cw system. We have measured the concentration and field dependence of the exponential decay of the photon echo, and the decays show simple exponential behavior.

We have measured electron-spin echo-modulation behavior associated with the $3/2 \rightarrow 1/2$ transition of the $^4A_2$ ground state of ruby.

Stimulated Raman scattering and four-wave parametric mixing has been studied in thallium vapor. The intensity distribution is approximately Gaussian with a half width divergence of 0.66 mrad. In the presence of SRS, the laser-beam divergence increases to 1.23 mrad. Generated Stokes energy appeared to be a function of thallium vapor pressure. The energy of the dye laser anti-Stokes pulse versus the product of the laser and Stokes energies is 0.96 ± 0.02.

III

13. ABSTRACT (cont'd)

We have studied two of the cascading single-photon fluorescences from cesium gas excited by two-photon absorption. The fluorescent pulsewidth is two to four times that of the laser at low incident power levels.

After reanalyzing published experimental data regarding the relaxation behavior of two- and three-pulse electron-spin echoes in dilute systems, we find excellent agreement with our recently published theory of spectral diffusion decay.

We have confirmed that the superradiant condition is unstable by both a theoretical mode analysis and straightforward numerical computation.

We have found a clear singularity in the temperature coefficient of viscosity for He^4 at the superfluid transitions (T_λ). The reduced viscosity difference $\Delta\eta/\eta$ depends on the reduced temperature difference $\epsilon = 2/3$ below T_λ, and $x = 0.9$ to 1.1 above T_λ. An experiment to detect the quantized rotation of superfluid helium by a thermal modulation technique is underway, and an apparatus to study mechanical properties of superfluid He^3 is nearing completion.

IV

COLUMBIA RADIATION LABORATORY

RESEARCH INVESTIGATION DIRECTED TOWARD
EXTENDING THE USEFUL RANGE OF THE
ELECTROMAGNETIC SPECTRUM

Progress Report No. 24

July 1, 1973 through June 30, 1974

Contract DAAB07-69-C-0383
[Continuation of Contract DA 28-043 AMC-00099(E)]

CU-6-74 C-0383 Physics

Object of the research:

Physical research in fields in which microwave frequency techniques
are employed; the development of microwave electronic and circuit
devices.

The research reported in this document was made possible through
support extended the Columbia Radiation Laboratory, Columbia Univer-
sity, by the Joint Services Electronics Program (U. S. Army Electro-
nics Command and U. S. Army Research Office, Office of Naval Research,
and the Air Force Office of Scientific Research) under Contract
DAAB07-69-C-0383.

Submitted by: S. R. HARTMANN and W. HAPPER, Co-Directors

Coordinated by: A. Owen, Editor

COLUMBIA UNIVERSITY

Division of Government-Aided Research

New York, N. Y. 10027

June 30, 1974

ii

TABLE OF CONTENTS

FACTUAL DATA, CONCLUSIONS, AND PROGRAMS
FOR THE NEXT INTERVAL

The names of the authors are arranged alphabetically.

PUBLICATIONS AND REPORTS

Publications

P. F. Liao[1] and S. R. Hartmann, "Determination of Cr-Al Hyperfine and Electric Quadrupole Interaction Parameters in Ruby using Spin-Echo Electron-Nuclear Double Resonance," Phys. Rev. B $\underline{8}$, 69 (1973).

G. R. Tomasevich, K. D. Tucker, and P. Thaddeus, "Hyperfine Structure of Furan," J. Chem. Phys. $\underline{59}$, 131 (1973).

R. Friedberg and S. R. Hartmann, "On the QED Approach to Frequency Shifts," Phys. Letters $\underline{44A}$, 311 (1973).

P. F. Liao and S. R. Hartmann, "Radiation Locked Photon Echoes and Optical Free Induction in Ruby," Phys. Letters $\underline{44A}$, 361 (1973).

W. Happer and H. Tang,[2] "Spin Exchange Shift and Narrowing of Magnetic Resonance Lines in Optically Pumped Alkali Vapors," Phys. Rev. Letters $\underline{31}$, 273 (1973).

R. Friedberg and S. R. Hartmann, "Influence of Resonant Frequency Shifts on Superradiant Damping," Coherence and Quantum Optics, L. Mandel and E. Wolf, eds. (Plenum Publishing Corp., New York, 1973).

P. F. Liao and S. R. Hartmann, "Magnetic Field- and Concentration-Dependent Photon-Echo Relaxation in Ruby with Simple Exponential Decay," Opt. Comm. $\underline{8}$, 310 (1973).

C. Tai,[3] R. Gupta, and W. Happer, "Hyperfine Structure of the $8^2P_{1/2}$ State of Cs^{133}," Phys. Rev. A $\underline{8}$, 1661 (1973).

---

1. Present Address: Bell Telephone Laboratories, Inc., Holmdel, New Jersey 07733.

2. Present Address: Bell Telephone Laboratories, Inc., Murray Hill, New Jersey 07922.

3. Present Address: Department of Physics, University of British Columbia, Vancouver, Canada.

N. A. Lin[4] and S. R. Hartmann, "Nuclear Spin-Lattice Relaxation in CaF_2 via Paramagnetic Centers for Short Correlation Time when Spin Diffusion is Inhibited," Phys. Rev. B <u>8</u>, 4079 (1973).

R. Gupta, W. Happer, L. K. Lam, and S. Svanberg,[5] "Hyperfine-Structure Measurements of Excited S States of the Stable Isotopes of Potassium, Rubidium, and Cesium by Cascade Radio-Frequency Spectroscopy," Phys. Rev. A <u>8</u>, 2792 (1973).

K. H. Liao, R. Gupta, and W. Happer, "Measurement of Hyperfine Structure of the $4^2S_{1/2}$ State of Na^{23} by Cascade Radio-Frequency Spectroscopy," Phys. Rev. <u>8</u>, 2811 (1973).

K. D. Tucker and G. R. Tomasevich, "Deuteron Quadrupole Coupling in Formaldehyde," J. Mol. Spectry. <u>48</u>, 475 (1973).

N. Takeuchi,[6] S. Chandra, Y. C. Chen, and S. R. Hartmann, "Photon Echoes in $LaF_3:Nd^{3+}$ and $YAG:Nd^{3+}$," Phys. Letters <u>46A</u>, 97 (1973).

S. Svanberg, "Spectroscopy of Highly Excited Levels in Alkali Atoms," <u>Proceedings of the Laser Spectroscopy Conference</u>, Vail, Colorado, June 25-29, 1973 (Plenum Publishing Corp., New York, 1974).

W. Happer and S. Svanberg, "Power-Series Analysis of Light Shifts in Optical Pumping Experiments," Phys. Rev. A <u>9</u>, 508 (1974).

P. F. Liao, P. Hu,[7] R. Leigh,[8] and S. R. Hartmann, "Photon-Echo Nuclear Double Resonance and its Application in Ruby," Phys. Rev. A <u>9</u>, 332 (1974).

---

4. Present Address: Chemtex Corporation, New York, New York 10022.

5. Present Address: Department of Physics, Chalmers University of Technology, Göteborg, Sweden.

6. Present Address: Electron Physics Section, Radio and Electrical Engineering Division, National Research Council of Canada, Ottawa 10, Ontario.

7. Present Address: Bell Telephone Laboratories, Inc., Murray Hill, New Jersey 07974.

8. Present Address: Department of Physics, City College of the CUNY, New York, New York 10031.

A Shih, D. Raskin, and P. Kusch, "Investigation of the Interaction
Potential between a Neutral Molecule and a Conducting
Surface," Phys. Rev. A $\underline{9}$, 652 (1974).

R. Gupta, W. Happer, G. Moe, and W. Park, "Nuclear Magnetic
Resonance of Diatomic Alkali Molecules in Optically
Pumped Alkali Vapors," Phys. Rev. Letters $\underline{32}$, 574 (1974).

R. Friedberg and S. R. Hartmann, "Superradiant Stability in
Specially Shaped Small Samples," Opt. Comm. $\underline{10}$, 298 (1974).

P. Hu and S. R. Hartmann, "Theory of Spectral Diffusion Decay
Using an Uncorrelated-Sudden-Jump Model," Phys. Rev.
B $\underline{9}$, 1 (1974).

K. H. Liao, L. Lam, R. Gupta, and W. Happer, "Cascade Anticross-
ing Measurement of the Anomalous Hyperfine Structure of
the 4^2D State of Rubidium," Phys. Rev. Letters $\underline{32}$, 1340
(1974).

Papers by CRL Staff Members Presented at Scientific Meetings

R. Gupta, "Non-P Excited States of the Alkali Atoms," Invited
Paper, Fifth Annual Meeting of the Division of Electron
and Atomic Physics, New Haven, Connecticut, December 10-
12, 1973, Bull. Am. Phys. Soc. II $\underline{18}$, 1499 (1973).

Fifth International Symposium on Magnetic Resonance, Bombay,
India, January 14-18, 1974.

S. R. Hartmann, "Photon Echoes in Ruby and Crystals Doped with
Neodymium," Invited paper.

S. R. Hartmann and P. Hu, "Theory and Support for an Uncorrelated
Sudden-Jump Model of Spectral Diffusion Decay."

American Physical Society Meeting, Chicago, Illinois, February
4-7, 1974.

R. A. Weingarten, A. Flusberg, and S. R. Hartmann, "Nonlinear
Optical Processes in Atomic Thallium Vapor," Bull. Am.
Phys. Soc. II $\underline{19}$, 53 (1974).

N. Takeuchi, S. Chandra, Y. C. Chen, and S. R. Hartmann, "Photon
Echoes in Trivalent Neodymium," Bull. Am. Phys. Soc. II
$\underline{19}$, 53 (1974).

S. R. Hartmann, "Superradiant Stability in Small Samples and
Spin- and Photon-Echo ENDOR in Ruby," U. S, Naval Research Conference, Washington, D. C., February 22, 1974.

R. Friedberg, "In Search of Dicke Decay," Seventh International
Quantum Electronics Conference, San Francisco, California,
June 10-13, 1974.

Lectures

S. Chandra, "Photon Echoes and PENDOR," Seminar, Department of
Physics, Fordham University, Bronx, New York, April 25,
1974.

R. Friedberg, "Small Sample Superradiant Stability," Seminar,
IBM T. J. Watson Research Center, Yorktown Heights, New
York, March 14, 1974.

R. W. Guernsey, "Anomalous Damping by He II," Colloquium, Department of Physics and Astronomy, Dartmouth College, Hanover,
New Hampshire, January 18, 1974.

R. Gupta, "Cascade Fluorescence Spectroscopy," Seminar, Department of Physics, City College of the CCNY, New York,
New York, February 15, 1974.

W. Happer, "Miniature Magnetometers," Colloquium, U. S. Naval
Ordnance Laboratory, Washington, D. C., February 5,
1974; "Cold Spins in Hot Alkali Vapors," Colloquium,
Department of Physics, University of Connecticut, Storrs,
Connecticut, March 15, 1974; id., Colloquium, University
of Tennessee, Knoxville, Tennessee, April 2, 1974.

S. R. Hartmann, "Spin- and Photon-Echo Behavior in Ruby,"
Seminar, Department of Physics, American University of
Beirut, Beirut, Lebanon, January 6, 1974; "Theory of
Spectral Diffusion Decay," Seminar, Department of Physics,
American University of Beirut, Beirut, Lebanon, January
7, 1974; "Superradiant Stability in Small Samples and
Spin- and Photon-Echo ENDOR in Ruby," Seminar, U. S.
Naval Research Laboratory, Washington, D. C., February
22, 1974, id., Seminar, Department of Physics, Yale
University, New Haven, Connecticut, February 13, 1974.

P. Thaddeus, "The Unidentified Interstellar Molecules," Colloquium, Department of Physics, University of Texas,
Austin, Texas, January 22, 1974; id., Colloquium, Department of Physics, University of Texas, Dallas, Texas,

January 23, 1974; id., Colloquium, Department of Physics, Columbia University, January 25, 1974; "A New Interstellar Molecule," Colloquium, Department of Physics, Princeton University, Princeton, New Jersey, January 31, 1974; id., Colloquium, National Radio Astronomy Observatory, Charlottesville, Virginia, February 7, 1974; "The Molecular Content of the Orion Association," Colloquium, Department of Physics, Columbia University, February 5, 1974; "The Unidentified Interstellar Lines," Seminar, Department of Physics, New York University, New York, New York, February 14, 1974; "An Abundant New Interstellar Molecule," Seminar, Department of Physics, Massachusetts Institute of Technology, Cambridge, Massachusetts, April 2, 1974; "New Cosmic Masers," Seminar, Bell Laboratories, Murray Hill, New Jersey, April 23, 1974; "Point Maser Sources of Vibrationally Excited SiO," Seminar, Department of Physics and Astronomy, University of Massachusetts, Amherst, Massachusetts, April 26, 1974; "Forecasting to the End of the Century," Seminar, Arden House, Columbia University, May 1, 1974; "Interstellar C_2H," Colloquium, Kitt Peak National Observatory, University of Arizona, Tucson, Arizona, June 3, 1974.

K. D. Tucker, "Molecular Properties of the Ethynyl Radical, C_2H, from Astronomical Observations," Colloquium, Department of Physics, Fordham University, Bronx, New York, May 14, 1974.

R. A. Weingarten, "Nonlinear Optics in Thallium Vapor," Colloquium, Optical Sciences Division, National Bureau of Standards, Washington, D. C., February 20, 1974; id., Seminar, Optics Branch, U. S. Naval Research Laboratory, Washington, D. C., February 21, 1974; id., Colloquium, Department of Physics and Astronomy, University of Toledo, Toledo, Ohio, May 16, 1974.

Radiation Laboratory Seminars

Meetings are held weekly at Columbia University, New York, New York, during the academic year and are open to all members of the Physics Department. Guest speakers are invited to discuss work in the general area of the research in the Columbia Radiation Laboratory.

S. Haroche, Ecole Normale Superieure de Paris, "Laser-Induced his Quantum Beats; Atoms Dressed by rf Photons," August 22, 1973.

J. Wynne, IBM Watson Research Center, "Toward the End of the Infrared, or How to Succeed in Nonlinear Optics by Switching from Solids to Vapors," September 7, 1973.

M. S. Feld, Massachusetts Institute of Technology, "Superradiance: Self-Induced Emission in Optically Pumped HF Gas," September 14, 1973.

M. Weger, Hebrew University, "Recent Aspects in the Theory of One-Dimensional Superconductivity," September 21, 1973.

D. L. Rousseau, Bell Telephone Laboratories, Inc., "Resonance Raman Scattering from Iodine," September 28, 1973.

R. Dalven, University of California at Berkeley, "Physics of Lead Salt Semiconductors," October 5, 1973.

H. Metcalf, State University of New York at Stonybrook, "Time-Resolved Excited-State Spectroscopy," October 12, 1973.

N. Swanson, National Bureau of Standards, "Resonant Structure in Near Threshold Electron Excitation of Krypton and Xenon," October 19, 1973.

R. W. Waynant, U. S. Naval Research Laboratory, "The Quest for the X-Ray Laser," October 26, 1973.

S. R. Ryan, Yale University, "Collisional Quenching of Metastable Hydrogen by Rare Gas Atoms," November 2, 1973.

H. W. Moos, Johns Hopkins University, "Phonons and Ions in Crystals," November 9, 1973.

P. W. Smith, Bell Telephone Laboratories, Inc., "Wave Guide Gas Lasers," November 16, 1973.

V. L. Telegdi, University of Chicago, "Hyperfine Structures of Muonium," November 30, 1973.

M. McDermott, University of Washington, "Differential Hyperfine Anomalies and Nuclear Magnetism," December 5, 1973.

L. Riseberg, GTG Laboratories, "Penning Collisions in Pulsed and Flowing Afterglows," December 7, 1973.

G. Gamota, Bell Telephone Laboratories, Inc., "Long-Range Coherence in Superfluid Helium," December 14, 1973.

H. J. Maris, Brown University, "The Dispersion Curve of Super-
    fluid Helium," January 25, 1974.

W. Fairbanks, Jr., Stanford University, "Detection of Individual
    Atoms using Resonance Fluorescence," February 1, 1974.

M. Nisenoff, U. S. Naval Research Laboratory, "Superconductiv-
    ity, Squids, and Magnetometry," February 8, 1974.

G. Flynn, Columbia University, "Energy Transfer in Polyatomic
    Molecules: Prerequisites for Infrared Photo-Chemistry,"
    February 22, 1974.

D. Klepner, Massachusetts Institute of Technology, "Magnetic
    Interactions in Alkali-Rare-Gas Molecules," March 1,
    1974.

S. Ezekiel, Massachusetts Institute of Technology, "Ultrahigh
    Resolution Spectroscopy Using cw Dye Lasers," March 22,
    1974.

L. Rimai, Ford Motor Company, "The Biophysical Applications of
    Raman Spectroscopy," March 27, 1974.

I. Lowe, University of Pittsburgh, "A New Method for Measuring
    Short Time Behavior of Free Induction Decay with
    Applications to CaF_2 and NH_4Cl," April 5, 1974.

L. Menegozzi, Yale University, "Theory of the Ring Laser,"
    April 12, 1974.

P. G. H. Sandars, Oxford University, "Atomic Quadrupole Moments:
    Experiments and Theory," April 19, 1974.

H. Kleinpoppin, University of Stirling, "Analysis of Electron-
    Atom Collisions," April 26, 1974.

ABSTRACT

A powerful new spectroscopic technique, cascade level anticrossing spectroscopy, has been developed and used to determine the complete hyperfine Hamiltonian of the 4_D state of rubidium. The anomalous magnetic hyperfine structure of this state is due to an anisotropic core polarization which has both a contact and a spin-dipole component. The spin-dipole component is so large that the sign of the net spin-dipole interaction is reversed with respect to the sign expected for the direct interaction between the nucleus and the valence electron. This is the first instance of a negative spin-dipole interaction ever discovered, and it may help in the formation of a satisfactory theory for the anomalous magnetic interactions in the D states of alkali atoms.

A number of new hyperfine interaction constants have been measured for S, P, D, and F states of the alkali atoms.

We have succeeded in obtaining narrow optical pumping signals in alkali vapors at vapor densities much higher than those previously attained, demonstrating the existence of a hitherto unsuspected high density optical pumping regime in which the Zeeman resonance frequency is shifted downward by a large factor and spin-exchange broadening vanishes. This new regime opens the way to miniature optically pumped devices, such as magnetometers, and affords important new possibilities for investigating basic interactions in dense alkali vapors.

Nuclear magnetic resonance signals from diatomic alkali molecules have been observed in optically pumped cesium and rubidium vapors. Some important rate constants have been deduced from the observed widths of these signals.

Hyperfine structure in the rotational spectrum of the heterocyclic rings pyrrole and pyridine has been resolved with a molecular beam maser. Pressure broadening of millimeter-wave lines of CO and HCN is being investigated as a function of temperature (down to dry ice temperature for HCN, and liquid nitrogen temperature for CO).

A quartet of new interstellar millimeter-wave lines has been discovered, and identified as the ethynyl radical C_2H, a molecule which has never previously been observed in the gas phase, even in the terrestrial laboratory. A radio telescope equipped with spectral line receivers for a sky survey of the carbon monoxide molecule has been completed, and is currently being installed on the roof of the Pupin Physics Laboratory.

We have detected photon echoes in $LaF_3:Nd^{3+}$ and $YAG:Nd^{3+}$ with amplitudes two to three orders of magnitude smaller than in $CaWO_4:Nd^{3+}$.

We observed a temperature-dependent decay which we attribute to photon-induced relaxation of the Orbach and Raman type. Magnetic field dependence results were also studied. For both crystals we observed modulation effects.

Using the Cr-Al interaction parameters determined from PENDOR studies and those determined from spin-echo ENDOR experiments, we have calculated photon-echo modulation behavior in ruby. The results compare favorably with our experimental data taken with an automated, gated cw system. We have measured the concentration and field dependence of the exponential decay of the photon echo, and the decays show simple exponential behavior.

We have measured electron-spin echo-modulation behavior associated with the $3/2 \rightarrow 1/2$ transition of the $^4A_2$ ground state of ruby.

Stimulated Raman scattering and four-wave parametric mixing has been studied in thallium vapor. The intensity distribution is approximately Gaussian with a half width divergence of 0.66 mrad. In the presence of SRS, the laser-beam divergence increases to 1.23 mrad. Generated Stokes energy appeared to be a function of thallium vapor pressure. The energy of the dye-laser anti-Stokes pulse versus the product of the laser and Stokes energies is 0.96 ± 0.02.

We have studied two of the cascading single-photon fluorescences from cesium gas excited by two-photon absorption. The fluorescent pulsewidth is two to four times that of the laser at low incident power levels.

After reanalyzing published experimental data regarding the relaxation behavior of two- and three-pulse electron-spin echoes in dilute systems, we find excellent agreement with our recently published theory of spectral diffusion decay.

We have confirmed that the superradiant condition is unstable by both a theoretical mode analysis and straightforward numerical computation.

We have found a clear singularity in the temperature coefficient of viscosity for He^4 at the superfluid transition (T_λ). The reduced viscosity difference $\Delta\eta/\eta$ depends on the reduced temperature difference $\epsilon = 2/3$ below T_λ, and $x = 0.9$ to 1.1 above T_λ. An experiment to detect the quantized rotation of superfluid helium by a thermal modulation technique is underway, and an apparatus to study mechanical properties of superfluid He^3 is nearing completion.

I. ATOMIC PHYSICS

A. HYPERFINE STRUCTURE OF EXCITED S STATES OF POTASSIUM, RUBIDIUM, AND CESIUM*

(R. Gupta, W. Happer, L. Lam, S. Svanberg)

We have completed measurements of the hyperfine structure (hfs) of the first and second excited S states of K^{39} and K^{41}, and of the first, second, and third excited states of Rb^{85}, Rb^{87}, and Cs^{133}. These systematic measurements of the hfs of several excited S states of each alkali metal have revealed some very interesting properties of these states. These measurements have been performed by the method of cascade radio-frequency spectroscopy, a technique developed in this Laboratory. This method of reaching the optically inaccessible states has been described in detail in the previous Progress Report, [1] and is also illustrated in Fig. 1.

The results of our measurements are shown in Table I. For completeness, we have included in Table I the well-known ground-state hfs constants of the alkali metal atoms. We have also included the hfs value [2] for the $4^2S_{1/2}$ state of sodium (see p. 10 below). Recently, Rosén and Lindgren [3] calculated hfs-coupling constants using restricted self-consistent field methods for the sequences of S and P states of alkali metal atoms. Also, Norcross [4] has calculated the A values for the 6, 7, 8, and 9 S states of cesium using a semiempirical model potential. Both of these calculations, as well as the results obtained from the semiempirical formula for S states, allow us to compare our experimental values with the theoretical A values for _sequences_ of S states. Some interesting conclusions can be drawn from these comparisons.

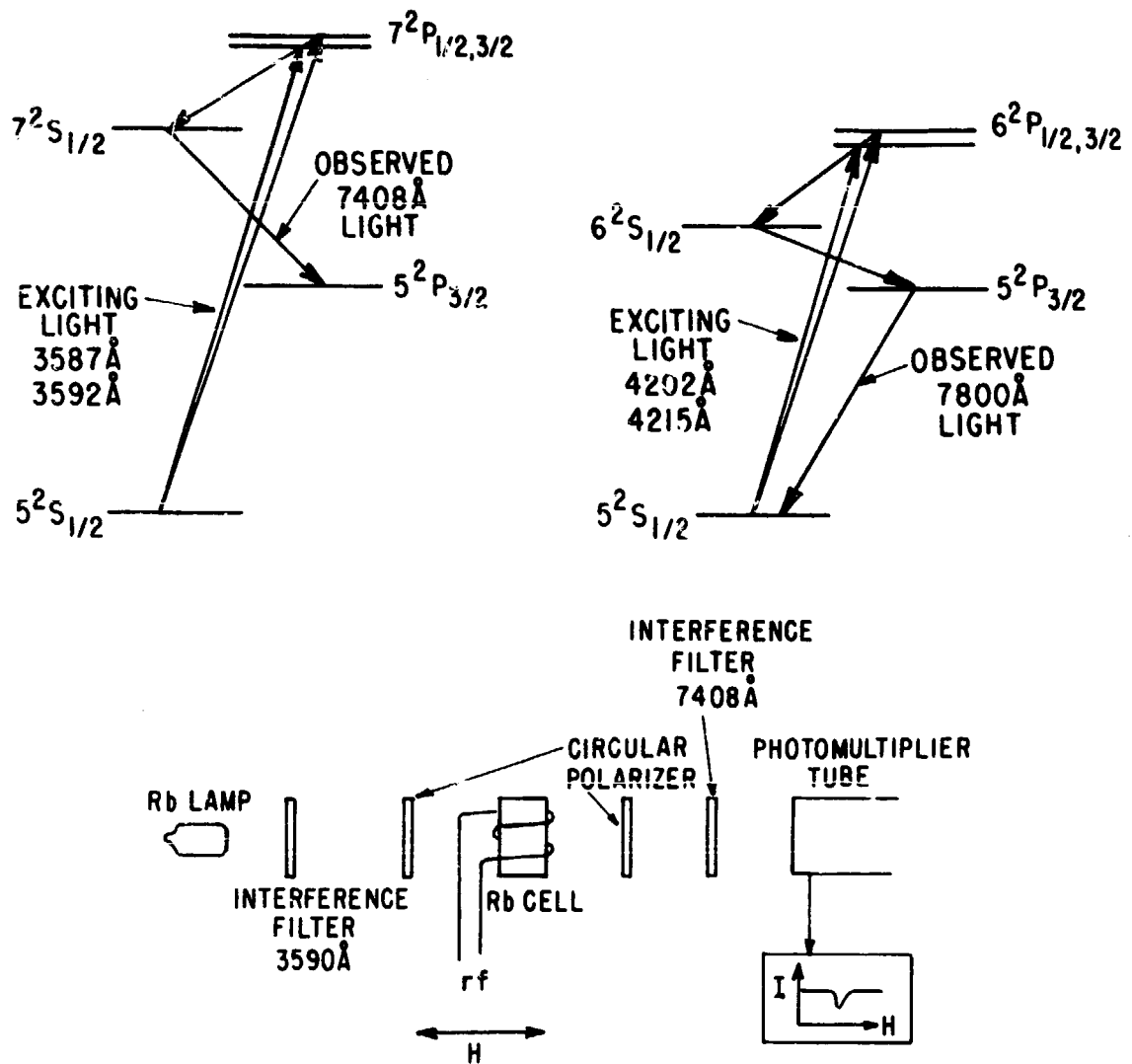Columns 4 through 10 of the table list some of the theoretical

3

Fig. 1. Schematic illustration of the method of cascade radio-frequency spectroscopy. The polarized P states are created by excitation with circularly polarized resonance light. The excited S states are populated and polarized by the spontaneous decay of these P states. The polarization of the excited S states is monitored by observing the circular polarization of the fluorescent light. Rf resonances in these states are observed as a decrease in the polarization of the fluorescent light.

4

TABLE I. Experimental and theoretical values of the hyperfine structure coupling constant A.

Isotope	State	A_{exp} (MHz)	A_{theo} (MHz)						
			SE	R L[b] HF	R L[b] IIS	R L[b] CHFS	RHF + CP[c]	RHF + RCP[b]	SEMP[a]
Na^{23}	$3^2S_{1/2}$	885.8	996.4	631.1	840.87	814.1	777.54 857.8 ± 6.0[d]	774.41	
	$4^2S_{1/2}$	202(3) [a]	228.45	151.8	199.8	198.9			
K^{39}	$4^2S_{1/2}$	230.85	248.3	150.9	222.0	195.6	184.49	187.79	
	$5^2S_{1/2}$	55.50(60)	59.98	39.76	56.57	53.42			
	$6^2S_{1/2}$	21.81(18)	23.62	16.15	22.38	21.72			
K^{41}	$4^2S_{1/2}$	127.00	136.0	82.94	122.0	108.1	101.40	103.21	
	$5^2S_{1/2}$	30.75(75)	32.85	21.85	31.09	29.36			
	$6^2S_{1/2}$	12.03(40)	12.99	8.876	12.30	11.94			
Rb^{85}	$5^2S_{1/2}$	1011.9	1084.8	668.6	1003	856.9	793.54	821.3	
	$6^2S_{1/2}$	239.3(1.2)	261.6	176.1	254.5	237.5			
	$7^2S_{1/2}$	94.00(44)	103.9	71.23	101.3	97.58			
	$8^2S_{1/2}$	45.5(2.0)	51.6	36.15	50.78	49.25			
Rb^{87}	$5^2S_{1/2}$	3417.3	3675.6	2266	3398	2904	2689.4	2783.4	
	$6^2S_{1/2}$	809.1(5.0)	885.6	596.7	862.5	804.8			
	$7^2S_{1/2}$	318.1(3.2)	351.6	241.4	343.4	330.7			
	$8^2S_{1/2}$	158.0(3.0)	174.9	123.5	172.1	166.9			
Cs^{133}	$6^2S_{1/2}$	2298.1	2342.3	1519	2289	1763	1683.45	1854.3	2449.8
	$7^2S_{1/2}$	546.3(3.0)	570.8	412.5	591.7	516.0			579.8
	$8^2S_{1/2}$	218.9(1.6)	230.5	172.1	239.3	218.1			231.9
	$9^2S_{1/2}$	109.5(2.0)	115.8	87.55	120.9	112.0			116.3

(a) K. H. Liao, R. Gupta, and W. Happer, Phys. Rev. A 8, 2811 (1973).
(b) A. Rosén and I. Lindgren, Physica Scripta 6, 109 (1972).
(c) L. Tterlikkis, S. D. Mahanti, and T. P. Das, Phys. Rev. 176, 10 (1968).
(d) T. Lee, N. C. Dutta, and T. P. Das, Phys. Rev. A 1, 995 (1970).
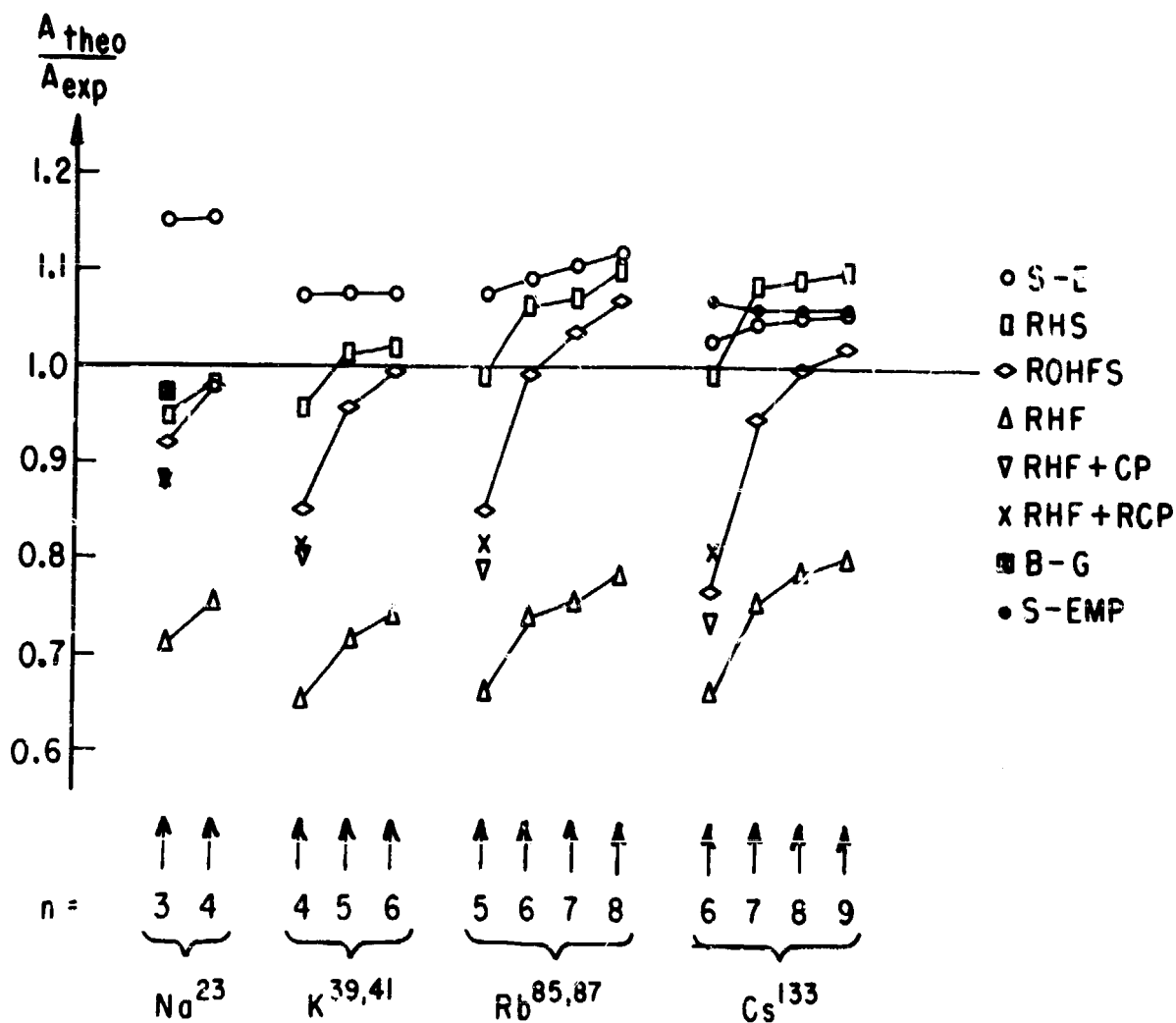(e) D. W. Norcross, Phys. Rev. A 7, 606 (1973).

5

Fig. 2. A pictorial representation of our experimental
results and some of the theoretical values of
the hyperfine interaction constant A. Ratios
of the experimental and theoretical values of
A have been plotted against the principal quan-
tum numbers of the states. The symbol SE repre-
sents the results of the semiempirical formula,
while RHS, RHF, and ROHFS represent the rela-
tivistic Hartree-Slater, Hartree-Fock, and op-
timized Hartree-Fock-Slater schemes, respec-
tively. The symbol RHF-CP is the results of
the relativistic Hartree-Fock method, includ-
ing core-polarization effects, while RHF-RCP
represents RHF-CP results corrected for rela-
tivistic effects in the core polarization
term. The symbol BG is the results of the
Brueckner-Goldstone manybody perturbation
theory, while S-EMP stands for the results
of a semiempirical model potential.

A values. Column 4 gives the values of the magnetic dipole-coupling constants calculated from the semiempirical formula[5]

$$A = \frac{8}{3} \frac{cR_\infty \alpha^2 Z g_I}{n_o^3} \left(1 - \frac{d\sigma}{dn}\right) F_r(j,Z)(1 - \epsilon)(1 - \delta).$$ (1)

Here, n_o is the _effective_ principal quantum number of the state, σ is the Rydberg correction, $F_r(j,Z)$ is the relativistic correction, and ϵ and δ are the corrections required by the distribution effects over the nuclear volume, respectively. All other symbols in Eq. (1) have their usual meaning. Both the effective quantum number n_o and the quantity $(d\sigma/dn)$ are deduced from the measured binding energies of the atomic states.[6] We have used the values of the correction terms $F_r(j,Z)$, ϵ, and δ listed in Kopfermann.[7] Columns 5, 6, and 7 of Table I give the A values calculated by Rosén and Lindgren using relativistic Hartree-Fock, Hartree-Slater, and optimized Hartree-Fock-Slater schemes, respectively. Column 8 shows the A values calculated by Tterlikkis et al.[8] They have taken into account both the core polarization and the relativistic effects, the former by a moment-perturbation procedure and the latter by a relativistic Hartree-Fock method. These calculations have been done only for the ground state of the alkali metal atoms. The ground-state hfs of sodium has also been calculated by Lee et al.,[9] using the Brueckner-Goldstone manybody perturbation theory (also shown in column 8). Tterlikkis' calculation does not take into account the relativistic effects in the core-polarization term itself. Rosén and Lindgren have applied a relativistic correction to Tterlikkis' core-polarization term, and the resulting A values are shown in column 9. The results of Norcross'[10] calculations using a semiempirical model potential are shown in column 10. In this calculation, two parameters in the model potential were chosen such that the spectroscopic term values of the 6^2S and the 6^2P states of Cs agree with those calculated using this potential. A graphical summary of the results of various calculations is shown in Fig. 2. The ratio of the theo-

7

retical and experimental A values has been plotted against the principal quantum numbers for various states. Referring to Fig. 2, we can make the following observations:

The values of A calculated by the semiempirical formula always lie higher than the experimental values. If Rosén and Lindgren's relativistic correction factors are used instead of those of Kopfermann, the theoretical A values will be even higher; i.e. the disagreement between the theoretical and experimental values will increase. Considering the simplicity and generality of the semiempirical formula, we find that the agreement with the experimental values that this formula provides (to within about 10%) is remarkable.

Of the restricted self-consistent field methods, the relativistic Hartree-Slater scheme gives the best agreement with the experimental A values, and the overall agreement is very good. It is worth noting that Rosén and Lindgren have not explicitly taken the core polarization into account, as their principal aim was to calculate new and more accurate relativistic correction factors for ^2S and ^2P states. Inclusion of core polarization explicitly will perhaps move all these theoretical hfs values somewhat higher. It is interesting that the ratio (A_{theo}/A_{exp}) systematically increases with increasing principal quantum number for all alkali-metal atoms that we have investigated and for all three schemes that Rosén and Lindgren have used. They have also calculated electron-binding energies by using the relativistic Hartree-Fock, Hartree-Slater, and the optimized Hartree-Slater schemes. We find that the ratios of the theoretical and experimental binding energies have exactly the same trend with the principal quantum number n as do the ratios of the theoretical and experimental hfs coupling constants A.

Tterlikkis' A values for the ground state, calculated by the relativistic Hartree-Fock method and _including_ core-polarization effects, are small compared to the experimental values. If the relativistic correction is applied to the core-polarization term,[11] the resulting A values are seen to agree better with the experimental values. Lee's A value for the ground state of sodium, calculated by the Brueckner-Goldstone manybody perturbation theory, agrees very

8

well with the experiment. This may indicate that electron correlation effects are quite important for S state hyperfine structure. An obvious question, however, is how well similar Brueckner-Goldstone calculations would work for the higher S states of sodium and for the S states of the other alkali atoms. Would the inclusion of electron-correlation effects remove the striking increase in A_{theo}/A_{exp} with principal quantum number?

The results of Norcross' calculations for the S states of Cs using a semiempirical model potential agree very well with the experimental values. It is remarkable that the ratio of Norcross' values to the experimental values is nearly independent of the principal quantum number, in striking contrast to the results of the self-consistent field calculations.

In summary, comparison of our measured values with various theoretical values shows that, although many creditable attempts have been made to calculate the S state hfs intervals of alkali atoms, no really precise theory seems to exist yet.

This project is now complete. Higher excited S states are now being investigated by dye-laser spectroscopy, as described in Part G of this Section.

(1)   CRL Progress Report, June 30, 1973, p. 3.

(2)   K. H. Liao, R. Gupta, and W. Happer, Phys. Rev. A $\underline{8}$, 2811 (1973).

(3)   A. Rosén and I. Lindgren, Physica Scripta $\underline{6}$, 109 (1972).

(4)   D. W. Norcross, Phys. Rev. A $\underline{7}$, 606 (1973).

(5)   H. Kopfermann, Nuclear Moments (Academic Press, New York 1968), p. 131.

(6)   C. F. Moore, NBS Circular No. 467 (U. S. GPO, Washington, D. C.).

(7)   H. Kopfermann, op. cit., p. 132 and 136.

(8)   L. Tterlikkis, S. D. Mahanti, and T. P. Das, Phys. Rev. $\underline{176}$, 10 (1968).

(9)   T. Lee, N. C. Dutta, and T. P. Das, Phys. Rev. A $\underline{1}$, 995 (1970).

(10) D. W. Norcross, op. cit., p. 606.

(11) A. Rosén and I. Lindgren, op. cit., p. 109.

B. HYPERFINE STRUCTURE OF EXCITED S STATES OF SODIUM*
(R. Gupta, W. Happer, K. Liao)

The measurement of the hyperfine structure of the $4S_{1/2}$ state of Na^{23} by cascade radio-frequency spectroscopy has been completed, and the results have been published.[1]

One of our experimental resonance curves is shown in Fig. 3. This resonance results from the $m_F = -2 \leftrightarrow m_F = -1$, $\Delta F = 0$ transition at about 147.5 MHz in an external field of about 117 G. At the peak of the resonance the polarization of the fluorescent light decreases by about 10%. Figure 4 shows a similar resonance at 231.5-G field strength. This resonance also comes from the $m_F = -2 \leftrightarrow m_F$, $\Delta F = 0$ transition, but the rf field has a frequency of about 405 MHz. The sharp dip at the low-field side of the $4^2S_{1/2}$ resonance results from a $4^2P_{3/2}$ state resonance. Unfortunately, a transition in the $3^2P_{3/2}$ state accidentally overlaps the $4^2S_{1/2}$ state transition at this field. Although the $3^2P_{3/2}$ resonance should be very weak and very broad, as the lifetime of this state is only 16 nsec, we are not sure that the $3^2P_{3/2}$ resonance does not slightly affect the observed position of the $4^2S_{1/2}$ state resonance. For this reason, we have used only the data for the 147-MHz transition frequency to deduce our final results. The 405-MHz resonance, however, serves to confirm our identification of the $4^2S_{1/2}$ resonance. For about 25 curves of the type shown in Fig. 3, we have deduced the hfs of the $4^2S_{1/2}$ state from the magnetic field at which these resonances are seen. We find, for the magnetic dipole coupling constant, a value of

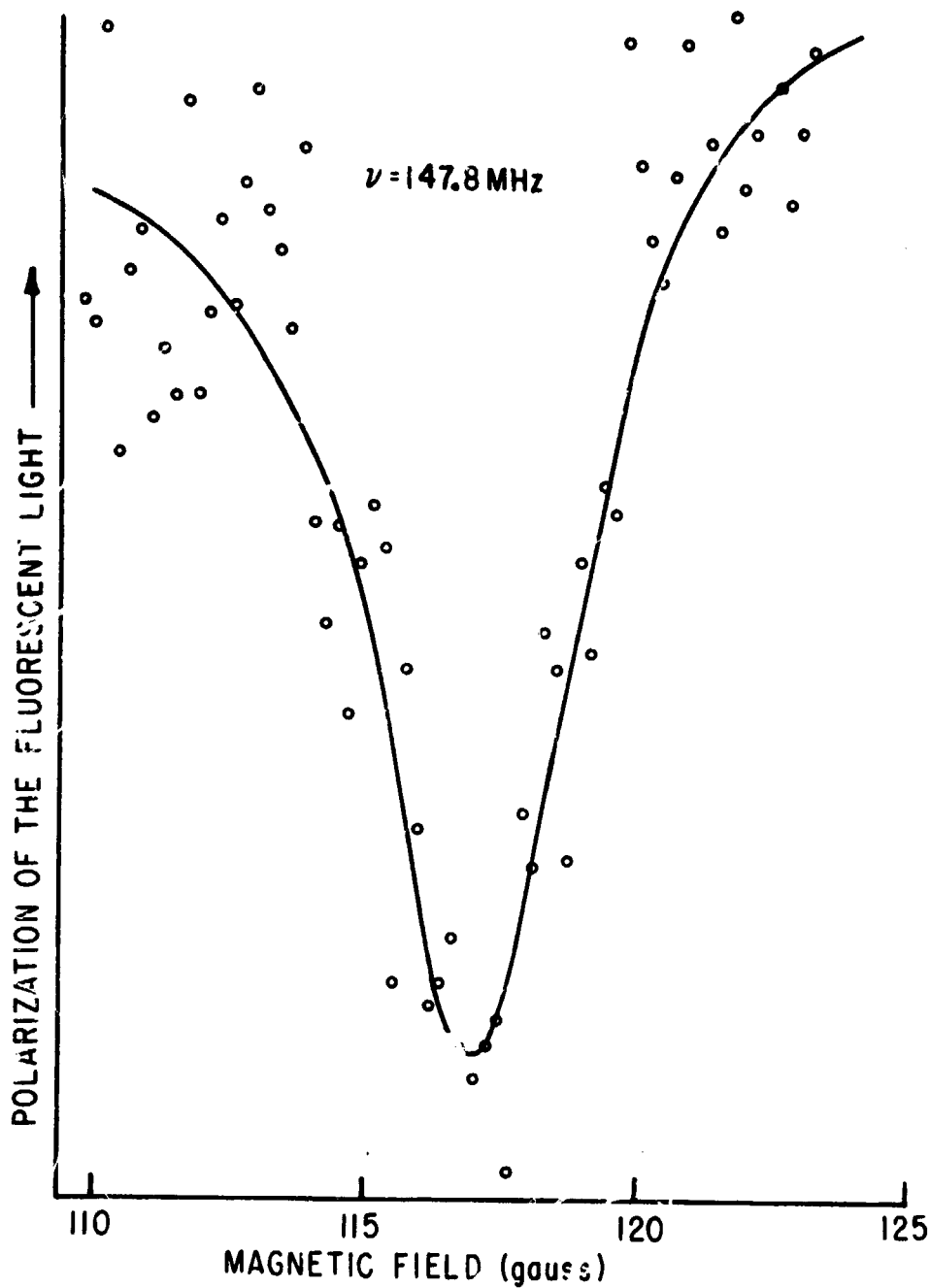$$A(4^2S_{1/2}) = 202 \pm 3 \text{ MHz.}$$

10

Fig. 3. Rf resonance curve for the $m_F = -2 \leftrightarrow m_F = -1$, $\Delta F = 0$ transition in the $4^2S_{1/2}$ state of Na^{23}. The transition frequency is 147.8 MHz. This curve represents ~3 hr of signal averaging.
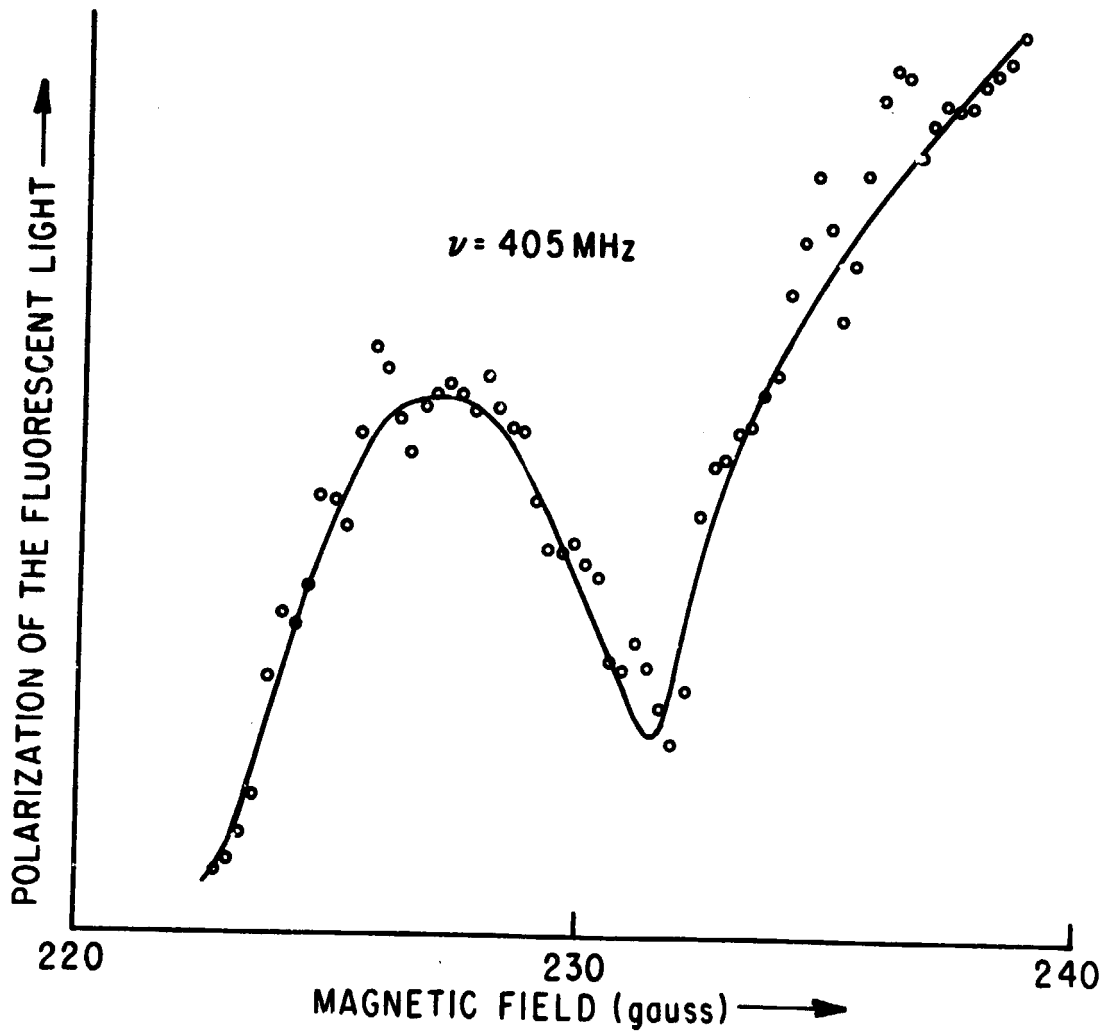
11

Fig. 4. Rf resonance curve due to the $m_F = -2 \leftrightarrow m_F = -1$, $\Delta F = 0$ transition at 405-MHz frequency in the $4^2S_{1/2}$ state of Na^{23}.

12

(1) K. H. Liao, R. Gupta, and W. Happer, Phys. Rev. A **8**, 2811 (1973).

C.   HYPERFINE STRUCTURE OF EXCITED $D_{5/2}$ AND $D_{3/2}$ STATES OF ALKALI ATOMS*

(R. Gupta, W. Happer, C. Tai)

We have measured the hyperfine structures of some of the excited D states of rubidium and cesium. A compilation of these results appears in Table II. The double-resonance data are obtained from the results of several repeated measurements, and the quoted error bars represent three standard deviations in the statistical spread of the results plus an allowance for possible systematic errors, such as errors in the magnetic-field calibration, etc. The hyperfine structure of the $8P_{1/2}$ state of cesium was also measured and is given in Table II. The methods we used to investigate the hfs of the D states are cascade-double-resonance, cascade-level-crossing, and cascade-decoupling spectroscopy. These were all discussed in last year's Progress Report.[1] Additional experimental results of this work are given in Figs. 5-13.

This year we have developed a new and powerful method to determine the sign of the hfs constant. In the measurement of the hyperfine constant of the Cs $6D_{3/2}$ state, we excite the ground-state atoms into the $8P_{1/2}$ state with circularly polarized helium 3888-Å light; we then get polarized D state atoms by the spontaneous decay of the atoms in the $8^2P_{1/2}$ state from Fig. 14. From Fig. 14, we see that we can approximate the excitation process by white light excitation from the ground-state F = 4 sublevel alone. After simple calculation, at a magnetic field low for the ground state but high for the associated excited states, we find out that, with helium σ_+ exciting light, the cesium $8P_{1/2}$ state is polarized, with the $m_J = -1/2$ sublevels unpopulated and the population of the $m_J = +1/2$ sublevels proportional to $(I + 1/2 + m_I)$. If rf transitions are induced between the sublevels, the resonance signals corresponding to sublevels with different m_I

13

TABLE II. Hyperfine coupling constants A measured in this work.

Element	State	Method	Measured Hyperfine coupling constant A (in MHz)	Calculated A
Rb^{87}	$5\,^2D_{3/2}$	Double-resonance and decoupling	14.43 ± 0.12	13.57
	$5\,^2D_{5/2}$	Double-resonance and decoupling	-7.44 ± 0.06	5.81
Rb^{85}	$5\,^2D_{3/2}$	Double-resonance and decoupling	4.18 ± 0.10	4.00
	$5\,^2D_{5/2}$	Double-resonance and decoupling	-2.14 ± 0.12	1.71
Cs^{133}	$6\,^2D_{3/2}$	Level-crossing and decoupling	16.5 ± 0.3	
	$6\,^2D_{3/2}$	Double-resonance and decoupling	16.38 ± 0.05	9.4
	$6\,D_{5/2}$	Decoupling	-3.0 ± 1.0	4.0
	$8\,P_{1/2}$	Decoupling and double-resonance	42.97 ± 0.10	

14
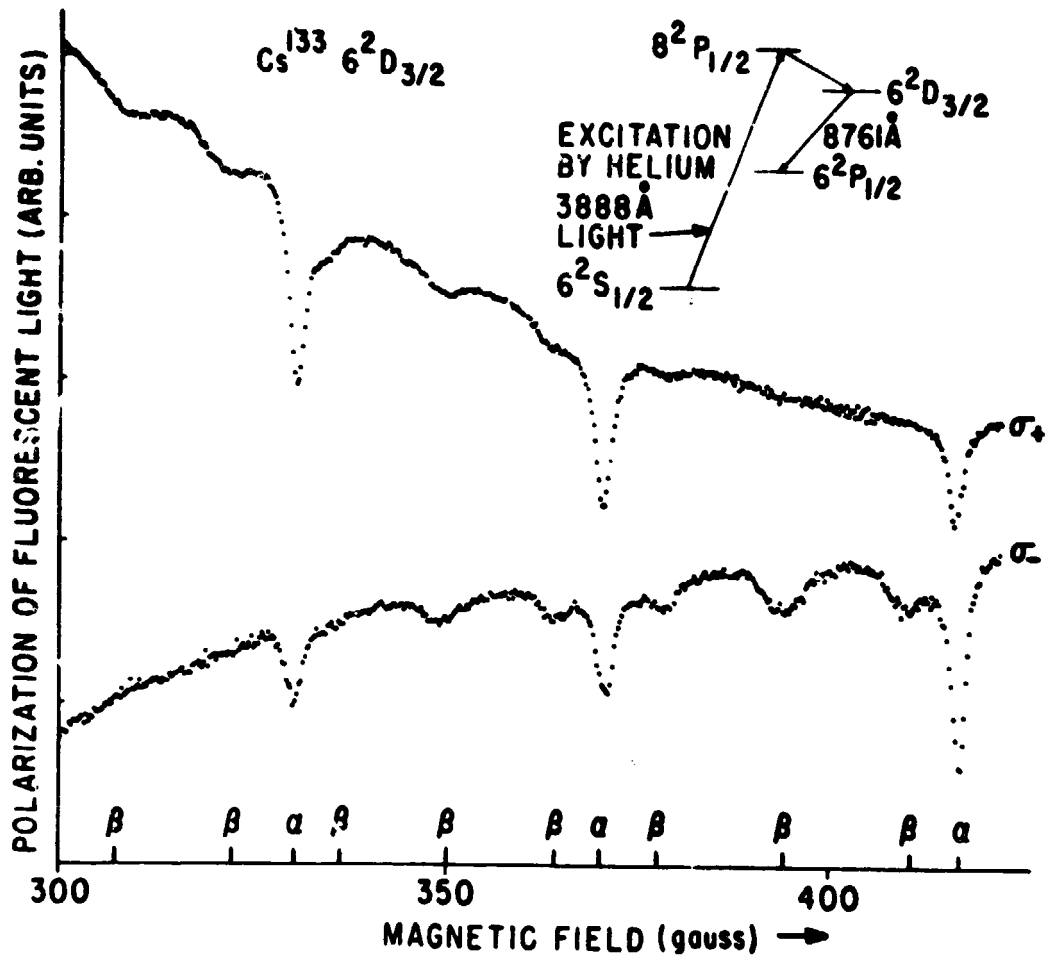
Fig. 5.   Observed radio-frequency resonances in Cs^{133}.   The
symbols α and β refer to rf resonances in the 8P$_{1/2}$
and 6D$_{3/2}$ states, respectively.   One division on
the ordinate corresponds to about a 5% change in
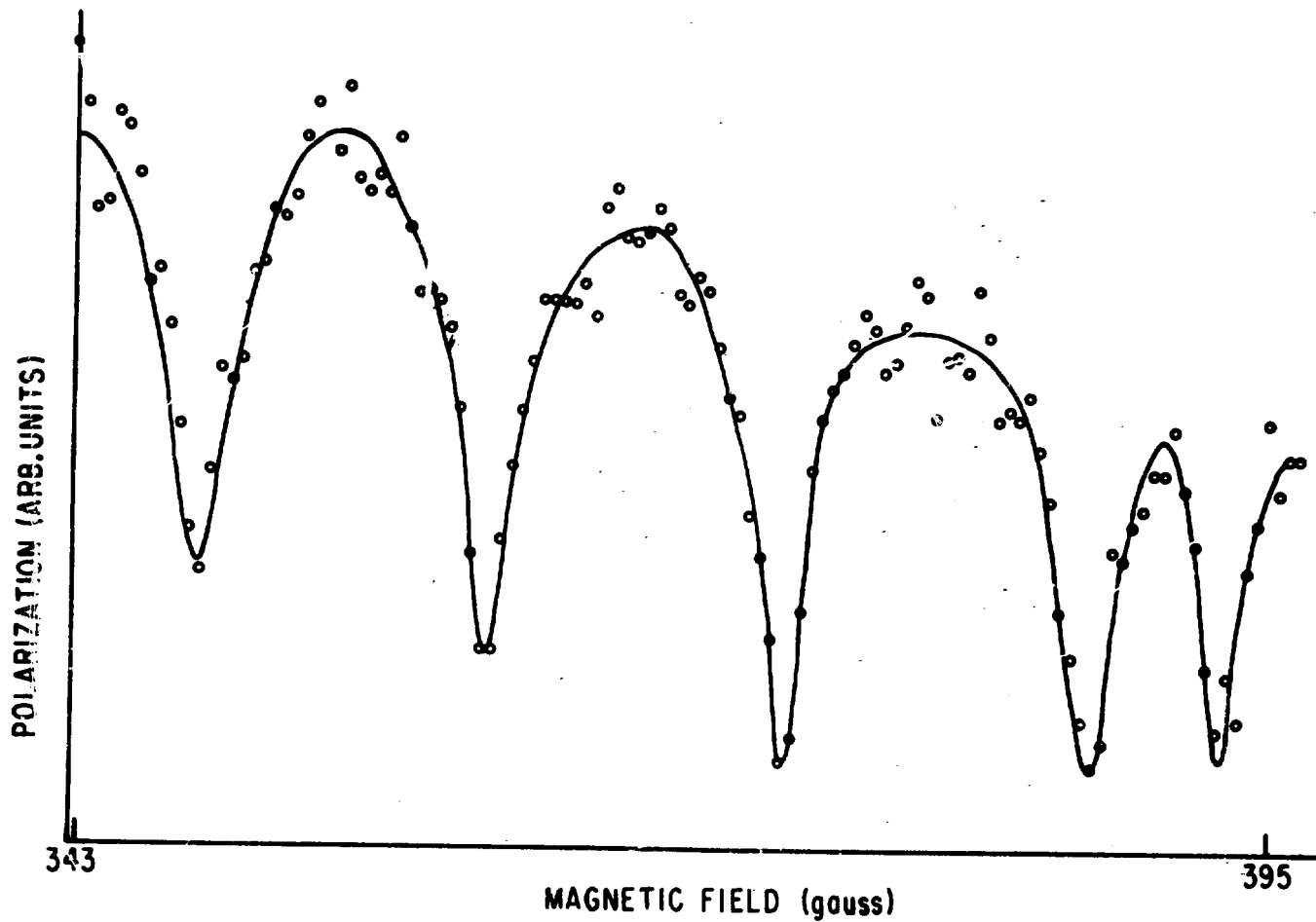the polarization of σ_- light and an 8% change in
the σ_+ light.

Fig. 6.   Observed radio-frequency resonances of Rb^{87} $5D_{3/2}$ states with Rb^{87} lamp. The resonance at highest H-field is an $8P_{1/2}$ resonance.   Radio frequency is 403 MHz.
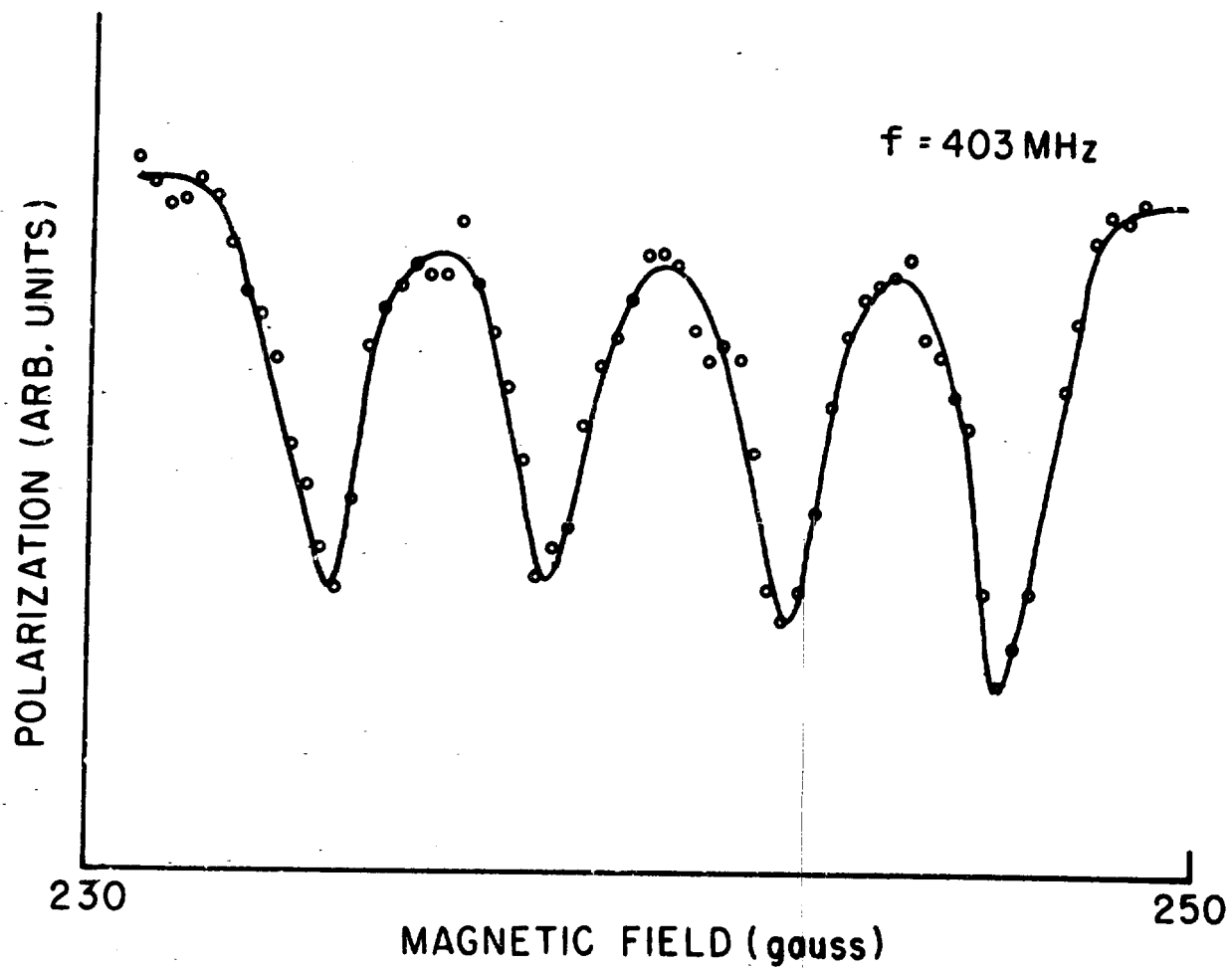
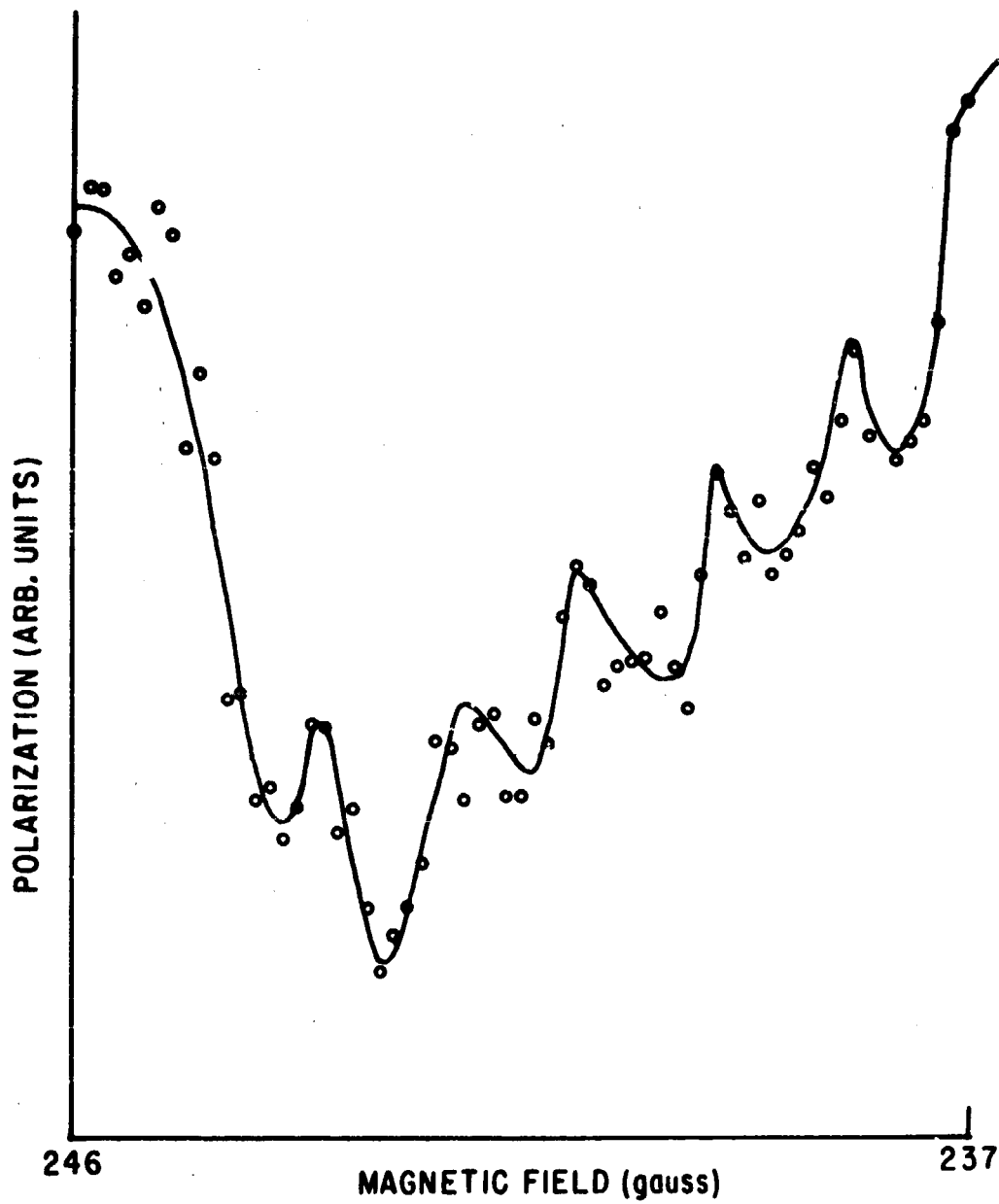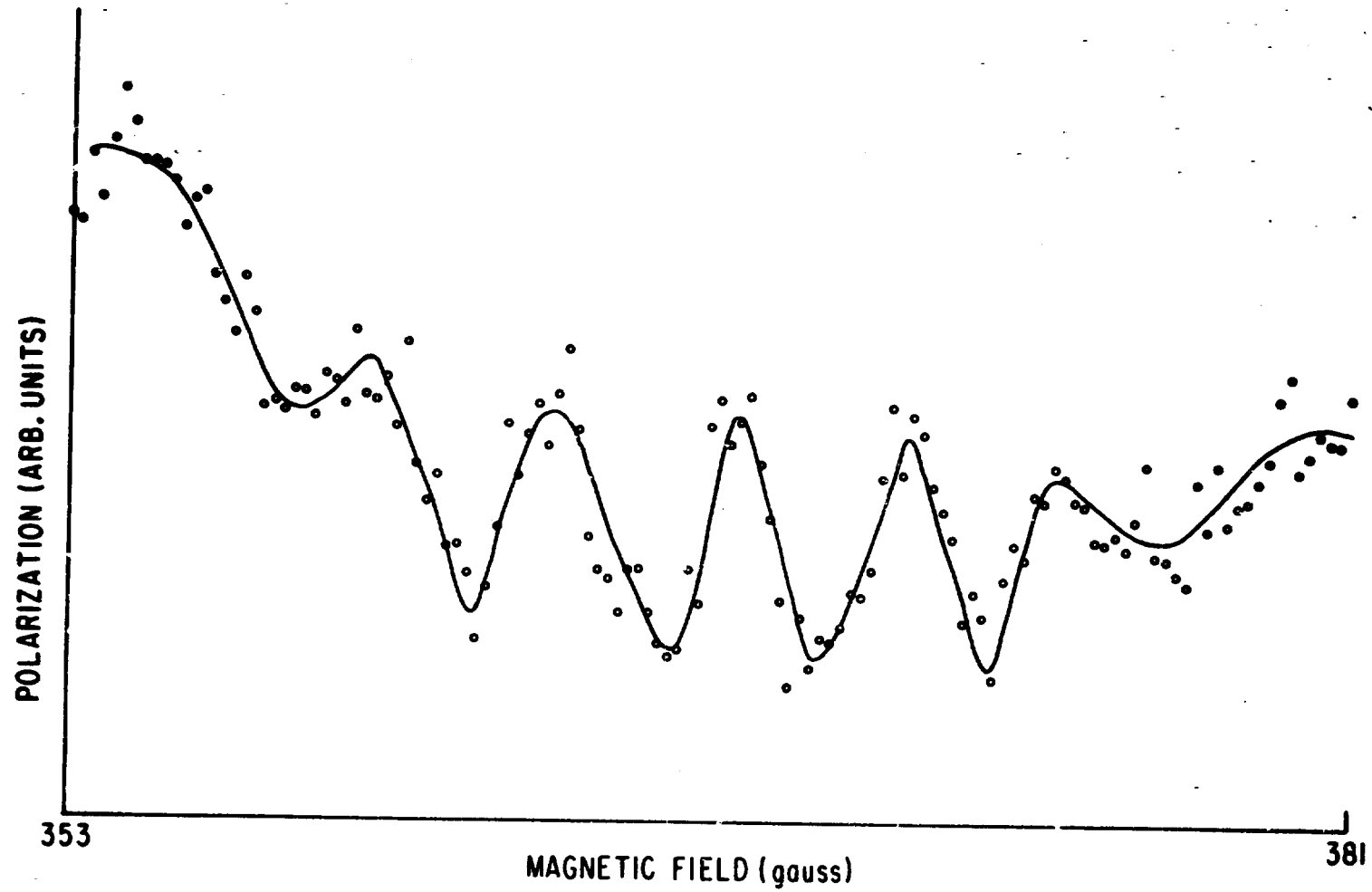Fig. 7.   Observed radio-frequency resonances of Rb^{87} 5D$_{5/2}$ states.

Fig. 8. Observed radio-frequency resonances of Rb^{85} $5D_{5/2}$
states. Radio frequency is 403 MHz.

Fig. 9. Observed radio-frequency resonances of Rb[85] $5D_{3/2}$ states. Radio frequency is 403 MHz.
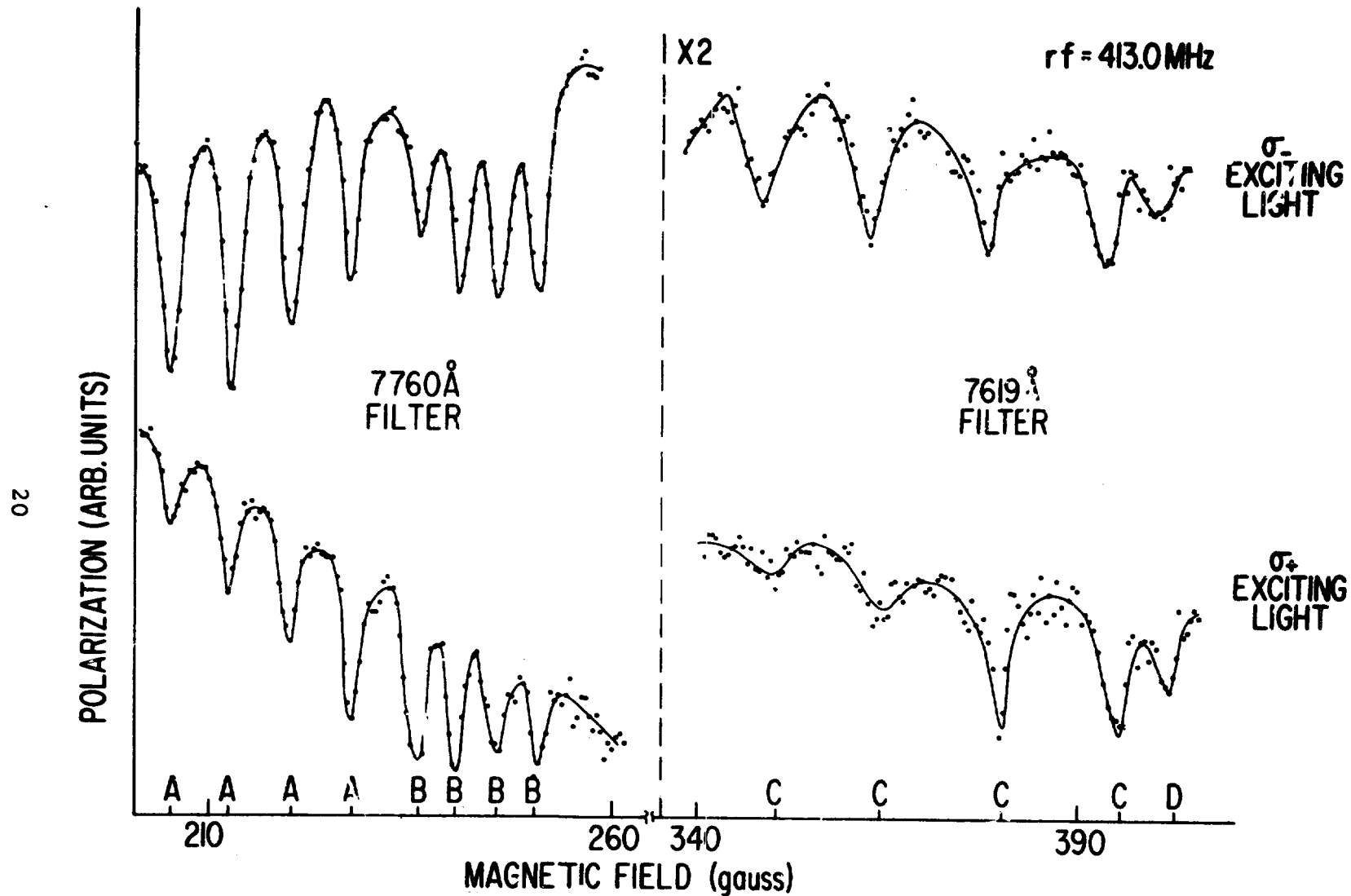
61

Fig. 10. Observed radio-frequency resonances of Rb^{87} 5D states with Rb^{85} lamp. The letters A, B, C, and D refer to radio-frequency resonances in the $7P_{3/2}$, $5D_{5/2}$, $5D_{3/2}$, and $7P_{1/2}$ states, respectively.
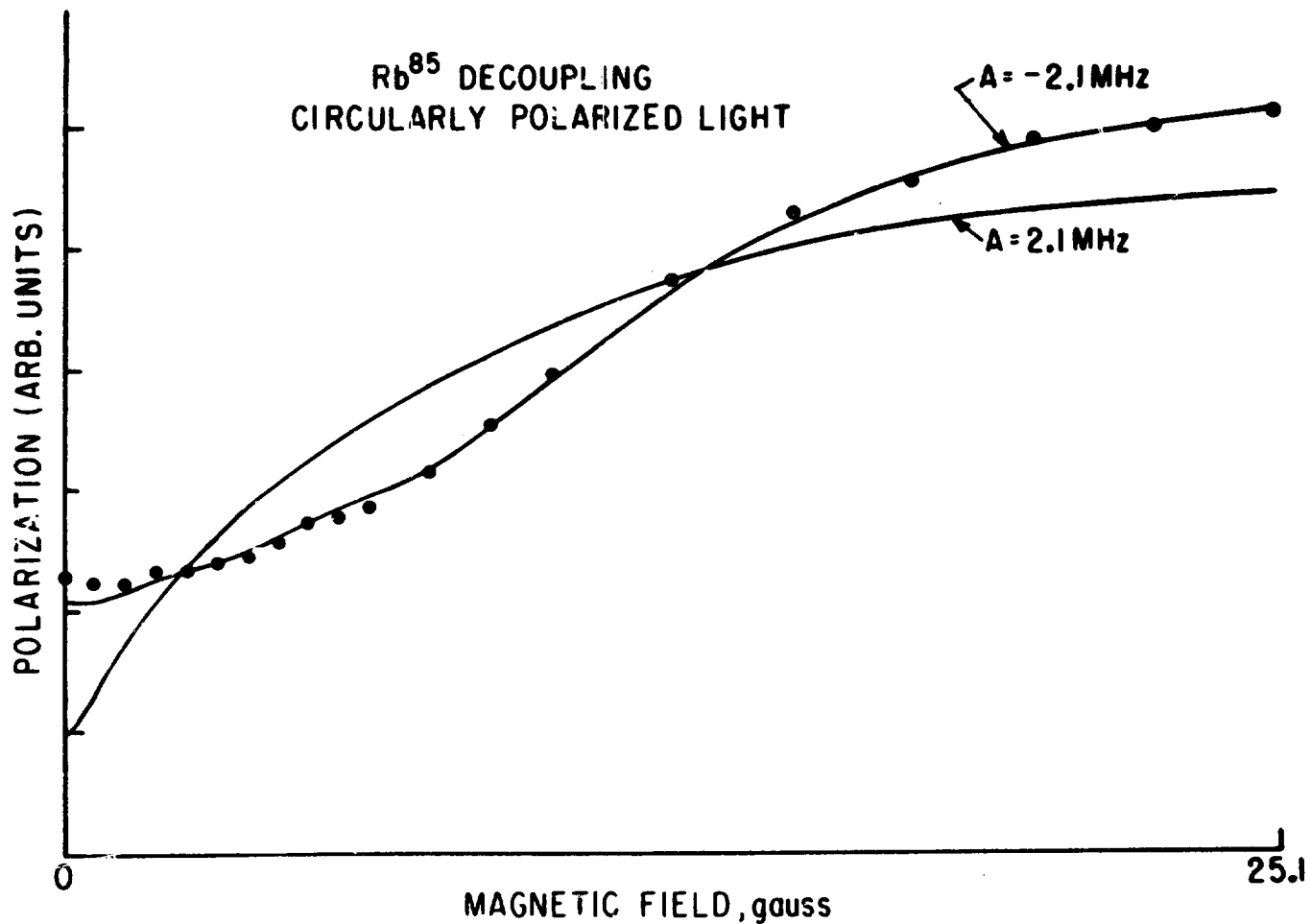
20

Fig. 11. Cascade-decoupling data for the $5D_{5/2}$ states of Rb^{85}. The points are experimental data. The solid lines are calculated from the hyperfine structure parameters indicated in the figure. These data determine the sign and the approximate magnitude of the D state A value.

Fig. 12. Cascade-decoupling data for the $5D_{3/2}$ states of Rb^{85}. The points are experimental data. The solid lines are calculated from the hyperfine structure parameters indicated in the figure. These data determine the sign and the approximate magnitude of the D state A value.
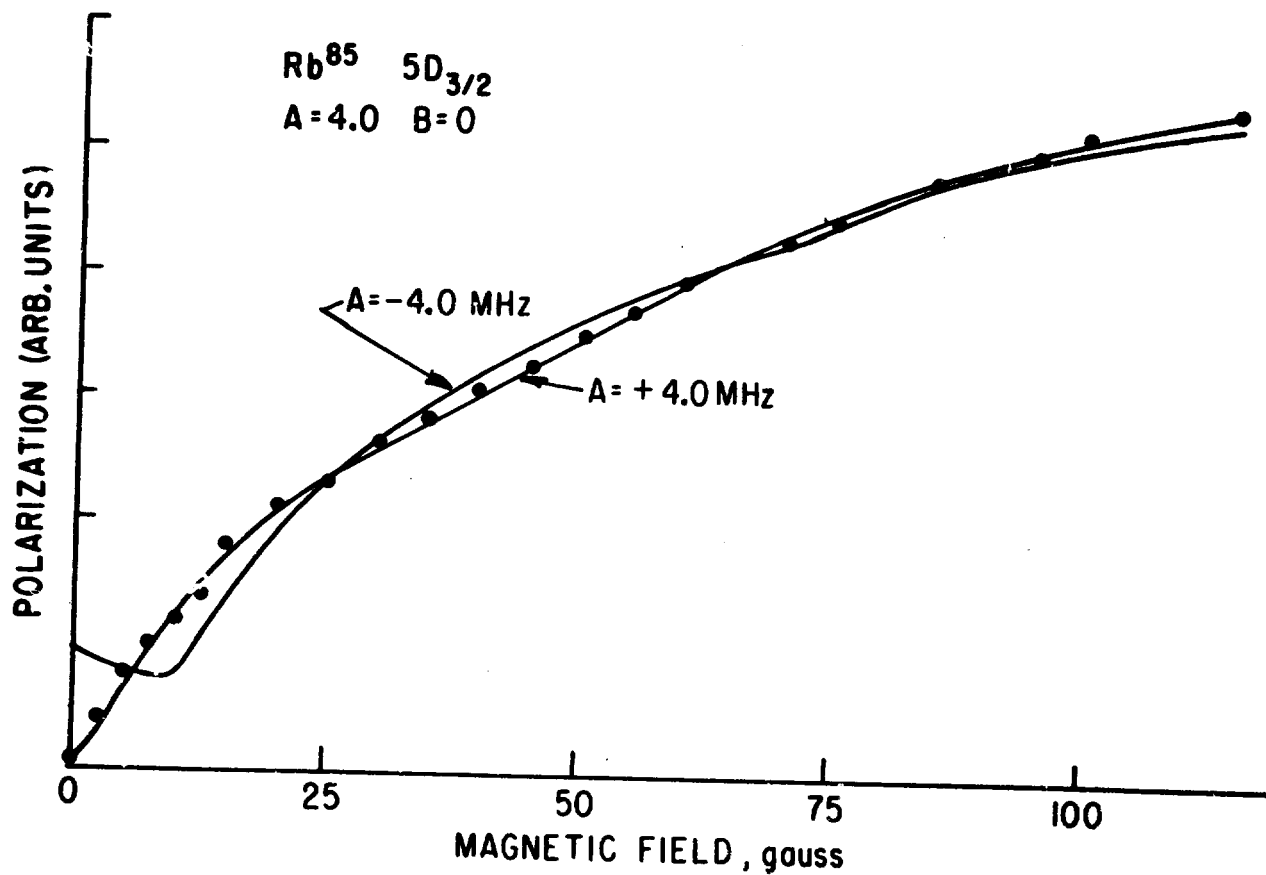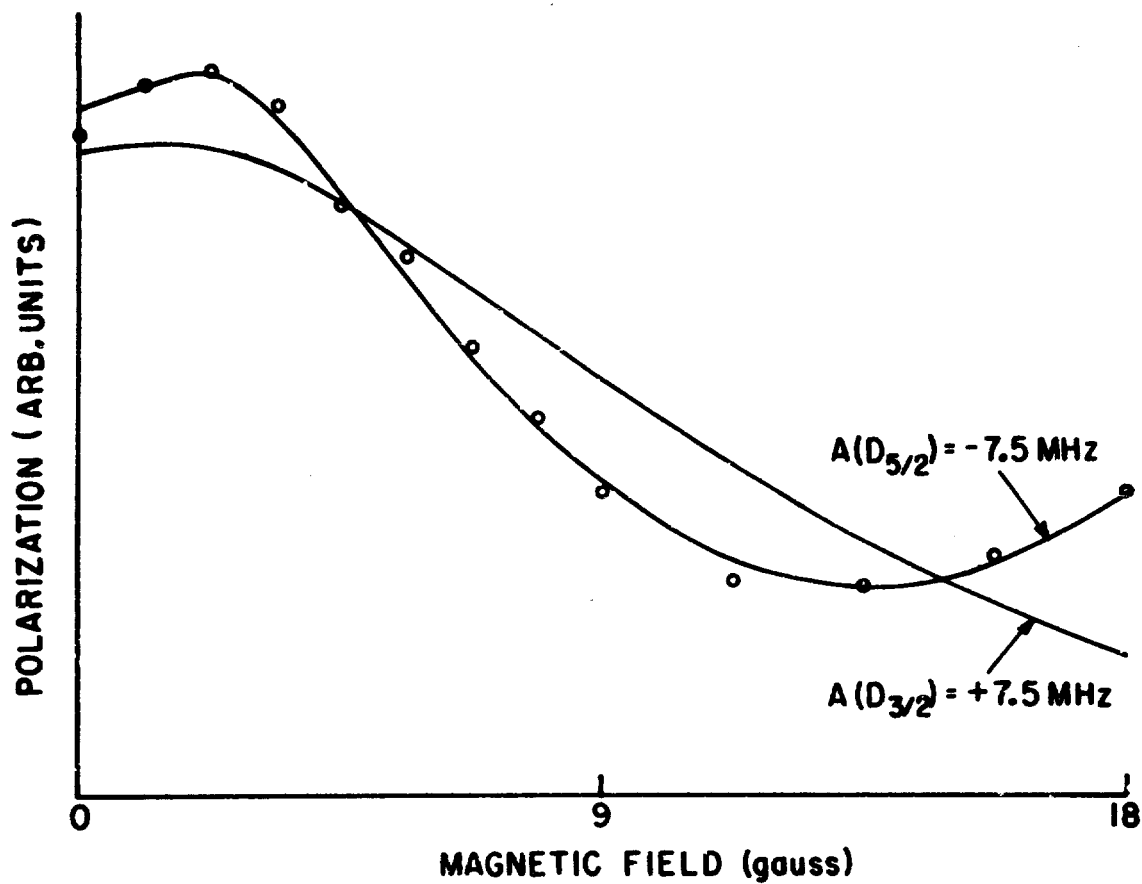
Fig. 13. Decoupling of Rb[87] $5D_{5/2}$ states with exciting light linearly polarized in the direction of the magnetic field.

$T = 400°K$

He 3888
RELATIVE EMISSION

$2^3S_1 \rightarrow 3^3P_2$

F=4

$2^3S_1 \rightarrow 3^3P_1$

F=3

Cs 3888
DOPPLER WIDTH"

.004 Å

$2^3S_1 \rightarrow 3^3P_0$

.026 Å .020 Å

.007

.036 Å

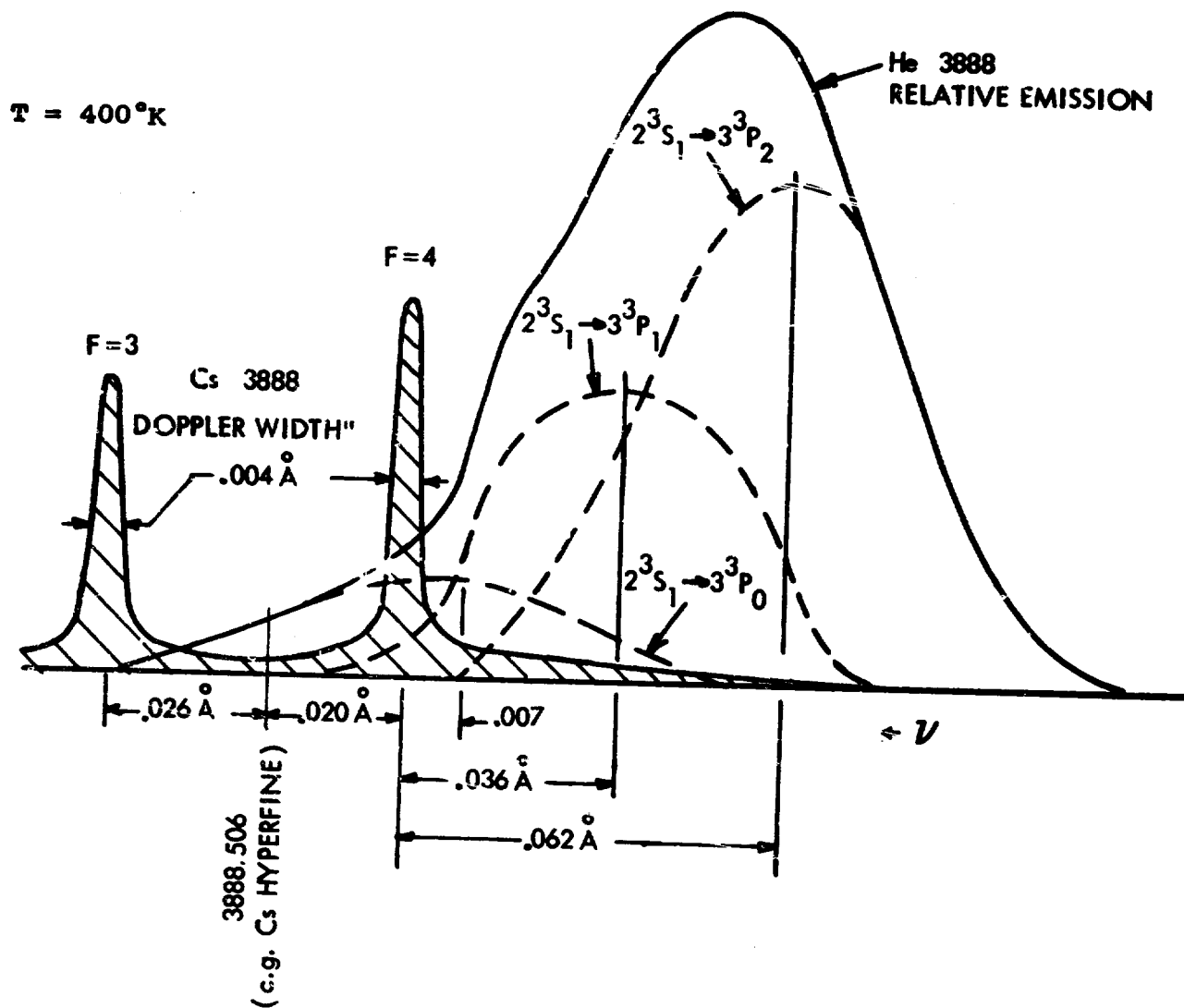.062 Å

$\leftarrow \nu$

3888.506
(c.g. Cs HYPERFINE)

24

Fig. 14. Helium and cesium lineshapes. (From P. Rabinowitz and S. Jacobs, Quantum Electronics, Proceedings of the Third International Congress, 1963 Paris Conference.)
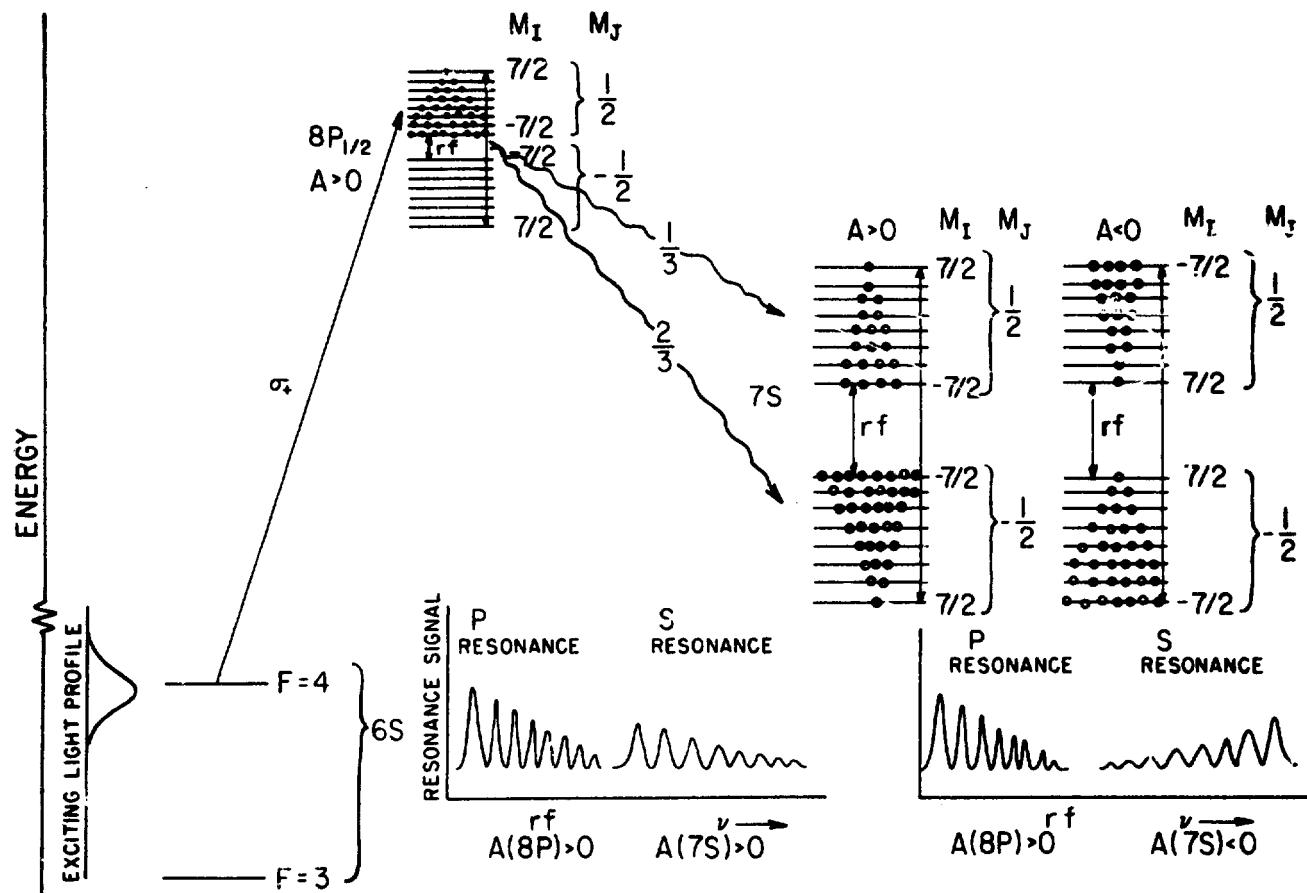
Fig. 15. Process of cascade double resonance of the $8P_{1/2}$ state of Cs^{133}; the Cs
cell is excited with circularly polarized light from a helium lamp. The
magnetic field is ~700 gauss. The relative amplitude of the resonance
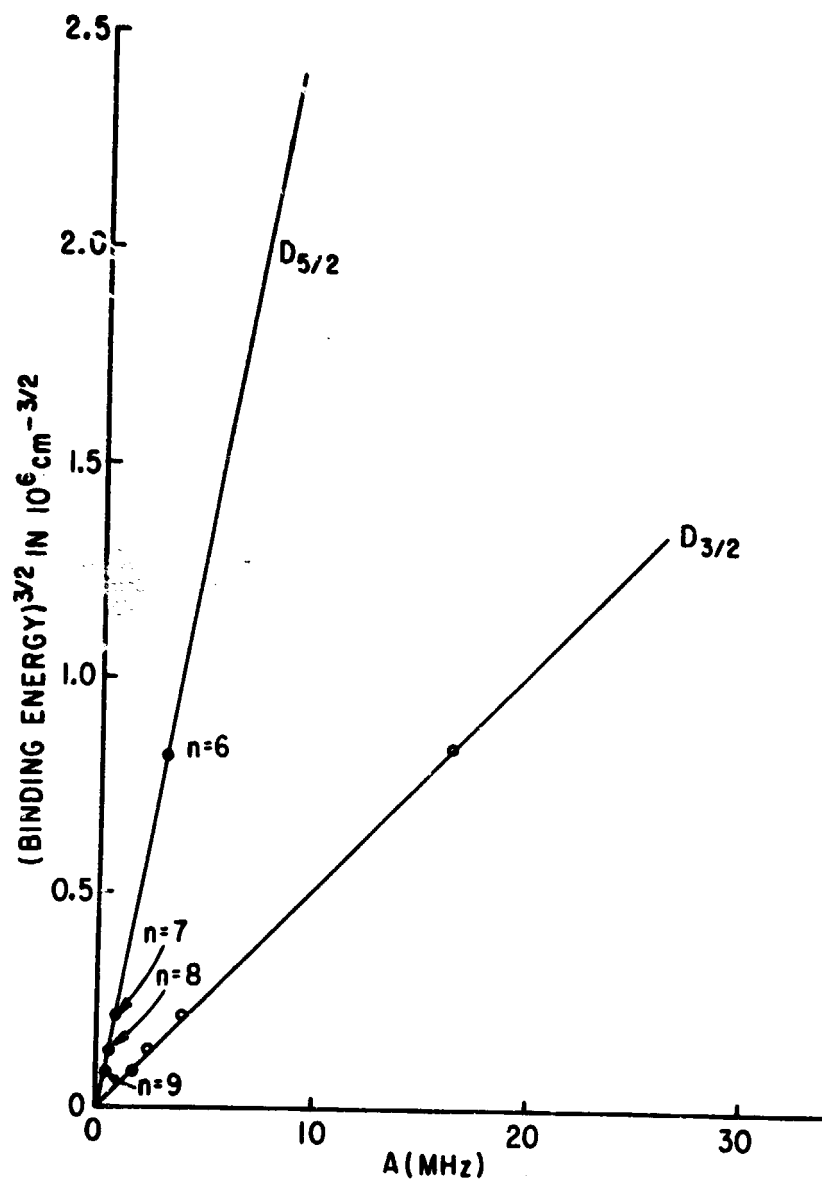signals can be used to determine the sign of the A values of the P and
S states.

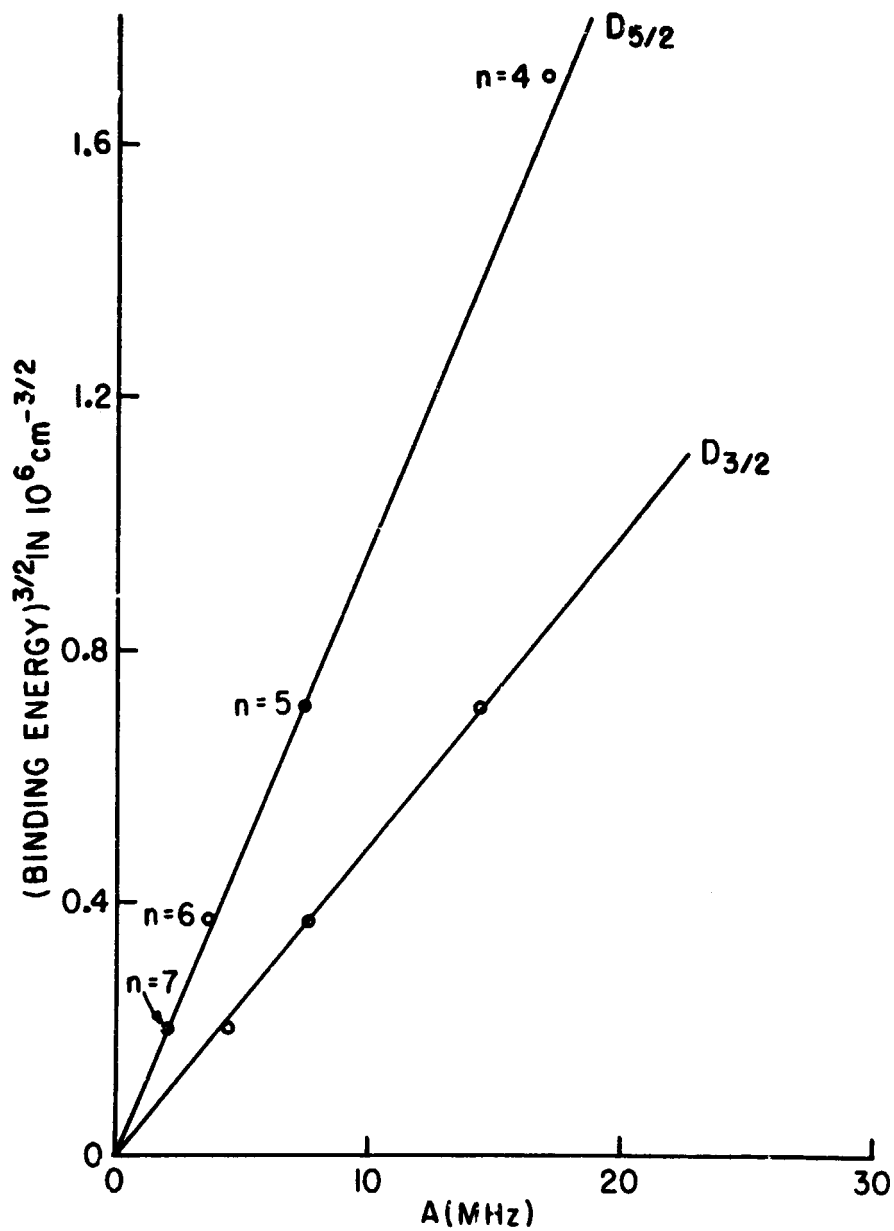Fig. 16.   Plot of measured A values of cesium D states vs
(binding energy)$^{3/2}$.

26

Fig. 17.   Plot of measured A values of Rb^{87} D states vs (binding energy)$^{3/2}$.

27

TABLE III. Recently measured D state hyperfine structure constants.[a]

Atom	State	A		
Rb^{87}	$4\,D_{5/2}$	(-)	16.9	(6)
	$6\,D_{3/2}$	(?)	7.72	(20)
	$6\,D_{5/2}$	(?)	3.6	(7)
	$7\,D_{3/2}$	(?)	4.52	(3)
	$7\,D_{5/2}$	(?)	2.2	(5)
	$8\,D_{3/2}$	(?)	2.85	(3)
	$8\,D_{5/2}$	(?)	1.2	(2)
	$8\,^2D_{3/2}$	(?)	3.98	(12)
	$8\,^2D_{5/2}$	(?)	0.9	(4)
	$9\,^2D_{3/2}$	(?)	2.37	(3)
	$9\,D_{5/2}$	(?)	0.3	(2)
	$10\,D_{3/2}$	(?)	1.52	(3)
	$10\,D_{5/2}$	(?)	0.4	(2)

(a) L. Lam (private communication); S. Svanberg, Proceedings, Laser Spectroscopy Conference, Vail, Colorado, 1973.

will have different amplitudes. If we sweep the rf frequency while keeping the magnetic field fixed, we get a resonance pattern as shown in Fig. 15. The relative amplitude determines the sign of the hfs constant. In the case of cascade excitation, since the nuclear polarization is not changed at all by spontaneous decay at high field, the nuclear polarization will be the same throughout the cascade process. Thus we can determine the sign of the hfs constant of the D state by this method. The whole process is illustrated in Fig. 15. The experimental results of double-resonance experiments with narrow band excitation are shown in Figs. 5 and 10. The sign of the hfs constants determined by this method is consistent with that given by the method of cascade decoupling, discussed previously, and no complicated computer calculation is needed in this method.

We have compared our results with some of the recently measured hfs of other excited D states of rubidium and cesium. A compilation of these results is shown in Table III. A plot of the measured value of A versus the ionization energy, $\mathcal{E}_n$, raised to the 3/2 power, is given in Figs. 16 and 17. The number n is the principal quantum number. Note that the sign of the hyperfine constants of the first, third, and higher D states are not fully determined. The fact that all the points lie in a straight line might indicate that all the $D_{5/2}$ hyperfine states are inverted and all the $D_{3/2}$ states are normal. The hyperfine structures of the excited D states of Rb and Cs depend on n only through the simple $(\mathcal{E}_n)^{3/2}$ relation, contrasting with the fine structures that do not scale according to this function. This completes our investigation of the hyperfine structure of the second excited $D_{5/2}$ and $D_{3/2}$ states of Rb and Cs.
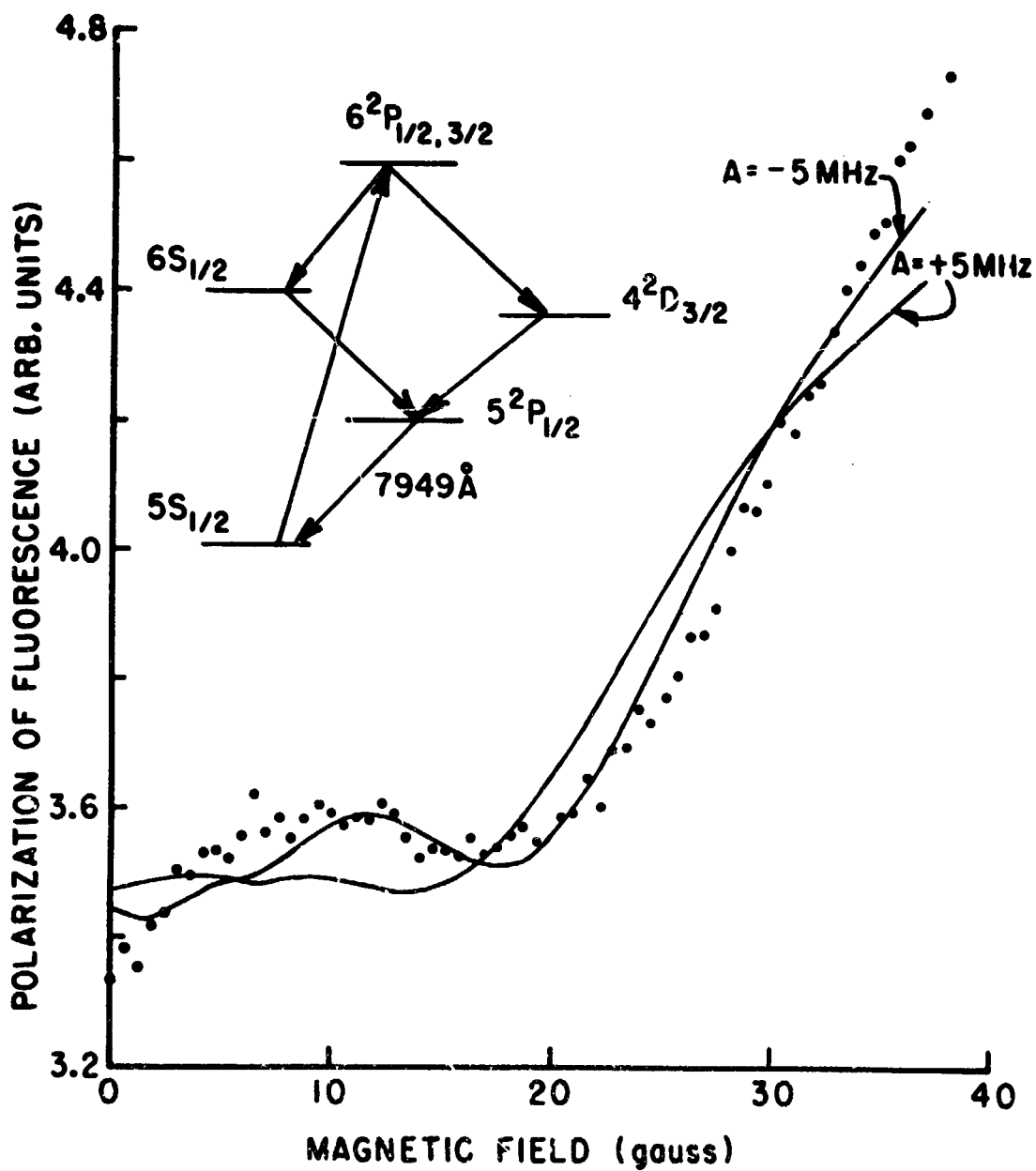
(1) CRL Progress Report, June 30, 1973, p. 10.

Fig. 18. Rb[85] cascade decoupling curve compared with fitted theoretical curves for $A(4^2D_{5/2})$ = +5 MHz and -5 MHz. The cascade scheme is shown in the upper right corner.

D. HYPERFINE STRUCTURE OF THE FIRST EXCITED S AND D STATES OF ALKALI ATOMS*

(R. Gupta, W. Happer, L. Lam)

We have already measured and reported the absolute magnitude of the magnetic dipole hfs constants for the $4\,^2D_{5/2}$ states of Rb.[1] We have determined the sign by measuring the change in the polarization of the fluorescence as the atoms decouple under increasing magnetic field. The data are shown with the theoretical curves in Fig. 18. Agreement between the experimental and theoretical curves is not good, although the curve for a negative value has the same general structure as the experimental curve. The discrepancy may result from inaccuracy in the theoretical branching ratios and imperfection of the circular polarizers and analyzers. We independently measured the relative rf-resonance signal amplitudes with nonwhite excitation (see Part C of this Section). Results for Rb^{85} and Rb^{87} are shown in Figs. 19 and 20, respectively. The change in the relative amplitude of the rf resonances is prominent for Rb^{85} and is clearly in opposite directions for the $4\,^2D_{5/2}$ and $6\,^2P_{3/2}$ states. Since the hfs of the $6\,^2P_{3/2}$ state is known to be normal, this suggests that the hfs of the $4\,^2D_{5/2}$ is inverted.

We have also performed cascade rf spectroscopy on the $4\,^2D_{3/2}$ states of Rb^{85} and Rb^{87}; the results are shown in Fig. 21. The $4\,^2D_{3/2}$ resonances are not of equal magnitude, and some of the smaller resonances cannot be resolved from the noise because of the recoupling of the electronic (J) and nuclear (I) spins in the fluorescing $5\,^2P_{1/2}$ state.[2] The fact that the $m_I = -I + 1/2$ group of resonances is small indicates that the magnetic dipole hfs constant for the $4\,^2D_{3/2}$ state of Rb is positive. The A values we obtained from the data, +7.3(5) MHz for Rb^{85} and +25.1(6) for Rb^{87}, are significantly smaller than those extrapolated from the higher-lying $^2D_{3/2}$ state. Values for the coupling constants of both $4\,^2D$ states are given in Table IV. The hfs measurements of the first excited S states of K, Rb, and Cs have been completed, and results are discussed in Part A of this
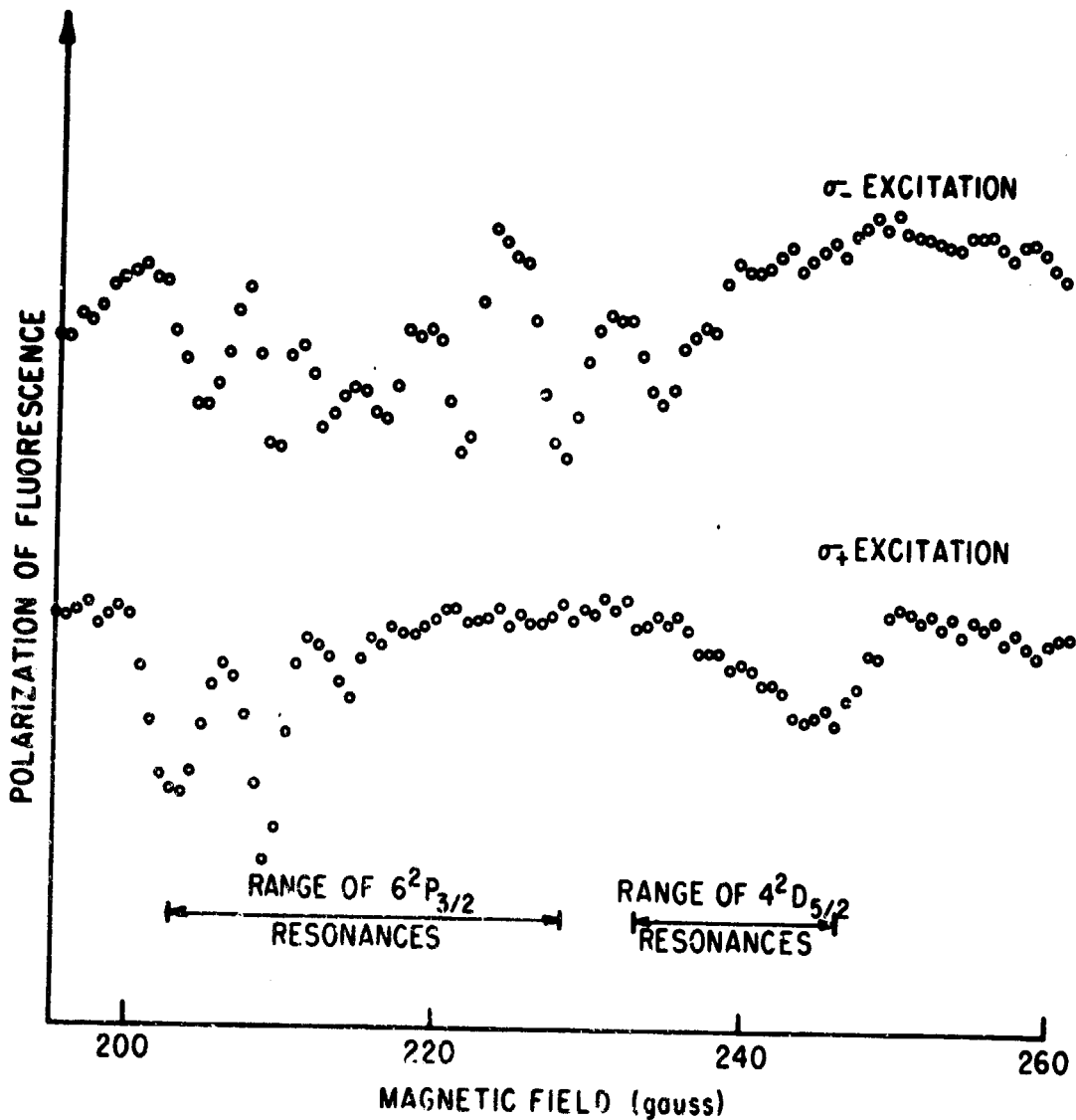
Fig. 19. The $6^2P_{3/2}$ and $4^2D_{5/2}$ rf resonances with an Rb^{85} cell excited by an Rb^{87} lamp. The $4^2D_{5/2}$ resonances are not resolved here. The relative amplitudes of the $P_{3/2}$ and $D_{5/2}$ resonances change in opposite directions as excitation changes from σ_+ to σ_-.

32
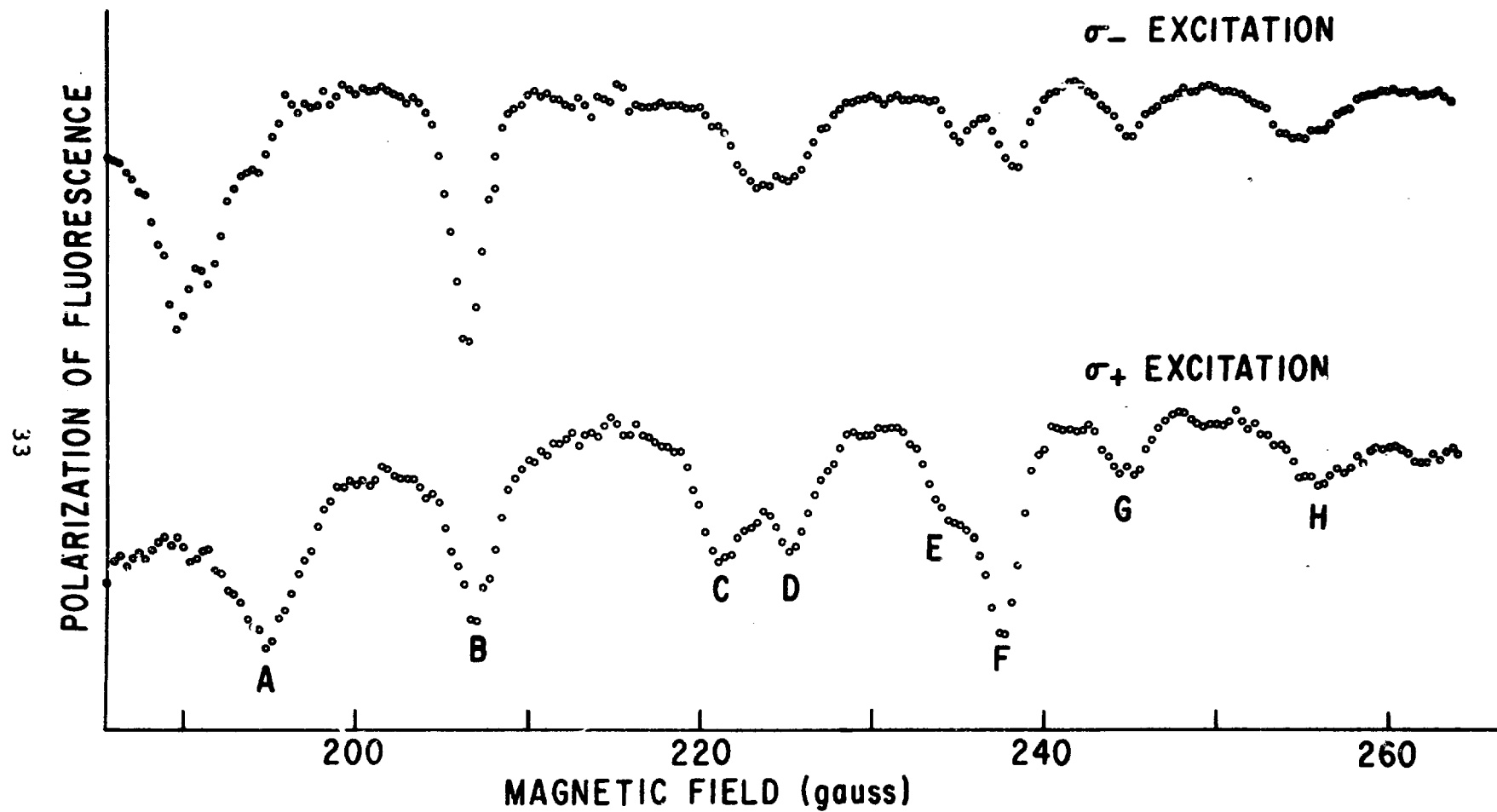
Fig. 20.   The $6\,^2P_{3/2}$ (A, B, C, F) and $4\,^2D_{5/2}$ (D, E, G, H) rf resonances with an Rb[87] cell excited by an Rb[85] lamp.
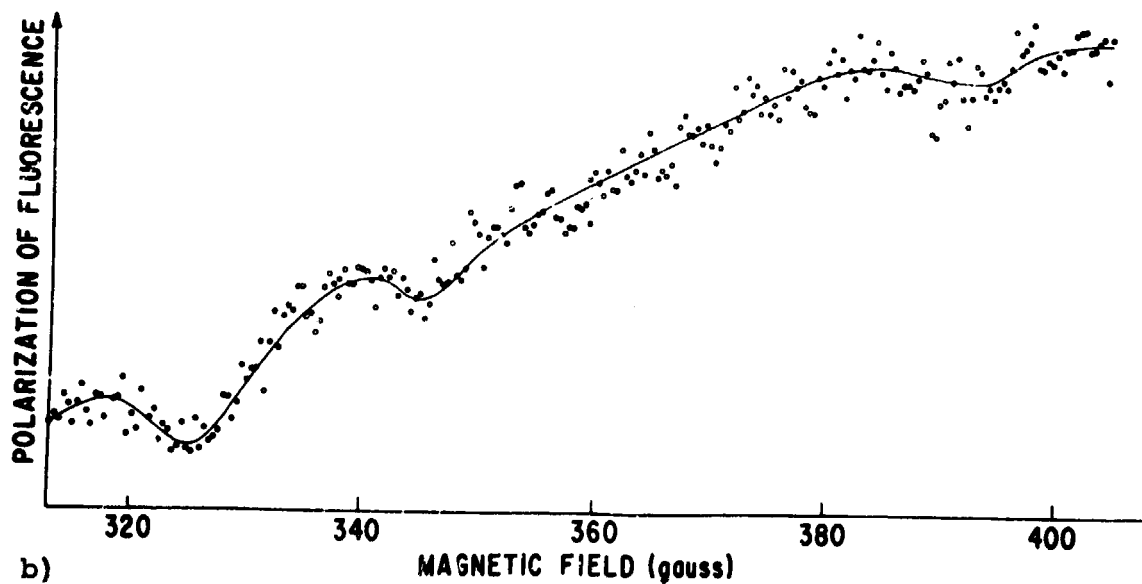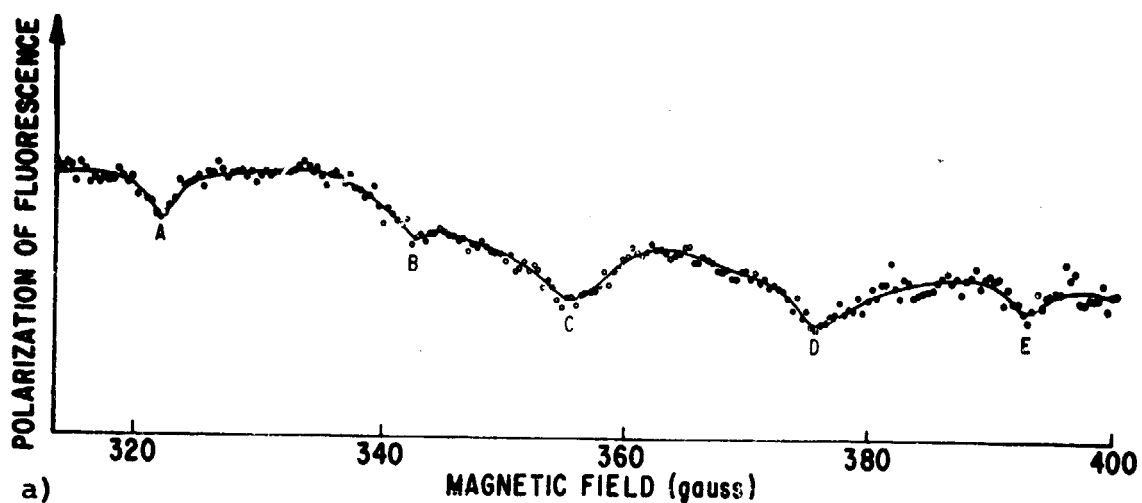
Fig. 21.   a)   The $4^2D_{3/2}$ rf resonances of Rb^{85} shown with
three $6^2P_{1/2}$ resonances, A, C, and E.   Point C
overlaps with some of the $6^2P_{1/2}$ resonances, while
B and D are identified $4^2D_{3/2}$ resonances.
b) Rb^{87} $4^2D_{3/2}$ rf resonances.

34

TABLE IV. Magnetic dipole hyperfine coupling constants of
the 4^2D states of rubidium.

	Rb^{85}	Rb^{87}
$4^2D_{3/2}$	+7.3(5) MHz	+25.1(6) MHz
$4^2D_{5/2}$	−5.2(3) MHz	−16.9(6) MHz

Section.

Program for the next interval: We will measure the hfs of the $5^2D_{3/2}$ and $5^2D_{5/2}$ states of cesium.

(1) CRL Progress Report, June 30, 1973, p. 21.

(2) R. Gupta, W. Happer, L. Lam, and S. Svanberg, Phys. Rev. A 8, 2792 (1973).

E.   CASCADE LEVEL ANTICROSSING SIGNALS*

(R. Gupta, W. Happer, K. Liao)

We have developed a cascade level anticrossing technique which can be used to measure the fine structures and to determine the complete hyperfine Hamiltonians of the states of atoms. In this method, two fine structure sublevels of an atom are excited at different rates by cascading from a higher state. In the absence of hyperfine structure, the fine structure levels can be made to "cross" by tuning them to the same energy with an external magnetic field. However, if hyperfine structure is present, each fine structure sublevel is split into (2I + 1) hyperfine sublevels (I is the nuclear spin), and those sublevels which have the same total magnetic quantum number $m_F = m_J + m_I$ may be prevented from crossing by the hyperfine interactions. Instead of crossing, the levels repel one another, and the wavefunctions of the two substates interchange their identities as the magnetic field strength is swept through the region of closest approach. This state mixing will equalize the population differences between these two particular sublevels. During one more cascading process, the dipole selection rules allow us to monitor the fluorescence which comes only from one of the two sublevels involved. Any changes in the detected fluorescence can be used to deduce the information about fine and hyperfine structures of the state. The 4D state of the rubidium alkali atom, due to its anomalously small fine structure splitting, serves as a good example to demonstrate our new

36

method.

Figure 22 shows the energy-level scheme of the relevant states of the rubidium atom and the Zeeman splittings of the fine structure levels of 4^2D state in a magnetic field. The Rb^{85} (or Rb^{87}) atoms in the $5S_{1/2}$ ground states are excited to 6P states by the σ-polarized light of the second resonance lines of Rb^{87} atoms in a microwave lamp. In the high field region where the nuclear-spin angular momentum, I, and the electronic-spin angular momentum, J, are decoupled, the magnetic sublevels of the 6P state that have higher m_J values are more strongly populated than those of lower m_J values. This follows from considerations of the lamp profile and the atomic absorption profile, and also from the selection rules for excitation by σ-polarized light. After spontaneous decay, the major part of this population imbalance is carried over to the 4D state. Now, application of an external magnetic field at about 3800 gauss will cause crossing of the $J = 3/2$, $m_J = 1/2$ and $J = 5/2$, $m_J = 5/2$ fine structure levels of the 4D term. Figure 23 shows the eight hyperfine structure levels of Rb^{87} that are involved in this crossing. The static perturbation which couples the levels and causes them to "anticross" is provided in this case by the electric quadrupole interaction between the nucleus and the electrons. Coupling occurs between pairs of levels having the same value of $m_F = m_J + m_I$, but different values of m_I. This coupling mixes the wavefunctions of the hyperfine sublevels and equalizes the population imbalance between them.

Because the fine structure sublevel with $m_J = 5/2$ of the $^2D_{5/2}$ state remains a pure $^2D_{5/2}$ state in high magnetic fields, atoms in this sublevel cannot decay to a $^2P_{1/2}$ state because of the dipole selection rule $\Delta m_J = 0, \pm 1$. However, in the neighborhood of 3800 gauss, the electric quadrupole interaction can cause the electrons to jump from the state with $m_J = 1/2$ while the magnetic quantum number of the nucleus changes from m_I to $(m_I + 2)$ to conserve angular momentum. Since the initial and final levels are "crossed," no energy has to be supplied and the static quadrupole interaction is adequate to cause the transition, provided that the quadrupole interaction energy is greater than the natural width, $\hbar/\tau$, of the crossing

37
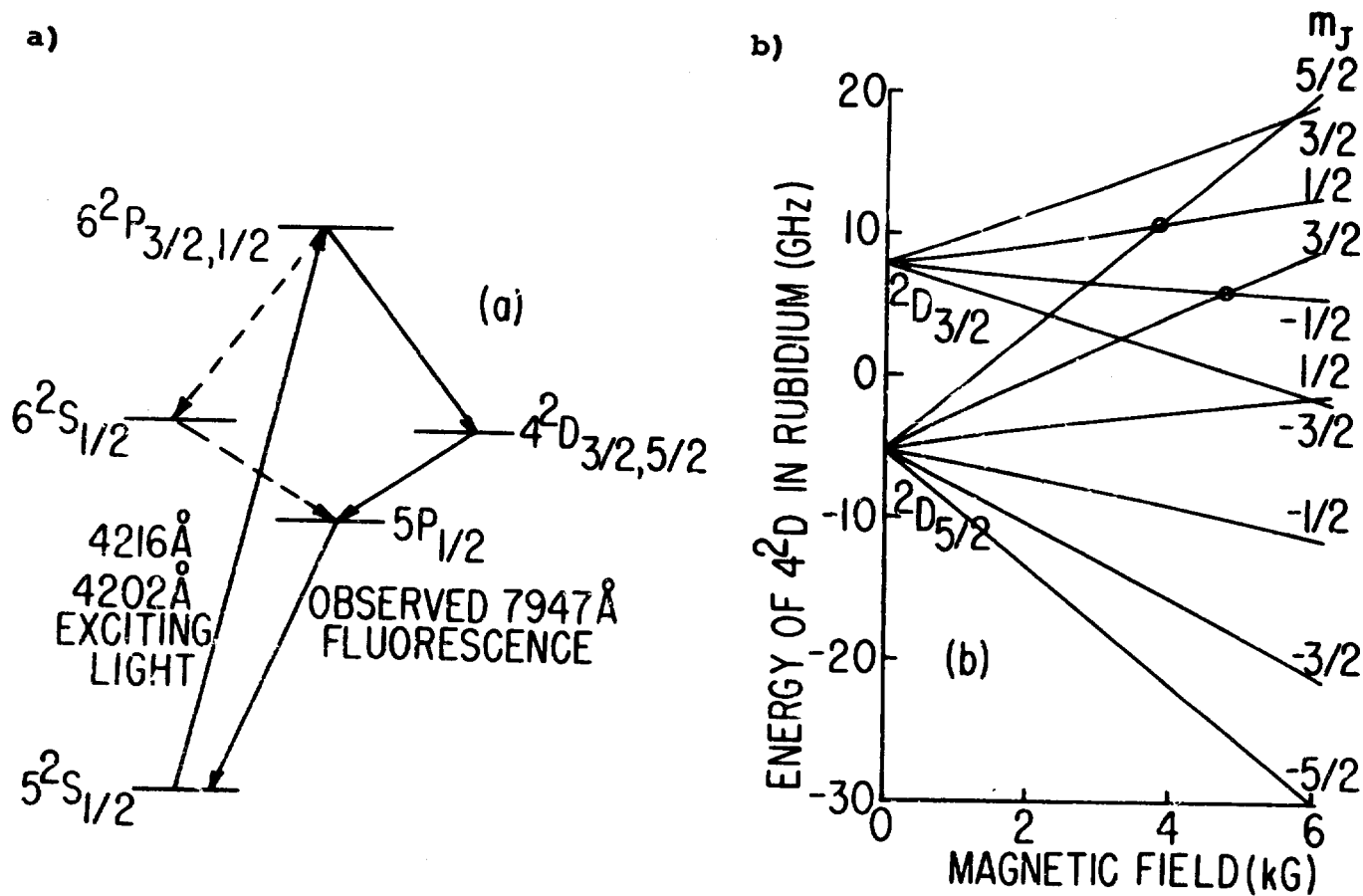
Fig. 22. a) The energy-level scheme of the relevant states in this work;
b) Zeeman splittings of the fine structure levels in the 4^2D state of
Rb in a magnetic field.

(m_F, m_I)
$(+1, -3/2)$
$(+2, -1/2)$
$(+3, 1/2)$
$(+4, 3/2)$
$(-1, -3/2)$
$(0, -1/2)$
$(+1, 1/2)$
$(+2, 3/2)$

$m_J = 5/2$

$m_J = 1/2$

(m_F, m_I)
$(-1, -3/2)$
$(0, -1/2)$
$(+1, 1/2)$
$(+2, 3/2)$

$(+1, -3/2)$
$(+2,$
$(+3,$
$(+4,$

$I = 3/2$

Fig. 23.   The hyperfine levels involved at the 3800-G crossing in the 4^2D state of Rb[87].   Circles indicate the positions of the anticrossings.

Fig. 24. Typical anticrossing signal recordings with σ exciting light. (Rb[87] resonance line has been used in both cases.) The magnitude of the anticrossing signals depends, among other things, on the polarization and the line profile of the exciting light.

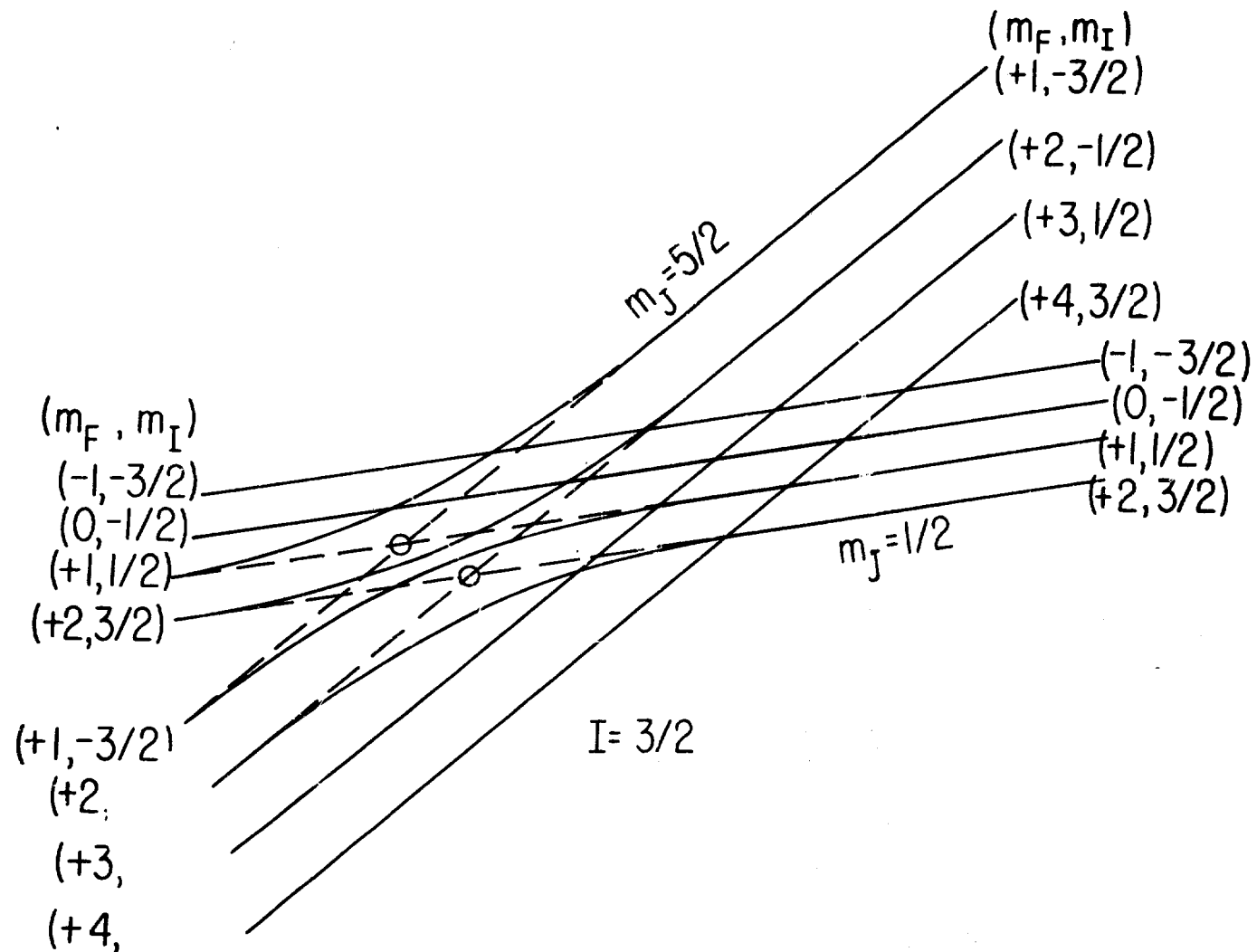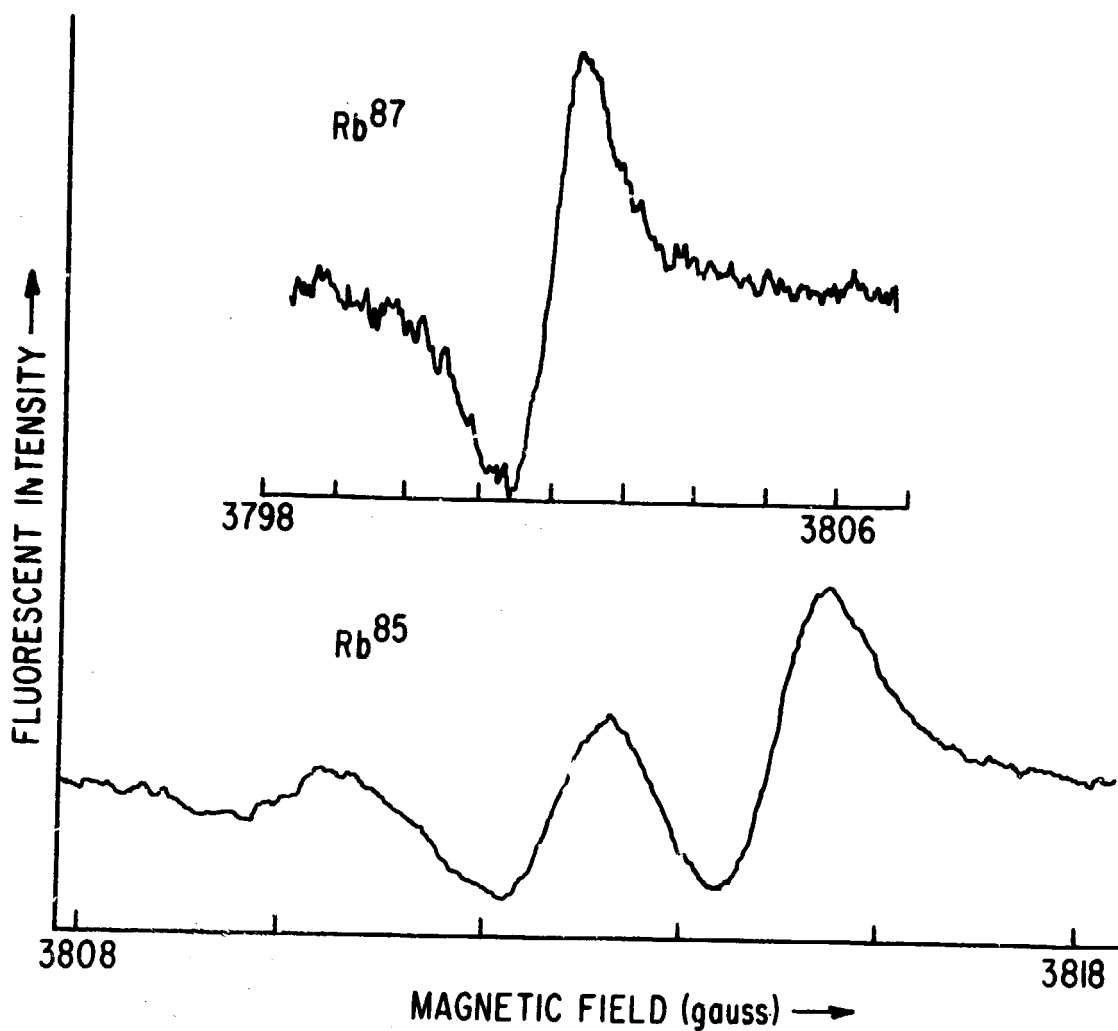levels (τ is the radiative lifetime of the 4D state atoms). When an atom has jumped from the $m_J = 5/2$ to the $m_J = 1/2$ sublevel, it is free to decay to the lower $P_{1/2}$ state, and the anticrossing should therefore be detectable as an increase in the fluorescence from the $5P_{1/2}$ state. In the case of Rb^{85} there are four such anticrossings corresponding to the $\Delta m_J = 2$ crossing between the $m_J = 5/2$ and $m_J = 1/2$ fine structure levels of the 4^2D state. In Rb^{87} there are only two anticrossings in the same region. Because the cascading steps wash out the transverse coherence of the excited atom, no level-crossing signals will be present to distort the anticrossing signals.

We modulate the magnetic field as the main field sweeps through the interesting region. A phase-sensitive lock-in technique is used in the detection process to suppress the background noise. We also use an nmr gaussmeter to measure the field very accurately.

Our preliminary experimental data for Rb^{85} and Rb^{87} are shown in Fig. 24. Some expected resonances are small, mainly because the overlapping of the profiles between the exciting light and the absorption spectrum of the atoms is rather poor. Since the lamp is located in a fringing field of less than a few gauss, while the atoms are sitting in the very high applied field, some exciting transitions may be only partially induced by the spectral distribution of our lamp. The data were taken with a sufficiently short time constant in the detector circuit and with a slow sweep rate of the magnetic field to avoid significant broadening from these sources. The modulation broadening has also been eliminated.[1] We deduce our electric quadrupole interaction from the distance from peak to peak of the modulated signal and the lifetime[2] of the 4D state of the rubidium atom. Our preliminary results are:

Hyperfine electric quadrupole interaction

$$B_\ell(Rb^{85}) = 6(3) \text{ MHz;}$$

$$B_\ell(Rb^{87}) = 3(2) \text{ MHz;}$$

Fine structure splitting = 13360(5) MHz.

41

We may obviously extend this method to measure the fine and hyperfine interactions of other states of alkali atoms. For example, if we apply a two-step excitation technique by using a cw tunable dye-laser to excite D states and then let them cascade down to F, or even G, states, the fine and hyperfine interactions of these states can be measured. Furthermore, if we put the results from these measurements together with the hyperfine interaction measurements from cascade radio-frequency spectroscopy, then for various interaction terms we can deduce core-polarization interactions and $\langle 1/r^3 \rangle$, values that are of particular interest in understanding atomic structures.

Program for the next interval: We will continue to make further measurements on this crossing and some other crossings at higher field region.

(1) H. Wahlquist, J. Chem. Phys. 35, 1708 (1961).

(2) O. S. Heavens, J. Opt. Soc. Am. 51, 1058 (1961).

F. TUNABLE DYE-LASER SPECTROSCOPY OF HIGHLY EXCITED STATES IN ALKALI ATOMS: I. D STATES*

(R. Gupta, W. Happer, P. Tsekeris)

We have continued the measurement of the hyperfine interaction constants (magnetic dipole and electric quadrupole constants) of the highly excited ^{2}D states in Rb^{87} and Cs^{133} by the two-step excitation method. In the first step of this process we excited the alkali atoms from the ground $^2S_{1/2}$ state to the first excited ^{2}P state, using the D_1 or D_2 resonance line from a powerful rf-discharge lamp; in the second step we excite the atoms from the ^{2}P state to the appropriate ^{2}D states using light from a tunable dye laser. We observe the polarization of the light which is emitted when atoms in the ^{2}D states decay to lower states; and, making use of the level-crossing and optical double-resonance methods, we measure the hyperfine interaction constants.

TABLE V. Experimentally determined values for the hyperfine interaction constants of the highly excited ^{2}D states of Rb^{87} and Cs^{133}.

Element	State	a (absolute value) (MHz)	b (absolute value) (MHz)
Rb^{87}	$6\,^2D_{3/2}$	7.84(5)	0.53(6)
	$7\,^2D_{3/2}$	4.53(3)	0.26(4)
	$7\,^2D_{5/2}$	2.2 (5)	
Cs^{133}	$9\,^2D_{3/2}$	2.73(3)	
	$10\,^2D_{3/2}$	1.52(3)	

We have repeated the measurements for the 6 and $7\,^2D_{3/2}$ states of Rb^{87} and the $9\,^2D_{3/2}$ of Cs^{133}, and we have also measured the $10\,^2D_{3/2}$ state of Cs^{133}. We have increased the precision of the measured hyperfine constants as shown in Table V.

The above experimental methods give us the absolute value of the hyperfine structure coupling constants. It is interesting to determine the algebraic sign of these constants, especially since experiments in the low-lying $^2D_{5/2}$ states give inverted signs.[1] We have therefore performed magnetic decoupling experiments to determine these signs. In the second step of the excitation process we use σ_+ or σ_- laser light. As the ^2D state decays to a lower ^2P state and finally to the ground ^2S state, we observe the polarization of the emitted light in this final step as a function of the magnetic field. The shape of the decoupling curve depends on the sign of the coupling constants. The experimental data are compared with computer-calculated curves, but unfortunately the shape of these curves depends critically on the spectral profile of the exciting laser light. Because of our lack of knowledge of the precise mode structure of the laser light, we have not yet succeeded in determining the signs of the magnetic dipole coupling constants. However, we have recently acquired a spectrum analyzer, which should now enable us to successfully apply the decoupling method.

We have also tried to find the signs of these coupling constants in Rb^{87} by exciting the atoms first with σ_+ or σ_- light from an Rb^{85} rf lamp and then with π-laser light to the $^2D_{3/2,5/2}$ states. We predict that this arrangement can create nuclear polarization in the ^2D states which would lead to asymmetry in the optical double-resonance signal. However, we have failed to see a definite indication of this asymmetry. We suspect that collisions and radiation trapping in the first ^2P state destroy its polarization.

(1) R. Gupta, S. Chang, C. Tai, and W. Happer, Phys. Rev. Letters 29, 655 (1972).

G. TUNABLE DYE-LASER SPECTROSCCPY OF HIGHLY EXCITED STATES IN ALKALI
    ATOMS: II. S STATES*
    (R. Gupta, W. Happer, P. Tsekeris)

Extensive measurements of the hyperfine structure of the excited
S states of alkali atoms, which have recently been carried out in
this Laboratory, have revealed some very interesting properties of
these states (see Part A of this Section). It is therefore desirable
to extend these measurements to the highly excited S states. The
measurements described in Part A, performed by the method of cascade
radio-frequency spectroscopy, have been confined to the first two or
three excited states. It is difficult to achieve significant popula-
tion of the highly excited S states by the method of cascade excita-
tion, since the oscillator strengths for highly excited P states are
very low. We have, therefore, used a two-step excitation method
(similar to the one used for D states described in Part F) to popu-
late the highly excited S states. Cesium atoms are excited to their
first excited P state $(6^2P_{3/2,1/2})$ by resonance light from an rf lamp.
Atoms in the $6^2P_{3/2}$ are excited to the $11^2S_{1/2}$ state by dye-laser
radiation of the 5746-Å fluorescent light. Our typical data are shown
in Fig. 25. We obtain, for the magnetic dipole coupling constant, a
value of A $(11^2S_{1/2}, Cs^{133}) = 39.4(2)$ MHz.

    Program for the next interval: We will extend these measure-
ments to other highly excited S states in Cs and Rb.

    *This research was also supported by the Air Force Office of
Scientific Research under Grant AFOSR-72-2180.

H. TUNABLE DYE-LASER SPECTROSCOPY OF HIGHLY EXCITED STATES IN
    ALKALI ATOMS: III. F STATES*
    (J. Farley, W. Happer)

Recent work at the Columbia Radiation Laboratory has resulted in
the development of the stepwise excitation method. We excite alkali
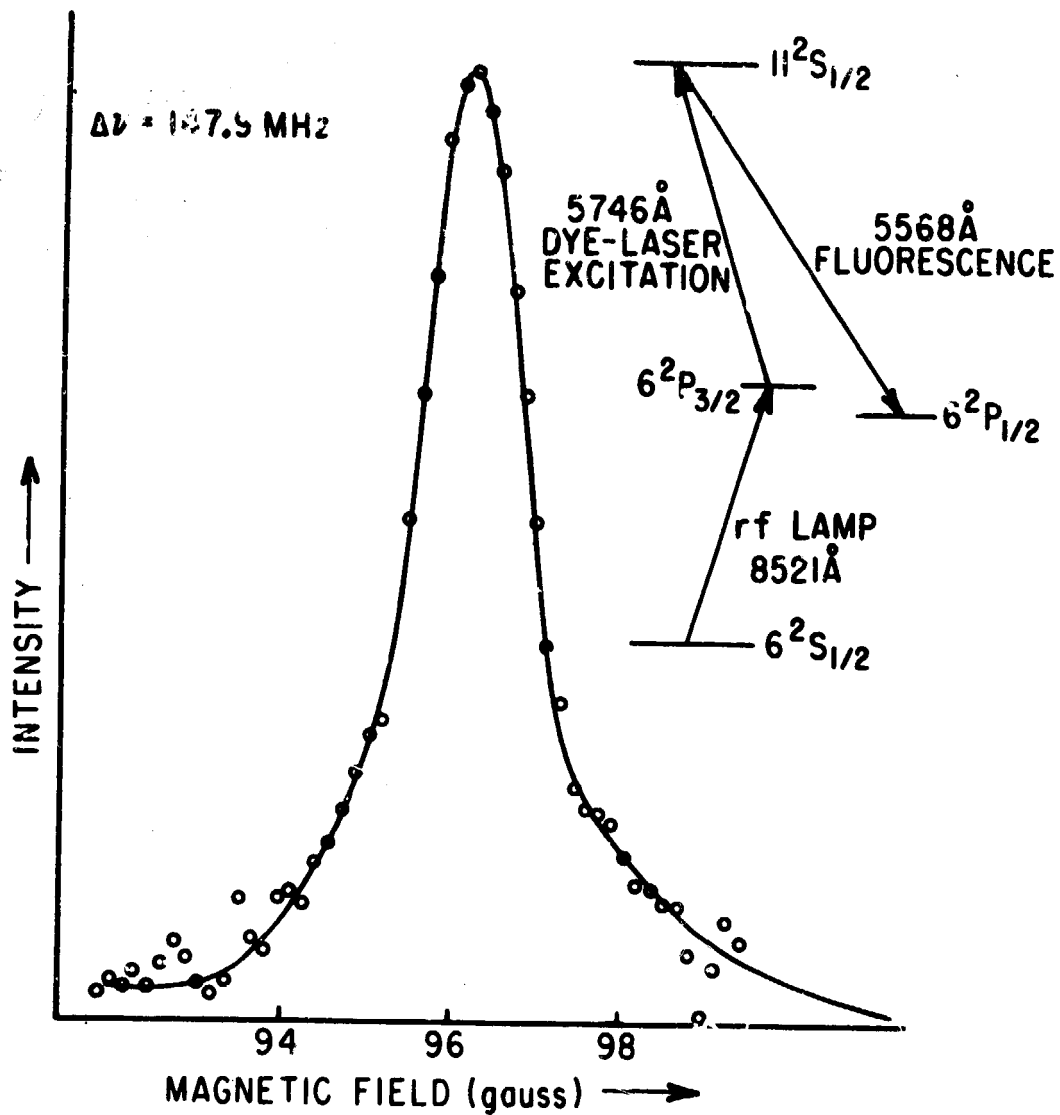atoms to P states with a conventional rf lamp, then to a D state with

Fig. 25. Radio-frequency resonance due to transitions
between F = 4, m_F = -4 ↔ m_F = -3 sublevels of
the $11^2S_{1/2}$ state of Cs^{133}. The transition
frequency is $\Delta\nu$ = 147.9 MHz.

a tunable dye laser. In our work, the D state decays to an F state, and we observe the subsequent fluorescence (see Fig. 26).

Using optical double resonance (ODR) spectroscopy, we obtained rough upper limits of the absolute value of the magnetic dipole coupling constant, a, for the $5F_{7/2}$ and $5F_{5/2}$ states of Cs^{133}. By using a least-squares fit of one set of experimental decoupling data with computer-generated curves, we have obtained a better value for the quantity a of the $6F_{7/2}$ state of Cs^{133}:

$$a = 0.05 \, {}^{+\, 0.17}_{-\, 0.12} \, \text{MHz}.$$

The fine structure intervals of the Rb 4F, 5F, and 6F states are very poorly known. Since they are listed as -0.01 cm^{-1} with no error given, the uncertainty may be nearly 100%. Moreover, they are inverted and hence of special interest.

In the investigation of the Rb 5F state with ODR, 7950-Å light from the $5S_{1/2} \to 5P_{1/2}$ line of the rf lamp excites Rb atoms in the sample to the $5P_{1/2}$ state, after which laser light at 5649 Å excites the atoms to the $7D_{3/2}$ state. After a spontaneous unobserved decay to the $5F_{5/2}$, and then to the $5D_{3/2}$, level, the observed decay back to the $5P_{1/2}$ state occurs at 7621 Å.

The direction of polarization of the laser light lies parallel to the magnetic field. Hence only $\Delta m = 0$ transitions are possible. Consequently, the F sublevels with high $|m_J|$ values are less populated than if the populations were statistical. When we apply an rf magnetic field to equalize the populations of a pair of sublevels, the fluorescent light has a more isotropic distribution. Our phototube, situated directly along the magnetic field from the sample, does not register π fluorescence. Hence we see an increase in fluorescent intensity at resonance.

We can calculate the theoretical position of the resonances for a given fine structure interval using the Breit-Rabi formula. From the observed positions of the resonances we deduce the fine structure interval. Similar considerations apply to the 4F fine structure.
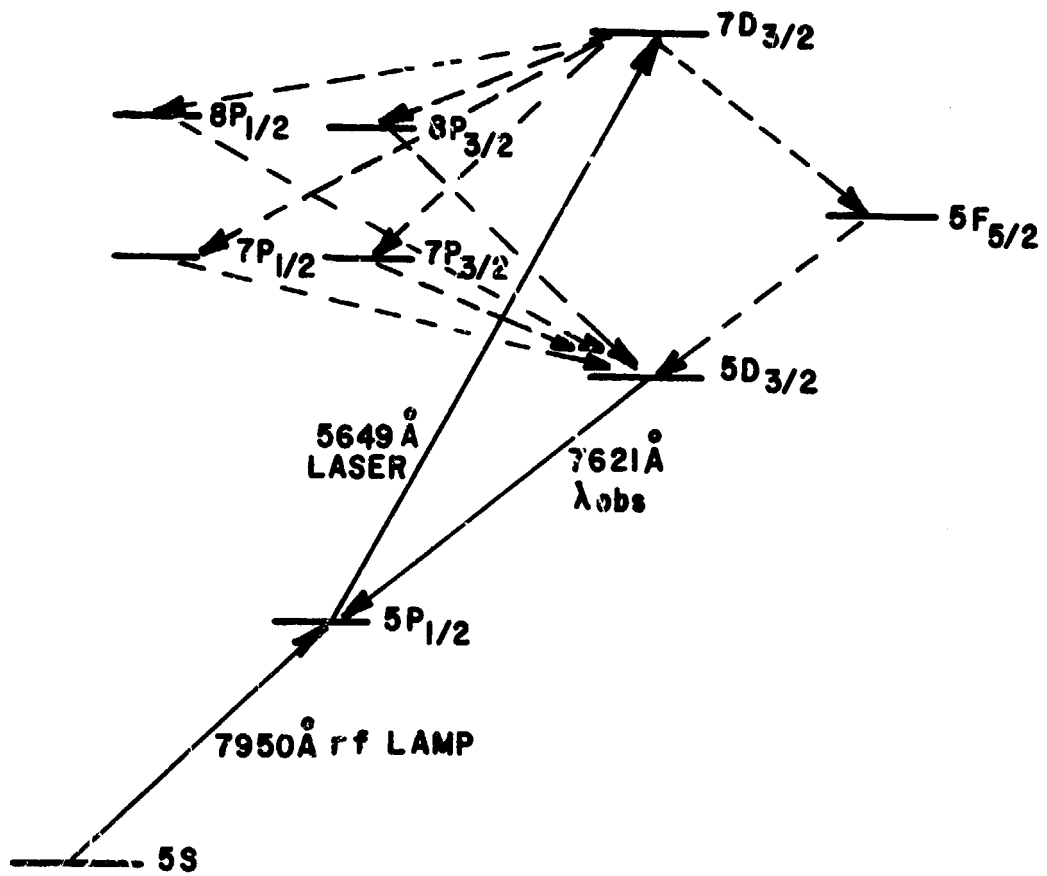
47

Fig. 26. Level diagram of the relevant states.

48

When new dyes or new solvents for the old dye are able to extend the wavelength range of the laser, we will study the 6F state of Rb.

Another program will utilize the fact that the $5D_{3/2}$ and $5D_{5/2}$ states of Cs^{133} are very long-lived (calculated lifetime of 960 nsec for the $5D_{3/2}$ state and 1400 nsec for the $5D_{5/2}$ state). Since atoms can decay into the 5D from the 5P states we can then use the 5D states as platforms for reaching highly excited F states with laser excitation. Since we would be exciting the F states directly (instead of using cascade excitation), we could perform level-crossing as well as ODR and decoupling experiments. The only problem is that we would detect almost the same wavelength (to within 50 Å) as the laser light. Normally this would mean that the laser background swamps the fluorescent signal, but we might overcome this if we increased the population of the 5D state by using lamps with elliptical reflectors, which have proven successful in other experiments.

I. HYPERFINE STRUCTURE OF THE 3^3S_1 STATE OF HE^3*
(W. Happer, A. Tam, H. Tang)

Because of changes in personnel, we have postponed work on this project.

J. STEPWISE EXCITATION AND LEVEL-CROSSING SPECTROSCOPY OF THE TRIPLET D STATE FINE STRUCTURE OF HE^4*
(W. Happer, A. Tam)

Fine and hyperfine structures of helium are of fundamental interest, as helium is the only multielectron system that can be treated theoretically with high precision, and accurate experimental
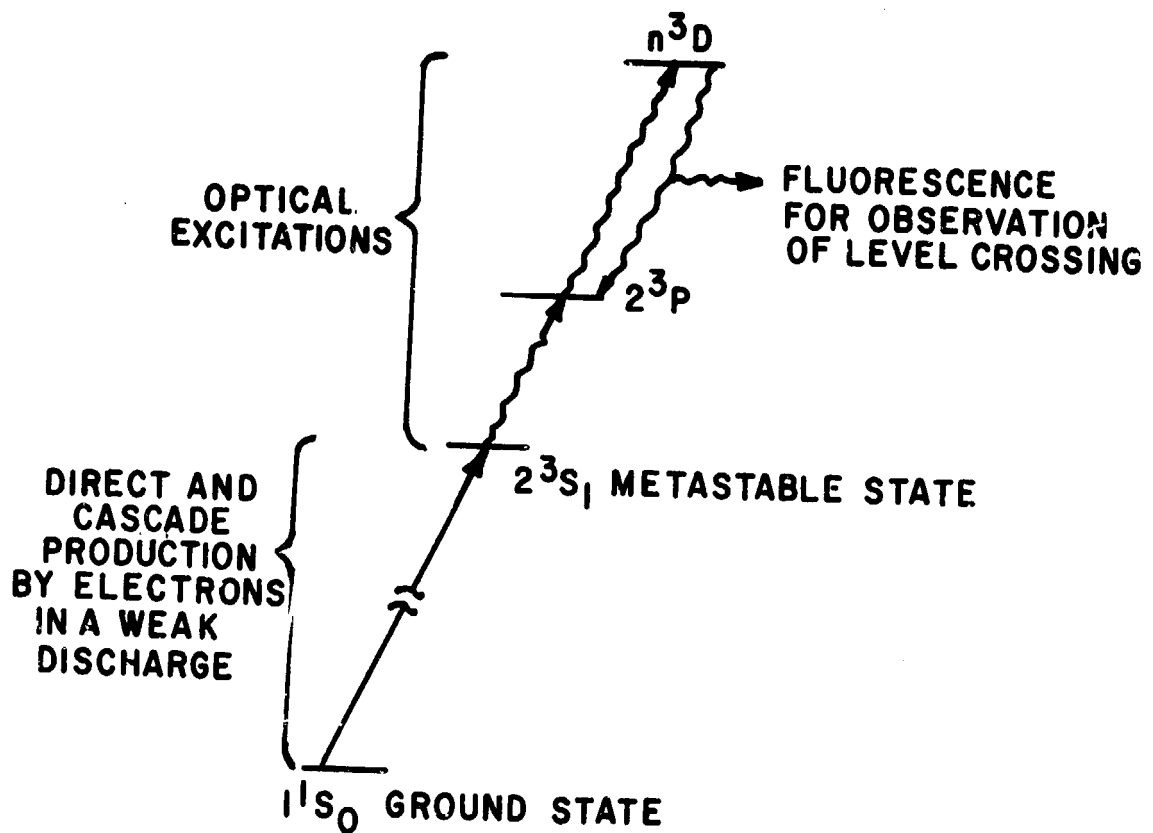
49

Fig. 27. Stepwise excitation scheme.

determination of the structures is needed to assess a theoretical calculation. This comparison is nontrivial, as different calculations using different wavefunctions and different approximations may predict very different structures or other properties of the excited states of helium. As an example, the existence of a large degree of singlet-triplet mixing in F states of helium has been established qualitatively by several electron-excitation experiments,[1] and various recent calculations[2,3] handling this problem predict vastly different degrees of singlet-triplet mixing and fine structures in the D, F, G,...states of He^4. (The S states are nonmixed, and the P states are essentially so.) Checking with experimentally determined fine structures in the ^3D states of He^4 would help us to evaluate the reliability of each calculation. Of course, experimental determinations of the fine structures in the F states are more useful for this comparison, but such determinations are difficult to achieve, as resonance lines involving F states are in the far-infrared region. We should note that the understanding of this singlet-triplet mixing in helium is essential to evaluate quantitively much applied research; e.g. studies of populations in a helium or helium-mixture plasma and their laser applications.

Some experimental studies on the ^3D state fine structures of He^4 have previously been done by optical spectroscopy,[4] electron-bombardment level-crossing spectroscopy,[5] ion-bombardment level-crossing spectroscopy,[6] and beam-foil quantum beats.[7] We have developed a new method to study the ^3D fine structures: use of a two-step optical excitation from the metastable 2^3S state and level-crossing spectroscopy.[8] This method is capable of achieving higher accuracy than all the other methods mentioned above and is less sensitive to systematic errors than the electron-bombardment method, as electron trajectories are seriously affected by the magnetic field applied for level crossing. The stepwise excitation is represented schematically in Fig. 27. We have obtained preliminary results for the fine structures of the 3^3D and 4^3D states. These are tabulated in Table VI, and Table VII also gives comparisons with other experiments and theory.

51

TABLE VI. Experimentally determined fine structure intervals of triplet D states of He^4.

	$3^3D_1 - 3^3D_3$	$3^3D_2 - 3^3D_2$	$4^3D_1 - 4^3D_3$	$4^3D_2 - 4^3D_3$
Present work (preliminary)	1400.7 ± 0.5	76 ± 1	590.8 ± 0.5	36 ± 1
Optical spectroscopy[a] (1957)	1448 ± 30	90 ± 24	$5?? \pm 30$	54 ± 30
Electron bombardment[b] (1969		72.5 ± 0.5		35.8 ± 0.4
Ion bombardment[c] (1968)	1399.9 ± 1.1			
Beam-foil quantum beat[d] (1972)	1420 ± 25	71 ± 2	576 ± 30	40 ± 5

(a) J. Brochard, R. Chabbal, H. Chantrel, and P. Jacquinot, J. Phys. Radium 18, 596 (195).

(b) J. P. Descoubes, Physics of the One- and Two-Electron Atom, F. Bopp and H. Kleinpoppen, eds. (North Holland Publishing Company, Amsterdam, 1969), p. 341.

(c) R. D. Kaul, J. Opt. Soc. Am. 58, 429 (1968).

(d) H. G. Berry, J. L. Subtil, and M. Carre, J. Physique 33, 947 (1972).

TABLE VII. Theoretically determined fine structure intervals of triplet D states of He^4.

	$3^3D_1 - 3^3D_3$	$3^3D_2 - 3^3D_3$	$4^3D_1 - 4^3D_3$	$4^3D_2 - 4^3D_3$
Prish and Mires[a] (1972)	1473	126	633	60
Van den Eynde et al.[b,c]	1414	85.8	600	41.8
Moser et al.[c,d] (1964, 1968)	1409	83.8	598	41.1
Bethe and Salpeter[e] (1957)	1390	92.5	587	39.1
Araki[f] (1937)	1353	75	567	28.5

(a)   R M. Parish and R. W. Mires, Phys. kev. A $\underline{4}$, 2145 (1971).

(b)   R. K. Van den Eynde, G. Wiebes, and T. Niemeyer, Physica $\underline{59}$, 401 (1972).

(c)   Fine structure given only implicitly by these workers.

(d)   N. Bessis, H. Lefebvre-Brion, and C. M. Moser, Phys. Rev. $\underline{135A}$, 957 (1964); C. Amboy, N. Bessis, and C. M Moser, Phys. Rev. $\underline{170}$, 131 (1968).

(e)   H. A. Bethe and E. E. Salpeter, Handbuch der Physik (Springer Verlag, Berlin, 1957), p. 88.

(f)   G. Araki, Proc. Phys.-Math Soc., Japan $\underline{19}$, 128 (1937).

We can see from the tables that good agreement between experiment and theory is still lacking. We hope that accurate experimental determinations of the fine structures will stimulate some better theoretical calculations which hopefully would also give us a better understanding of the degree of singlet-triplet mixings in helium.

Further refinement and extension of our triplet D state measurements is underway.

(1) R. B. Kay and R. H. Hughes, Phys. Rev. 154, 61 (1967); R. B. Kay and J. G. Showalter, Phys. Rev. A 3, 1998 (1971).

(2) R. M. Parish and R. W. Mires, Phys. Rev. A 4, 2145 (1971).

(3) R. K. Van den Eynde, G. Wiebes, and T. Niemeyer, Physica 59, 401 (1972).

(4) J. Brochard, R. Chabbal, H. Chantrel, and P. Jacquinot, J. Phys. Radium 18, 596 (1957).

(5) J. P. Descoubes, Physics of the One- and Two-Electron Atom, F. Bopp and H. Kleinpoppen, eds. (North Holland Publishing Company, Amsterdam, 1969), p. 341.

(6) R. D. Kaul, J. Opt. Soc. Am. 58, 429 (1968).

(7) H. G. Berry, J. L. Subtil, and M. Carré, J. Physique 33, 947 (1972).

(8) P. A. Franken, Phys. Rev. 121, 508 (1961).

K. FORBIDDEN TRANSITION RATES IN HELIUM*
   (W. Happer, H. Tang)

Due to changes in personnel this research has been terminated.

L. LIFETIME MEASUREMENTS OF OPTICALLY INACCESSIBLE EXCITED STATES*
   (R. Gupta, W. Happer, C. Tai)

We are continuing our measurements of the lifetimes of the optically inaccessible excited states. Table VIII gives a compilation of
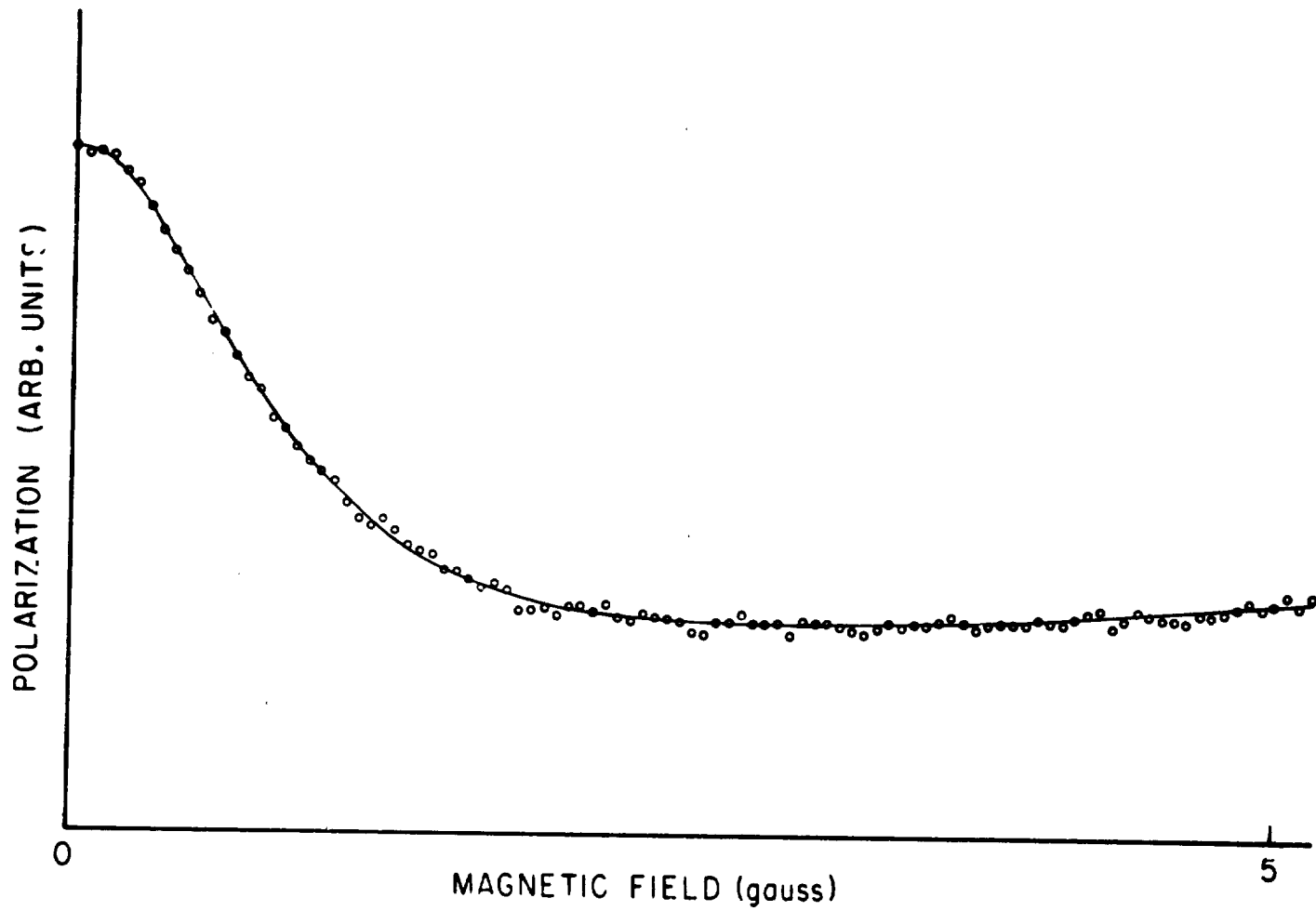
55

Fig. 28. Rb^{87} $5D_{3/2}$ state Hanle-effect data fitted with $\tau(D_{3/2}) = 210$ nsec.
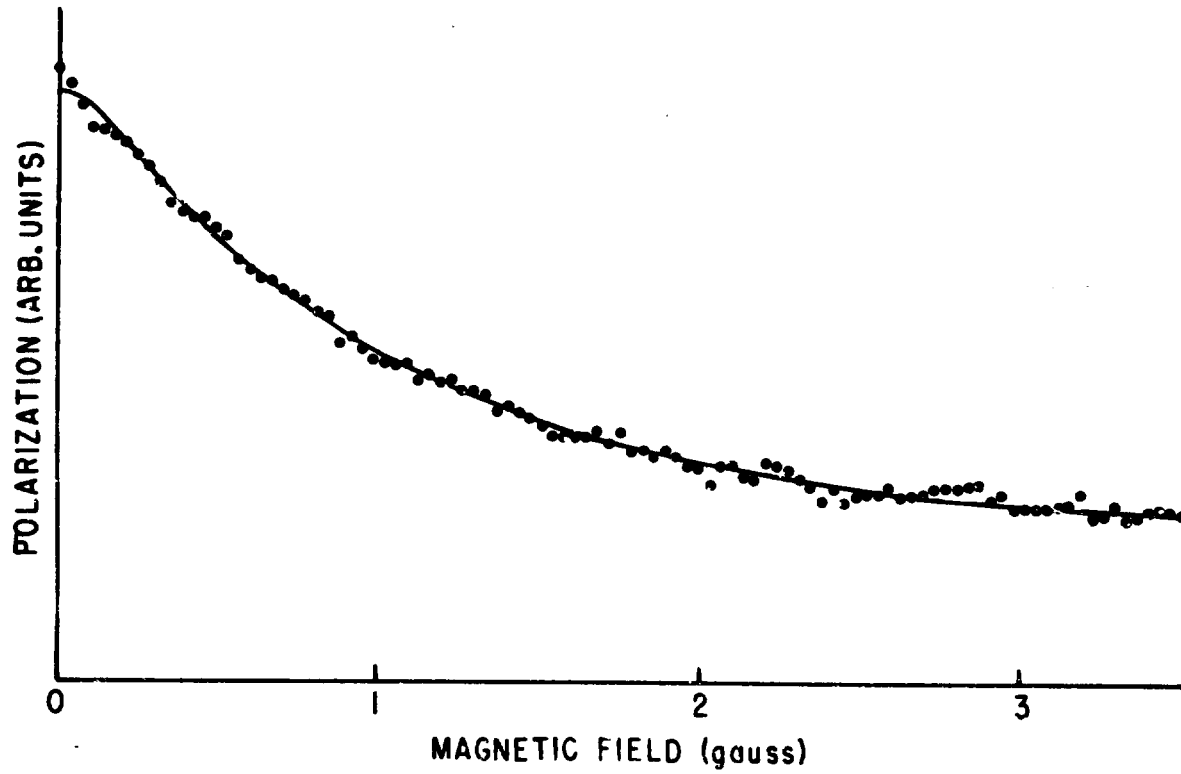
Fig. 29.   Cesium $6D_{3/2}$ Hanle effect; τ = 50 nsec.

the experimental results, while experimental data together with a least-squares fit are shown in Figs. 28 and 29. A compilation of the P state hfs and lifetime data which we used in the calculation of the Hanle-type curves is shown in Table IX. We used the cascade-Hanle method discussed in last year's Progress Report[1] to investigate the lifetimes of these states.

TABLE VIII. D state lifetimes.

Atom	State	Calculated[a] τ (nsec)	Measured τ (nsec)
Rb^{87}	$5D_{3/2}$	241	205 ± 40
Cs^{133}	$6D_{3/2}$	64.5	57 ± 15

(a) O. S. Heavens, J. Opt. Soc. Am. 51, 1058 (1961).

The comparatively large error bar associated with our results arises partly from the uncertainty in the lifetimes of the P states.

Program for next interval: We will continue to collect and analyze Hanle-effect data on other S and D states of alkali atoms.

(1) CRL Progress Report, June 30, 1973, p. 40.

M. LIGHT SHIFTS OF ZEEMAN RESONANCES IN OPTICALLY PUMPED ATOMIC VAPORS*

(W. Happer, S. Svanberg)

A relatively simple perturbation method to calculate light shifts of the Zeeman resonance frequencies of atoms has been developed, and the results are summarized in The Physical Review.[1] This work is now complete.

TABLE IX. P state hyperfine constants.

Atom	I	μ_I [a]	State	A (MHz)	B (MHz)	Lifetime (nsec)
Rb^{85}	5/2	1.3527	$7\,^2P_{1/2}$	17.65(2) [b]		
			$7\,^2P_{3/2}$	3.71(1) [c]	3.68(10) [d]	240 ± 20 [e]
Rb^{87}	3/2	2.7506	$7\,^2P_{1/2}$	59.92 [f]		
			$7\,^2P_{3/2}$	6.75(3) [g]	0.96(6) [h]	
Cs^{133}	7/2	2.579	$8\,^2P_{1/2}$	42.97(10) [i]		330 ± 30 [j]
			$8\,^2P_{3/2}$	7.626(5) [k]	-0.049(42) [l]	

58

[a] G. H. Fuller and V. W. Cohen, Nuclear Moments (Appendix 1 to Nuclear Data Sheets, (1965).

[b] D. Feiertag and G. zu Putlitz, Z. Phys. 208, 447 (1968).

[c] H. Bucka, G. zu Putlitz, and R. Rabold, Z. Phys. 213, 101 (1968).

[d] Ibid., p. 101.

[e] Ibid., p. 101.

[f] D. Feiertag and G. zu Putlitz, Z. Phys. 261, 1 (1973).

[g] G. zu Putlitz and D. V. Venkataramu, Z. Phys. 209, 470 (1968).

[h] Ibid., p. 470.

[i] C. Tai, R. Gupta, and W. Happer, Phys. Rev. A 8, 1661 (1973).

[j] E. L. Atman, Opt. Spectry. (USSR) 28, 556 (1970).

[k] H. Bucka and G. von Oppen, Ann. Physik 10, 119 (1962).

[l] Ibid., p. 119.

Scientific Research under Grant AFOSR-72-2180.

(1) W. Happer and S. Svanberg, Phys. Rev. A $\underline{9}$, 508 (1974).

N. SPIN-EXCHANGE SHIFT AND NARROWING OF MAGNETIC RESONANCE LINES IN ALKALI VAPORS*

(W. Happer, G. Moe, H. Tang)

In our previous Progress Report[1] we presented some preliminary results of an experiment to study the effects of very rapid spin-exchange collision rates on the magnetic resonance lines of an alkali vapor. In this Report we present some data obtained during the past interval which conclusively demonstrate that when the spin-exchange collision rate greatly exceeds the unperturbed Larmor frequency of the alkali vapor, the magnetic resonance frequency decreases dramatically, while the spin-exchange broadening of the resonance line vanishes. We were able to observe magnetic resonance lines with 200-Hz widths at atomic densities of greater than 10^{14} cm^{-3}. These results point out the possibilities of constructing miniaturized optically pumped devices such as magnetometers. Smaller devices would require higher atomic densities to achieve the required optical density, and up to now spin-exchange broadening of the magnetic resonance lines has placed an upper limit on the atomic densities one can use, and, therefore, on the smallness of the device. We are presently studying the feasibility of constructing optically pumped devices as much as 1000 times smaller than usual.

To review the theory of spin-exchange shifts and narrowing we refer to Eqs. (9) through (12) in the previous Report, which we rewrite here as

$$\frac{d}{dt}\langle S_+ \rangle = -\left(A + \gamma - \frac{i\omega_0}{[I]}\right)\langle S_+ \rangle + \left(B + \frac{2\gamma}{[I]^2} + \frac{i\omega_0}{[I]}\right)\langle I_+ \rangle, \qquad (1)$$

$$\frac{d}{dt}\langle I_+ \rangle = \left(A + \frac{4i\omega_0 I(I+1)}{[I]}\right)\langle S_+ \rangle - \left(B + \frac{2\gamma}{[I]^2} + \frac{i\omega_0}{[I]}\right)\langle I_+ \rangle, \qquad (2)$$

where

$$A = \frac{1}{T} \frac{8I(I + 1)}{3[I]^2} \, ,$$

(3)

$$B = \frac{1}{T} \frac{2}{[I]^2} \, ,$$

(4)

and

$$[I] = (2I + 1).$$

(5)

Here, I is the nuclear spin of the alkali atom, T is the mean time between spin-exchange collisions, ω_0 is the unperturbed Larmor frequency [$\omega_0 = 2\mu_0 H/(2I + 1)\hbar$], and γ is the electronic spin-depolarization rate due to buffer gas and wall collision. Equations (1) and (2) are a set of linearized coupled equations describing the motions of the electronic and nuclear spins, and they are written here for the transverse components $\langle S_+ \rangle$ and $\langle I_+ \rangle$ which rotate about the z-axis in the right-hand sense. These equations can be obtained from the density matrix of the atoms in the vapor. For a derivation of the density matrix of atoms undergoing spin-exchange collisions, one can refer to the works of Grossetête[2] and Gibbs.[3] In deriving Eqs. (1) and (2), we assumed weak polarization and the absence of hyperfine structure coherence. The eigensolutions of Eqs. (1) and (2) are of the form

$$\langle S_+ \rangle = a \exp (\lambda t),$$

and

$$\langle I_+ \rangle = b \exp (\lambda t)$$

with eigenvalues

$$\lambda_\pm = -\frac{1}{2} \left(A + B + \gamma + \frac{2\gamma}{[I]^2} \right) \pm \frac{1}{2} \Big[\left(A + B + \gamma + \frac{2\gamma}{[I]^2} \right)^2$$

$$- 4\gamma \left(B + \frac{2\gamma}{[I]^2} \right) + \frac{4i\omega_0}{[I]} (\gamma + [I]^2 B) - 4\omega_0^2 \Big]^{1/2}$$

(7)

$$= -\Gamma_\pm \pm i\omega.$$

60

The imaginary parts of the eigenvalues can be interpreted as precession frequencies, while the real parts can be interpreted as damping rates. The positive precession frequency would correspond to a resonance of the upper Zeeman multiplet while the negative precession frequency would correspond to a resonance of the lower Zeeman multiplet. If one applied a linearly polarized oscillating field, one would then observe both resonances. The two damping rates determine the widths of the two resonances. Figure 30 shows a plot of the two damping rates and the magnitude of the resonance frequency as a function of the spin-exchange collision rate for the case of Rb^{85} ($I = 5/2$). We see that the positive frequency damping rate first increases, reaches a maximum, and then decreases with increasing spin-exchange rate, eventually going to a limiting value determined by γ. The negative frequency damping rate is seen to always increase with increasing spin-exchange rate. This means that at high spin-exchange rates, the negative frequency resonance is "broadened out of existence," and only the positive frequency resonance can be observed. The magnitude of the resonance frequency is seen to start out at the unperturbed Larmor frequency. As the spin-exchange collision rate increases, the resonance frequency drops rapidly and eventually goes to the high density limit as given by Eq. (8) of the last Report. The magnetic resonance signal one observes when applying an oscillating magnetic field is proportional to the longitudinal torque on the spins due to the applied field. For an applied field of the form

$$\vec{H} = H_1(\cos\omega t \ \hat{e}_x + \sin\omega t \ \hat{e}_y),$$ (8)

the longitudinal torque, $T_{\parallel}$, can be written as

$$T_{\parallel} = \frac{2\mu_0 H_1}{\hbar}[I] \ \text{Im} \ \exp -i\omega t \ \langle S_+ \rangle.$$ (9)

The magnetic resonance lineshapes using Eq. (9) are plotted in Fig. 31 as a function of temperature for the case of Rb^{85}. In computing these
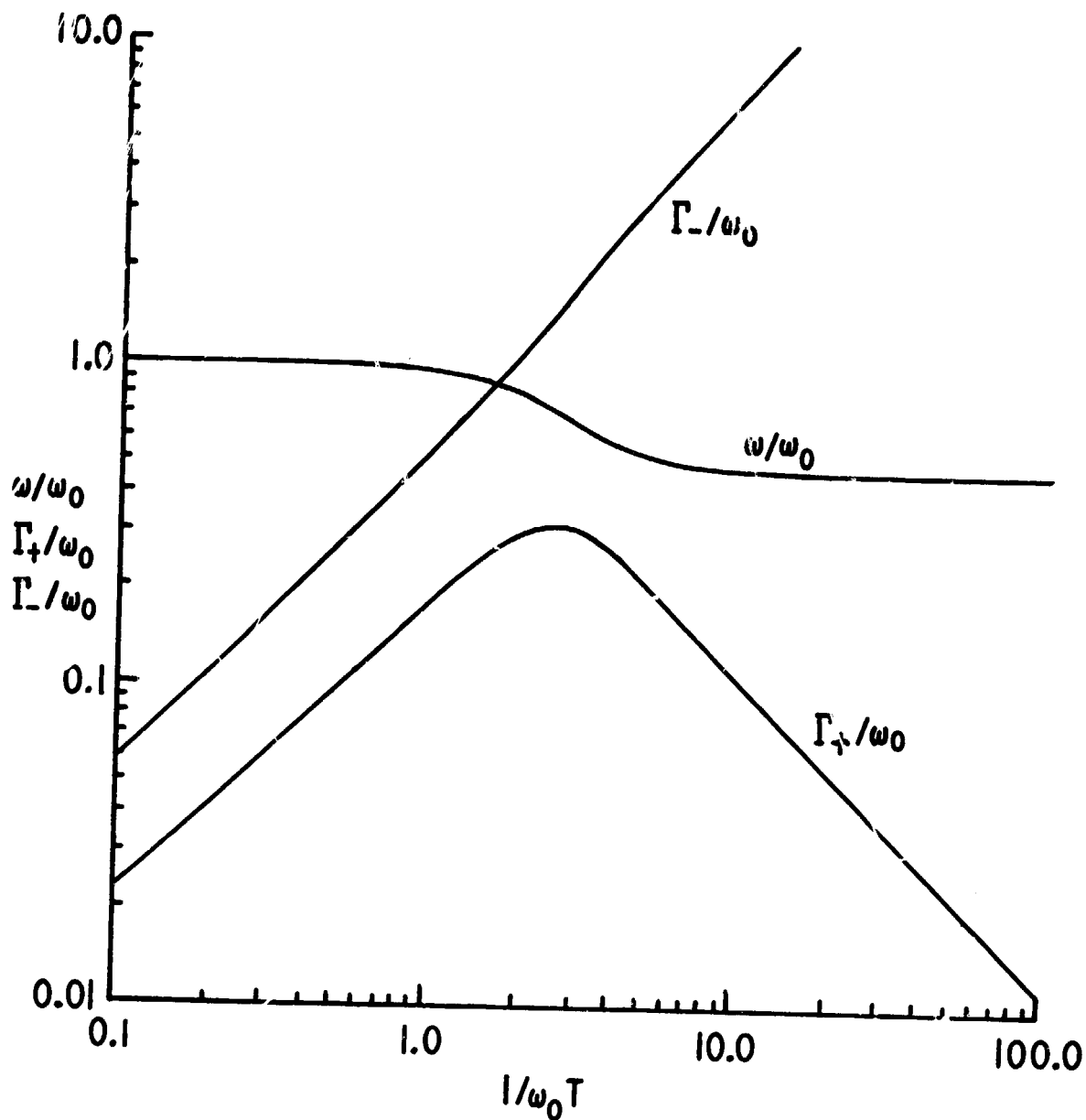
61

Fig. 30. Theoretical plot of the damping rates Γ_+ and Γ_- for the positive and negative frequency resonances and the observed Larmor frequency ω vs the spin-exchange rate $1/T$ for the case of Rb^{85}, which has nuclear spin $I = 5/2$. The above quantities have been normalized with respect to the Larmor frequency without spin exchange, ω_o.

62

TEMP. = 94°C
$N = 4.1 \times 10^{12} \, cm^{-3}$
$T = 1/N\bar{v}\sigma = 3.1 \times 10^{-4} sec$
$(\bar{v}\sigma = 7.9 \times 10^{-10} cm^3 sec^{-1})$

-1000 0 1000

TEMP. = 115°C
$N = 1.1 \times 10^{13} \, cm^{-3}$
$T = 1/N\bar{v}\sigma = 1.2 \times 10^{-4} sec$

-1000 0 1000

TEMP. = 136°C
$N = 5.0 \times 10^{13} cm^{-3}$
$T = 1/N\bar{v}\sigma = 2.5 \times 10^{-5} sec$

-1000 0 1000

TEMP. = 146°C
$N = 8.5 \times 10^{13} cm^{-3}$
$T = 1/N\bar{v}\sigma = 1.5 \times 10^{-5} sec$

-1000 0 1000

TEMP. = 156°C
$N = 1.4 \times 10^{14} cm^{-3}$
$T = 1/N\bar{v}\sigma = 9.0 \times 10^{-6} sec$

-1000 0 1000

TEMP. = 165°C
$N = 2.2 \times 10^{14} cm^{-3}$
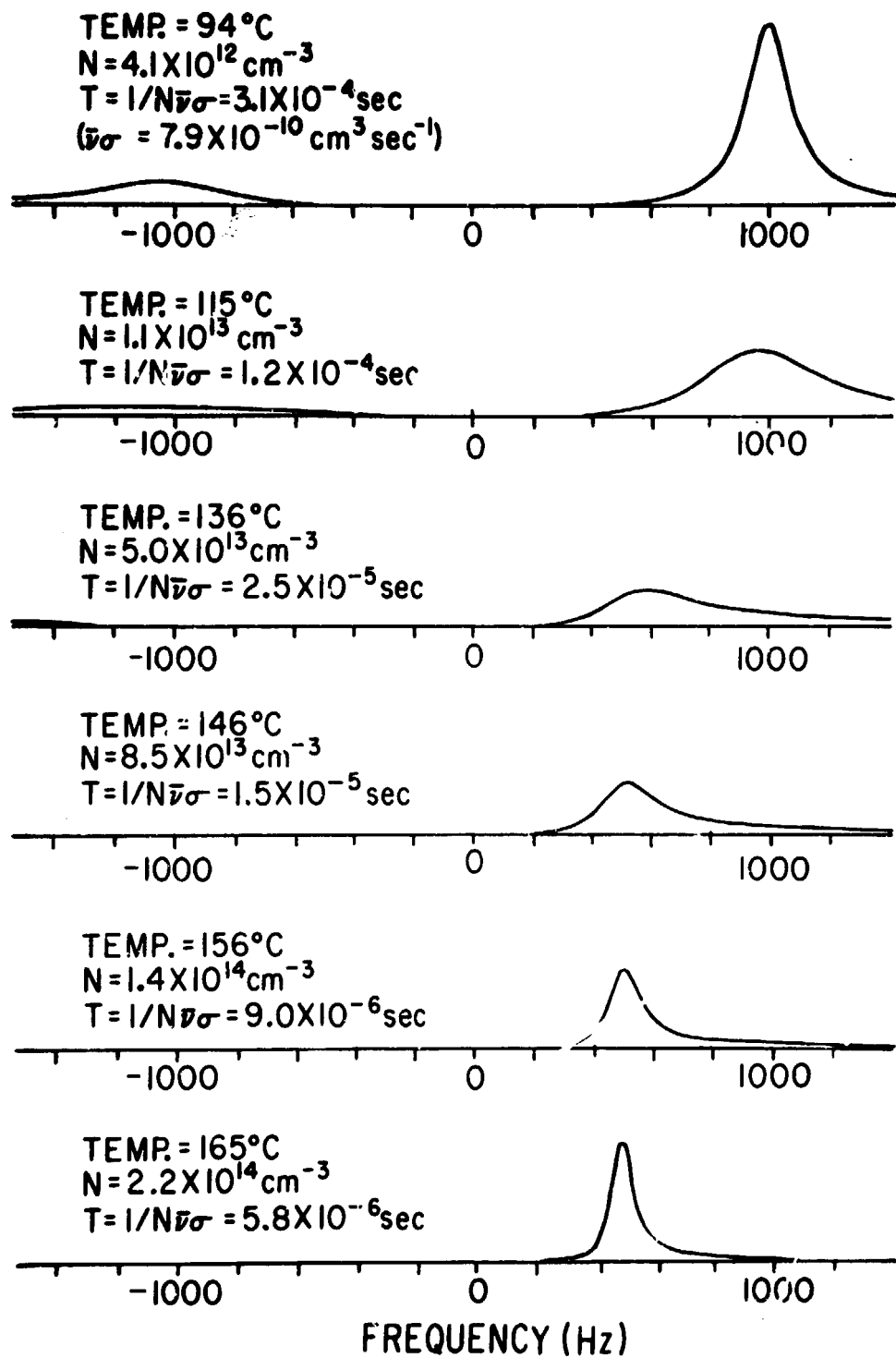$T = 1/N\bar{v}\sigma = 5.8 \times 10^{-6} sec$

-1000 0 1000

FREQUENCY (Hz)

Fig. 31. Theoretical magnetic resonance lineshapes for
different values of the spin-exchange rate 1/T,
showing the effects of spin-exchange frequency
shift and narrowing.

63

theoretical lineshapes we have used the spin-exchange collision constant $\bar{v}\sigma$ for Rb^{85} measured by Gibbs and Hull[4] to compute the atomic density N, which corresponds to a certain spin-exchange collision rate $(1/T = N\bar{v})$; then the Rb vapor pressure versus temperature data of Killian[5] were used to deduce the vapor temperature corresponding to a certain spin-exchange collision rate. We can see from these theoretical lineshapes that as the vapor temperature is initially increased, both the positive and negative frequency resonance lines broaden, with the negative frequency resonance being the broader of the two. While the negative frequency resonance continues to broaden with temperature until it can no longer be observed, the positive frequency resonance reaches a maximum width and then becomes narrower with increasing temperature. Furthermore, the positive frequency resonance has shifted to a much lower frequency at high temperatures. At intermediate temperatures, the theoretical lineshape is seen to be quite asymmetric.

The experimental apparatus is shown in Fig. 26 of the previous Report. Since according to the theory, the narrowing and shift become prominent only when the spin-exchange collision rate is comparable to or exceeds the magnetic resonance frequency, it is advantageous to work at as low a frequency as possible. Therefore, a set of two concentric cylindrical μ-metal shields were used to shield out the earth's field as well as other stray fields in the laboratory. The static magnetic field was applied by means of a coaxial solenoid inside the shields. The shields also served to make the fields inside the solenoid more uniform, thus greatly reducing the broadening of the resonance lines due to field inhomogeneities.[6] The rest of the apparatus is rather conventional optical pumping apparatus, except for the resonance cell. In order to reduce the optical thickness of the vapor at high temperatures, very thin resonance cells were used. The Pyrex cells were 2 in. in diameter and about 1 mm thick. In order to ensure a long diffusion time for the atoms in the cell, high buffer gas pressures were used (~2000 torr of He at 300°C). Fortunately, the high buffer gas pressure also greatly broadened the optical absorption line,[7] thus further reducing the optical thickness of the vapor.

The cells were made by first distilling the alkali metal into the cell; then the vacuum system was filled with about 700 torr of He gas, and the cell was cooled to liquid nitrogen temperatures before it was sealed off. Using cells made in this way, we were able to detect optical pumping signals in Cs^{133} vapor up to a density of about 6×10^{14} cm^{-3}. Plots of resonance frequency and linewidths versus temperature for Rb^{85} and Cs^{133} vapors are shown in Fig. 32. The points represent the experimental data, while the lines represent the theory. The theoretical curves were computed using the spin-exchange constant of Gibbs and Hull[8] and the vapor pressure versus temperature data of Killian.[9] The value of the spin-exchange constant has an experimental uncertainty of about 10%, while the uncertainty in the vapor pressure is unknown. We note that Cs^{133}, because of its higher nuclear spin ($I = 7/2$), exhibits a larger shift in resonance frequency between its low and high density values. The noise in the data resulted principally from magnetic noise in the laboratory. Although the μ-metal shields greatly reduced this noise, it was still the dominant noise in our experiment. The experimental magnetic resonance lines of Rb^{85} vapor are shown in Fig. 33. Again, the noise mainly arises from magnetic noise. In the experiment, a linearly oscillating magnetic field was used so that the magnetic resonance signal observed is the sum of a large positive frequency signal and a small negative frequency signal.

At low temperatures we start out with a symmetric lineshape which becomes broader as the temperature is increased. This broadening reaches a maximum and begins to decrease with temperature in the high temperature regime. The size of the signal is decreased at high temperatures owing to the vapor becoming optically thick. The lineshape becomes quite asymmetric at intermediate temperatures, while remaining symmetric in both the low and high temperature regimes, which is in agreement with the theory. The frequency at the peak of the line, which started out at about 1 kHz, has shifted to about 500 Hz at 170°C, also in agreement with the theory.

Since the spin-exchange rate must be greater than the magnetic resonance frequency for the frequency shift and narrowing to become
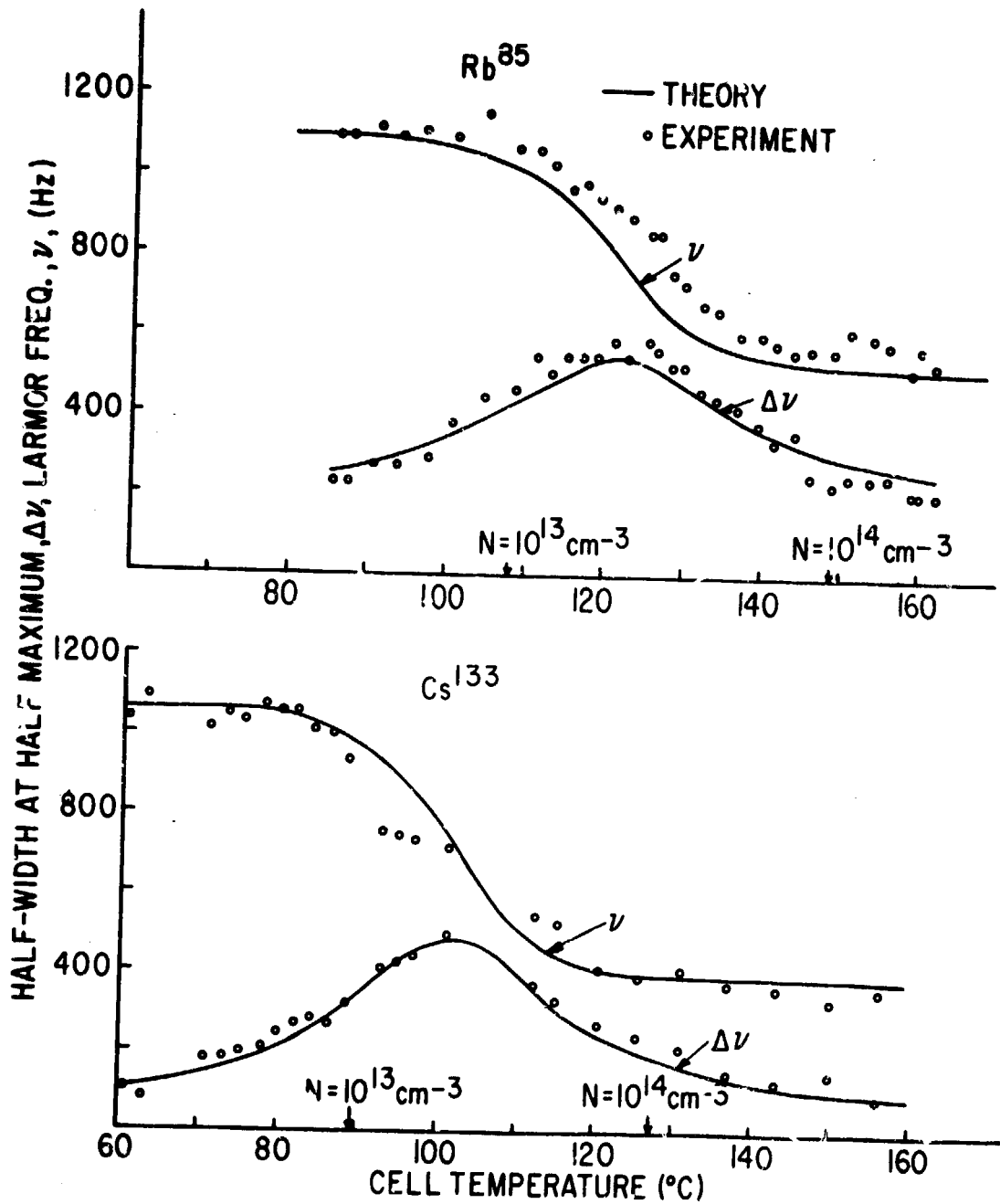
Fig. 32. Magnetic resonance frequency, ν, and half width at half maximum, $\Delta\nu$, of the magnetic resonance line in Rb^{85} and Cs^{133} vs the cell temperature.
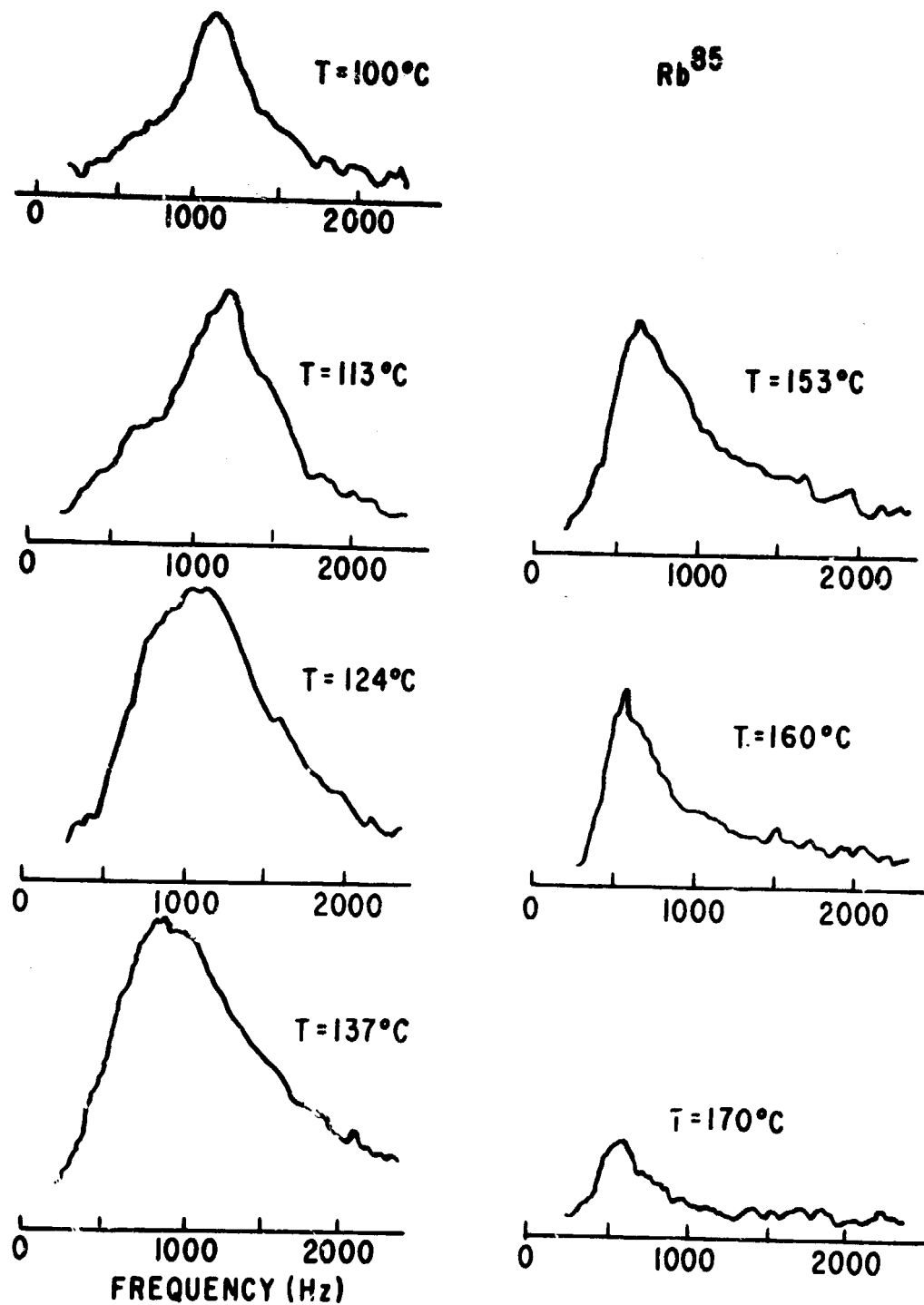
Fig. 33. Experimental magnetic resonance lines of Rb[85] vapor for different temperatures, showing the effects of spin-exchange frequency shift and narrowing.

67

appreciable, it is desirable to greatly increase the Cs-vapor density in order to allow operation in stronger magnetic fields. To observe optical pumping signals at higher densities, however, some means must be found to decrease the optical thickness of the vapor. The quality of the observed signal decreased rapidly with increasing vapor density when more than approximately 50% of the light is absorbed. In addition, when the optical thickness becomes very great, the photons are absorbed and reemitted many times, thus depolarizing the vapor.

One possible way to circumvent this difficulty is to pump the vapor with light that is less strongly absorbed than the D_1 line normally used, which excites the Cs atoms, for example, from the $6\,^2S_{1/2}$ ground state to the $6\,^2P_{1/2}$ first excited state. The transition to the $8\,^2P_{1/2}$ third P state in Cs has an oscillator strength smaller than the D_1 line by a factor of approximately 300.[10] There is a fortunate coincidence between this transition and the 3888-Å line in helium, and since an intense helium lamp was already available in the Laboratory, we attempted to optically pump Cs with the helium lamp, even though preliminary calculations showed the signal-to-noise ratio that would be obtained would be quite marginal. While pumping with the He lamp was envisioned as a simple, quick means of obtaining optical pumping signals at densities intermediate (on the order of 10^{16} atoms/cm^3) between those previously obtained and our ultimate objective ($\sim 10^{18}$ cm^{-3}), we discovered this to be an unexpectedly complicated system. Once excited to the $8\,^2P_{1/2}$ state, the Cs atoms have, at a vapor density of 10^{16} atoms/cm^3, a high probability of colliding with ground-state Cs atoms and undergoing nonradiative deexcitation, probably largely by forming Cs_2^+ molecules by the process of associative ionization.[11] The Cs_2^+ molecules thus formed are likely to recombine with an electron in the process of dissociative recombination,[12] apparently dissociating into two excited Cs atoms in the 6P first excited state. By this means, as well as by direct cascade fluorescence from the $8\,^2P_{1/2}$ state, most of the energy incident as 3888-Å photons is subsequently reemitted in the form of the 6P → 6S D-line photons we were trying to avoid. These photons are strongly trapped, and they depolarize the vapor. We at-

tempted to quench this fluorescence by using nitrogen as a buffer gas, but this introduced an additional complication because nitrogen reacts with the Cs to form an azide, CsN_3. While we believe the CsN_3 is sufficiently dissociated at 300°C to provide an adequate buffer gas pressure,[13] it is possible that CsN_3 molecules could also be present, providing a relaxation mechanism via spin exchange. At any rate, our attempt to pump Cs with the He lamp was unsuccessful, but the lack of success almost certainly resulted from the complicated phenomena involved and not from any fundamental problem with the spin-exchange narrowing mechanism itself.

A second method for decreasing the optical thickness of the vapor is to use much higher buffer gas pressure to obtain large collision broadening of the optical absorption profile. We are currently evaluating methods for constructing very small Cs-absorption cells with buffer gas pressures up to 100 atm. Since collision broadening proceeds at a rate of approximately 1 Å/atm in argon,[14] for example, this will result in absorption linewidths on the order of 100 Å. This should allow us to pump Cs vapors at very high densities with a GaAs injection laser. This would be a major step in the direction of miniature, cheap, optically pumped devices of great potential usefulness.

(1) CRL Progress Report, June 30, 1973, p. 34.

(2) F. Grossetête, J. Physique $\underline{25}$,383 (1965); F. Grosstête, J. Physique $\underline{29}$, 456 (1968).

(3) H. M. Gibbs, Phys. Rev. 139, A1374 (1965).

(4) H. M. Gibbs and R. J. Hull, Phys. Rev. $\underline{153}$, 132 (1967).

(5) T. J. Killian, Phys. Rev. $\underline{27}$, 578 (1926).

(6) R. J. Hansen and F. M. Pipkin, Rev. Sci. Instr. $\underline{36}$, 179 (1965).

(7) R. O. Garrett and S. Y. Ch'en, Phys. Rev. $\underline{144}$, 66, (1966).

(8) H. M. Gibbs and R. J. Hull, op. cit., p. 132.

(9) T. J. Killian, op. cit., p. 578.

(10) B. Warner, Mon. Not. R. Astron. Soc. $\underline{139}$, 115 (1968).

(11) F. L. Mohler and C. Boeckner, J. Res. Natl. Bur. Std. (U.S.) $\underline{5}$, 51 (1930).

(12) J. N. Bardsley and M. A. Biondi, "Dissociative Recombination," Advances in Atomic and Molecular Physics, D. R. Bates and I. Esterman, eds. (Academic Press, New York, 1970), p. 1.

(13) C. E. Mosheim, "Cesium," The Encyclopedia of the Chemical Elements, A. Hampel, ed. (Reinhold, New York, 1968), p. 130.

(14) S. Y. Ch'en and R. O. Garrett, op. cit., p. 59.

O. NUCLEAR MAGNETIC RESONANCE OF DIATOMIC ALKALI MOLECULES IN OPTICALLY PUMPED ALKALI VAPORS*

(R. Gupta, W. Happer, G. Moe, W. Park)

We have observed nuclear magnetic resonance signals which originate in diatomic alkali molecules in optically pumped cesium and rubidium vapors. Although the molecular number density is a small fraction of the atomic number density ($\sim 5 \times 10^{-4}$ at 350°K), the rate of transfer of angular momentum between the atoms and molecules is still sufficient for the Cs_2 molecules to have an appreciable influence on the atomic spin polarization. Good signals are therefore observable. The behavior of the molecules is strongly affected by the temperature and buffer gas pressure, and these experiments afford a unique and simple way to observe simple gas-phase chemical reaction rates for a system in thermal equilibrium. These seem to be the first measurement of the formation and breakup rates of alkali molecules. The molecules also represent a new factor that must be taken into consideration when designing miniature optically pumped devices for operation at high temperature (see Part N of this Section).

Our data were obtained with the apparatus sketched in Fig. 34. We distilled cesium metal into cylindrical Pyrex absorption cells, 5 cm in diameter and 1 cm in height. We then introduced various amounts of inert gas into these cells and measured the room-temperature (~ 22°C) pressure before seal-off. The cells were placed in an oven, which controlled the temperature and hence the pressure of the saturated cesium vapor. The cells were optically pumped with circularly polarized D_1 (8943-Å) resonance radiation from a cesium lamp, and we monitored the transmitted pumping light with a photomultipler
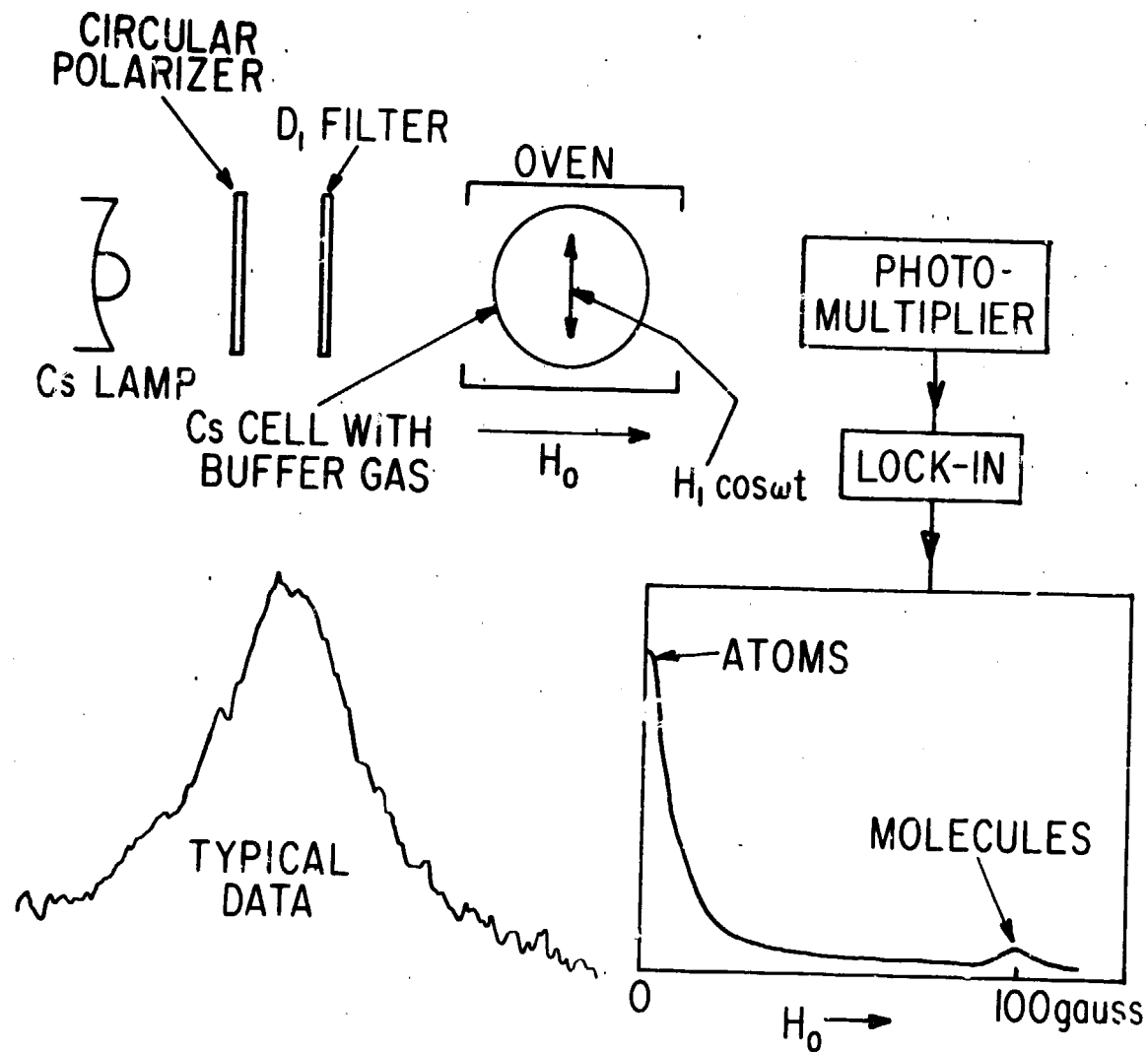
Fig. 34.   Schematic diagram of the experimental arrangement
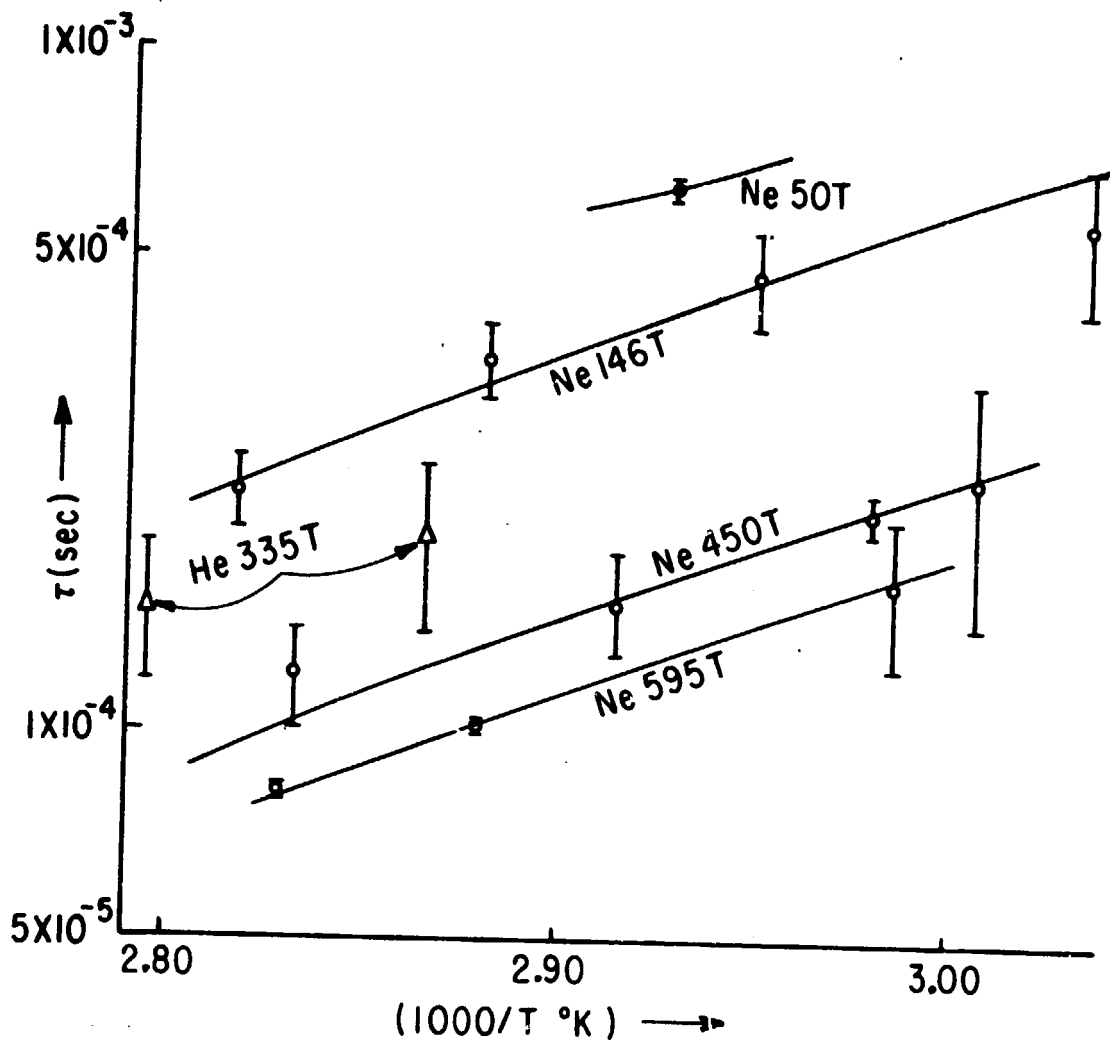and sketches of typical data.

71

Fig. 35. Relaxation time of nuclear spins in Cs_2 as a function of temperature and the pressure of buffer gas. The curves are the fit to the data based on the rate constants given in the text.

72

tube. We applied a large rf field with a peak amplitude of as much as 10 G and a frequency of 55 kHz to the cells. The rf field was square-wave modulated on and off at 13 Hz, and the synchronous component of the transmitted light intensity was detected with a lock-in amplifier and displayed on a chart recorder.

Figure 34 shows signals of the type recorded when a static magnetic field H_o was swept from zero to several hundred gauss. The large signal near zero magnetic field presumably resulted from magnetic resonance of the cesium atoms, although the rf-field amplitude was so large and the frequency so low that the conventional Bloch solutions for the magnetic resonance lineshape clearly need some revision to apply to our conditions. At a field of about 100 G we usually observed a second resonance. The high field resonance arises from nuclear magnetic resonance in molecules. A typical recording of the molecular signal is sketched in Fig. 34.

The mechanism for detection of the nmr signals in our work is very similar to that of Dehmelt's[1] original spin-exchange work, and we shall limit ourselves to a qualitative description of the process. The reactions (1) and (6), to be described below, can be expected to conserve both the electronic and nuclear spins of the cesium atoms and molecules. If these reactions proceed at a sufficiently rapid rate, the spin angular momentum of the molecules will be tightly coupled to the spin angular momentum of the atoms, and saturation of the nuclear spin polarization of the molecules with an rf field will also diminish the atomic spin polarization, which is monitored by the transmitted pumping light.

By obtaining magnetic resonance curves for a series of rf powers and extrapolating to zero rf power to determine the residual width Γ, which is the inverse of the transverse relaxation time τ of the nuclear spins, we were able to obtain the data summarized in Fig. 35 for the temperature of the saturated cesium vapor. The most striking feature of the data of Fig. 35 is the decrease of the relaxation time with increasing pressure and increasing temperature. This behavior can be understood most simply by assuming that the molecules are being broken up into atoms by the reaction

$$Cs_2 + Ne \rightarrow Cs + Cs + Ne. \tag{1}$$
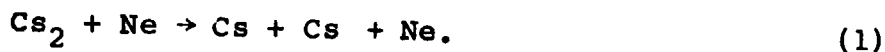
Of course, the inverse of Eq. (1), the three-body association of cesium atoms into molecules, must also occur. Since the mean thermal energy of the neon atoms ($\sim$0.03 eV) is much smaller than the dissociation energy[2] (0.396 eV) of the cesium molecules, one would expect that only a small fraction of the collisions between Cs_2 and the buffer gas atoms would lead to molecular dissociation. One would also expect the rate for the process (1) to be strongly temperature dependent, and to be characterized by an activation energy on the order of the molecular dissociation energy. Indeed, we find that the high-pressure data of Fig. 35 can be fit very well if we assume that the rate for the process (1) is

$$\frac{1}{\tau_g} = \langle v\sigma \rangle_g \exp\left(\frac{-4520}{T}\right)[Ne], \tag{2}$$

where T is the absolute temperature, [Ne] is the number density of neon atoms, and the rate constant is

$$\langle v\sigma \rangle_g = 2 \times 10^{-10} \; cm^3 \; sec^{-1}. \tag{3}$$

The characteristic temperature, 4520°K, corresponds to an activation energy of 0.39 eV, which agrees very well with the 0.396-eV dissociation energy[3] of Cs_2.

Another important experimental fact is the absence of any hyperfine structure of the nmr signals. The diatomic alkali molecules are known to have a fairly large hyperfine structure due to the electrostatic interaction between the nuclear quadrupole moment Q and the electric field gradient q produced by the atomic electrons. Logan, Cote, and Kusch[4] find eqQ/h = 230 kHz for $^{133}Cs_2$ and eqQ/h = -1100 kHz for $^{85}Rb_2$. Because of the rapid reorientation of the rotational angular momentum J of the molecule due to collisions with the buffer gas atoms, there should be a pronounced motional narrowing of the hfs, and the quadrupole interaction should manifest itself by causing the

74

nuclear spins to relax at a rate[5]

$$\frac{1}{\tau_Q} = \frac{3}{40} \frac{2I + 3}{I^2(2I - 1)} \left(\frac{eqQ}{\hbar}\right)^{1/2} \tau_J,$$ (4)

where I is the nuclear spin, and τ_J is the characteristic time for reorientation of J. We expect $(\tau_J)^{-1}$ to be proportional to the buffer gas pressure, i.e.

$$\frac{1}{\tau_J} = \langle v\sigma \rangle_J \ [Ne].$$ (5)

In contrast to molecular breakup [Eq. (1)], for which the electronic and nuclear spins should be conserved, the quadrupolar relaxation of Eq. (4) represents a loss of nuclear spin angular momentum to translational and rotational angular momentum of the molecules and buffer gas atoms. Because of the factor τ_J in Eq. (4), we expect the quadrupolar relaxation rate to vary inversely as the buffer gas pressure. The diffusion rate of the molecules to the cell walls also varies inversely with the pressure. However, the diffusion rates at one atmosphere should not exceed 3 sec^{-1}, and the diffusion rates were therefore too small to have had a noticeable influence on the rates measured in this work.

Before concluding our discussion of quadrupolar relaxation, let us note that a third process, chemical exchange, may also contribute to the nmr linewidth:

$$Cs(1)Cs(2) + Cs(3) \rightarrow Cs(1) + Cs(2)Cs(3).$$ (6)
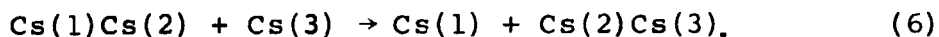
Although chemical exchange is known to occur at a very slow rate in hydrogen and deuterium,[6] recent experiments by Whitehead and Grice[7] indicate that the chemical exchange rates in the alkali atoms are quite fast, and thermal energy cross sections for the Process (6) are on the order of 10^{-14} cm^2. Although we expect that chemical exchange will conserve the electronic and nuclear spins of the reactants

in Eq. (6), the exchange collisions will contribute an amount $1/\tau_{ce}$ to the relaxation rate of the nuclear spins of the molecules:

$$\frac{1}{\tau_{ce}} = \langle v\sigma \rangle_{ce} [Cs].$$ (7)

Here $\langle v\sigma \rangle_{ce}$ is the rate constant, and [Cs] is the number density of cesium atoms. [8]

The accuracy of our data is too poor to allow us to make a very accurate determination of the relaxation rates due to chemical exchange and molecular hfs. However, from the data of Fig. 36 it is clear that something in addition to molecular breakup is limiting the relaxation time, since the relaxation time at lower pressures is too short to be explained solely by Eq. (2). We can obtain a fairly good fit to the data of Fig. 35 by choosing the rate constant for chemical exchange on the order of

$$\langle v\sigma \rangle_{ce} \simeq 10^{-10} \text{ cm}^3 \text{ sec}^{-1}.$$ (8)

The quadrupolar relaxation rate is then

$$\frac{1}{\tau_Q} \simeq 7 \times 10^{20} \text{ [Ne]}^{-1} \text{cm}^{-3} \text{ sec}^{-1},$$ (9)

which together with Eqs. (4) and (5) and the measured values [9] of eqQ/h, yields a rate constant for relaxation of the rotational angular momentum of the molecules

$$\langle v\sigma \rangle_J \simeq 3 \times 10^{-11} \text{ cm}^3 \text{ sec}^{-1}.$$ (10)

We note that the rate constant for the randomization of J corresponds to a mean cross section on the order of 10^{-15} cm^2, while the cross section for relaxation due to chemical exchange would be on the order of 10^{-14} cm^2. Although the numbers of Eqs. (8), (9), and (10) are physically reasonable, they can only be considered as order-of-magnitude estimates at this time because our data have been taken over such a limited range of temperature and pressure.

We have also observed good nmr signals for Cs^{133} in helium and argon buffer gases, and some measured relaxation rates for Cs in 338-torr helium buffer gas are shown in Fig. 35. The rates for breakup reactions such as Eq. (1) do not appear to be very sensitive to the nature of the inert gas.

(1)   H. G. Dehmelt, Phys. Rev. 109, 381 (1958).

(2)   P. Kusch and M. M. Hessel, J. Mol. Spectry. 32, 181 (1969).

(3)   Ibid., p. 181.

(4)   R. A. Logan, R. E. Coté, and P. Kusch, Phys. Rev. 86, 280 (1952).

(5)   A. Abragam, The Principles of Nuclear Magnetism (Oxford University Press, London, 1961), p. 314.

(6)   A. A. Westenberg and N. de Haas, J. Chem. Phys. 47, 1393 (1967).

(7)   J. C. Whitehead and R. Grice, Faraday Discussions Chem. Soc. 55, 320 (1973).

(8)   R. W. Ditchburn and J. C. Gilmour, Rev. Mod. Phys. 13, 310 (1941).

(9)   R. A. Logan et al., op. cit., p. 280.

II.   PHYSICS OF MOLECULES

A.   MICROWAVE SPECTROSCOPY*
(S. Green, R. Nerf, P. Thaddeus, K. D. Tucker)

1.   Pressure Broadening

The program of millimeter microwave pressure-broadening measurements on molecules of astrophysical interest is continuing. These measurements are part of a joint theoretical-experimental approach to the study of rotational excitation of molecules. The intermolecular potential, which determines collisional excitation, can neither be measured directly, nor calculated with complete confidence. However, collision cross sections obtained from pressure broadening can be used to fix some of the parameters of the potential, and so allow calculation of excitation rates.

At present, preliminary data have been taken on broadening of carbon monoxide by CO, H_2, D_2, and He. Measurements have been made at both room temperatures and liquid nitrogen temperatures, and will shortly be extended to dry-ice temperatures. During the next few months work on this molecule will be completed.

Studies have also begun on hydrogen cyanide at room and dry-ice temperatures. This molecules is a more difficult subject than molecules previously studied because of hyperfine structure in the observed transition; the $J = 0 \rightarrow 1$ line consists of three components separated by 1- 2 MHz. Since this splitting is neither large with respect to the Doppler widths of the lines, nor small with respect to the widest line the spectrometer can measure, the analysis of the observed spectrum is quite complex. It is also possible that interference effects may exist in the overlapping spectra. To facilitate the re-

duction of the HCN data, the spectrometer has been modified to allow output on digital magnetic tape. Nonlinear least-squares fitting techniques are then used to obtain the lineshape parameters from the observed spectra.

2. Spectroscopy

Recently a quartet of unidentified interstellar lines was discovered near 87.3 GHz; the observations strongly hinted that at least three, and possibly all four, of the lines were caused by the same molecule. As part of a systematic attempt to identify the source of the lines, the spectra of some twenty molecules were investigated in the neighborhood of the unkown lines. The molecules so studied can be characterized as simple enough to occur in the interstellar medium, and complex enough to prohibit the calculation of their spectra to the requisite accuracy. None of the molecules investigated could reasonably account for more than one of the unknown lines. The failure of the laboratory investigations to identify the unknown molecule prompted further theoretical studies. We evaluated a number of free radicals whose molecular constants were only poorly known. These investigations showed that all four of the unknown lines were from the ethynyl radical C_2H, which has never been observed in the gas phase in the laboratory.

B. MOLECULAR BEAM MASER SPECTROSCOPY*
(L. Gaines, P. Thaddeus, G. Tomasevich, K. Tucker)

We have completed our program to measure the hyperfine structure of the normal isotopic species of the organic ring molecule pyrrole, C_4H_5N, by studying rotational transitions of the type $J_{J0} \rightarrow J_{J1}$ in our high resolution maser spectrometer (see Table X). The $J = 1$ through 4 and $J = 10$ spectra determined the hyperfine parameters, which correctly predicted the $J = 9$ manifold (see Figs. 36 and 37

TABLE X. Theoretical center of mass frequencies for pyrrole.

J	F_N	F_N'	ν
1	2	2	4469447.399 ± 0.014
2	2	1	4341698.974 ± 0.006
	2	3	4341945.132
	2	2	4342399.876
	3	3	4342816.467
	1	1	4343046.967
	3	2	434271.1933
	1	2	4343747.871
3	3	3	4157979.419 ± 0.002
	4	1	4158186.423
	2	2	4158258.922
4	4	4	3921627.390 ± 0.006
	5	5	3921747.294
	3	3	3921778.402
9	8 → 8 9 → 9 10 → 10		2303432.383 ± 0.030
10	9 → 10 10 → 10 11 → 11		1973084.456 ± 0.008

TABLE XI. Molecular hyperfine parameters of pyrrole and furan, and internuclear distances of pyrrole.

Atom	Parameter (Hz)	Pyrrole	Furan
H 1 or 2	M_{aa}	-590 ± 14	-537 ± 3
	M_{bb}	686 ± 13	611 ± 5
	M_{cc}	-428 ± 111	-548 ± 13
H 3 or 4	M_{aa}	347 ± 14	253 ± 4
	M_{bb}	-137 ± 14	-189 ± 5
	M_{cc}	-486 ± 101	-512 ± 17
H 5	M_{aa}	852 ± 14	
	M_{bb}	-870 ± 16	
	M_{cc}	143 ± 104	
N	M_{aa}	1319 ± 7	
	M_{bb}	889 ± 7	
	M_{cc}	-405 ± 25	
	eQq_{aa}	1405532 ± 29	
	eQq_{bb}	1294109 ± 60	

Pyrrole Internuclear Distances (Å)	This work	Rotational Analysis[a]
a_{13}	2.591 ± 0.007	2.6055 ± 0.008
a_1	1.404 ± 0.010	1.362 ± 0.008
a_{56}	1.040 ± 0.002	0.996 ± 0.004
b_{12}	4.195 ± 0.011	$4.210 \quad 0.008$
b_{34}	2.712 ± 0.007	2.716 ± 0.008

(a) Lisa Nygaard, J. Tormod Nielsen, Jørgen Kirchheiner, Gudrun Maltesen, J. Rastrup-Andersen, and G. Ole Sørensen, J. Mol. Structure 3, 491 (1969).
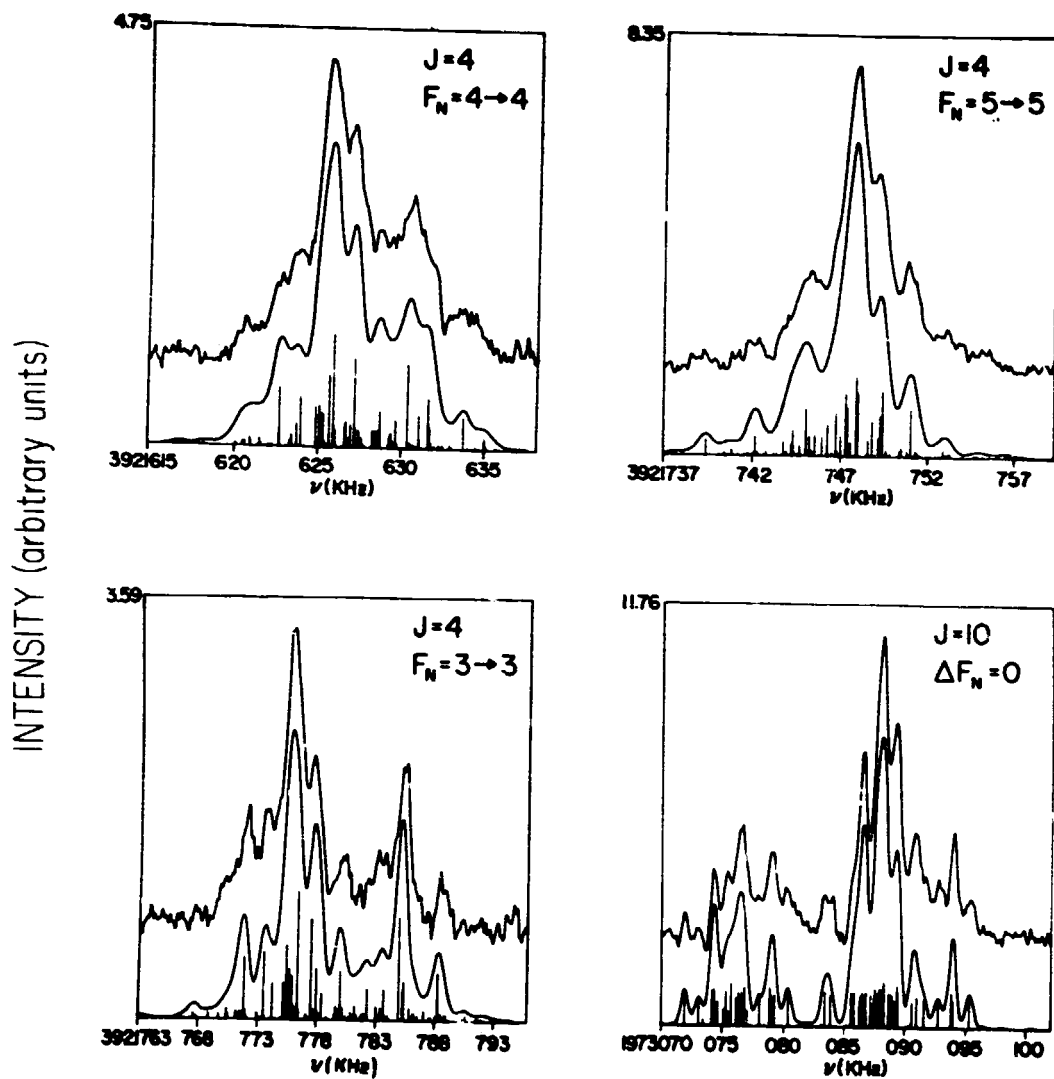
Fig. 36. Representative pyrrole spectra. Upper trace is experimental spectrum with best-fit theoretical below.
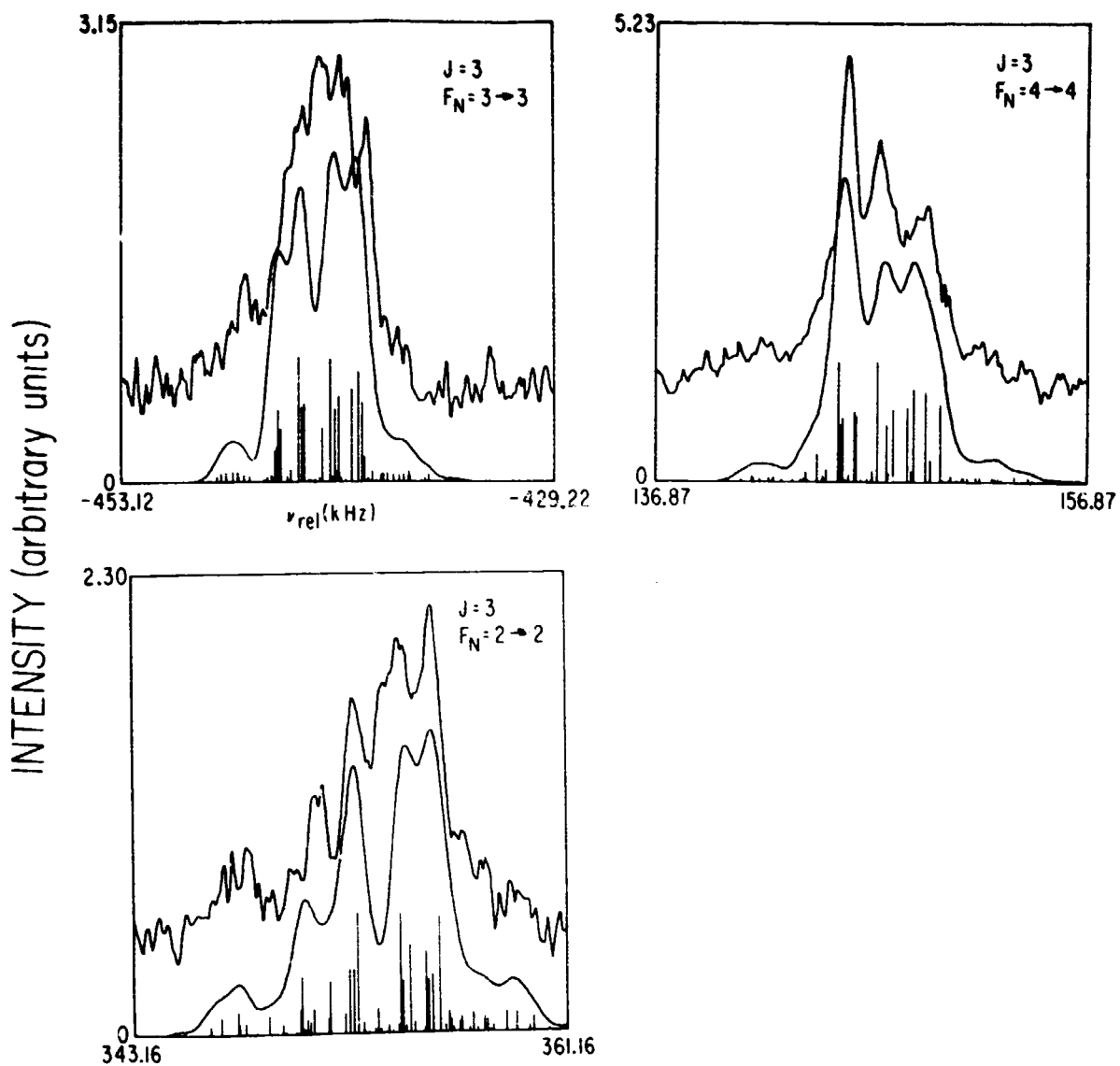
82

Fig. 37. Preliminary pyridine spectra. Experimental spectra
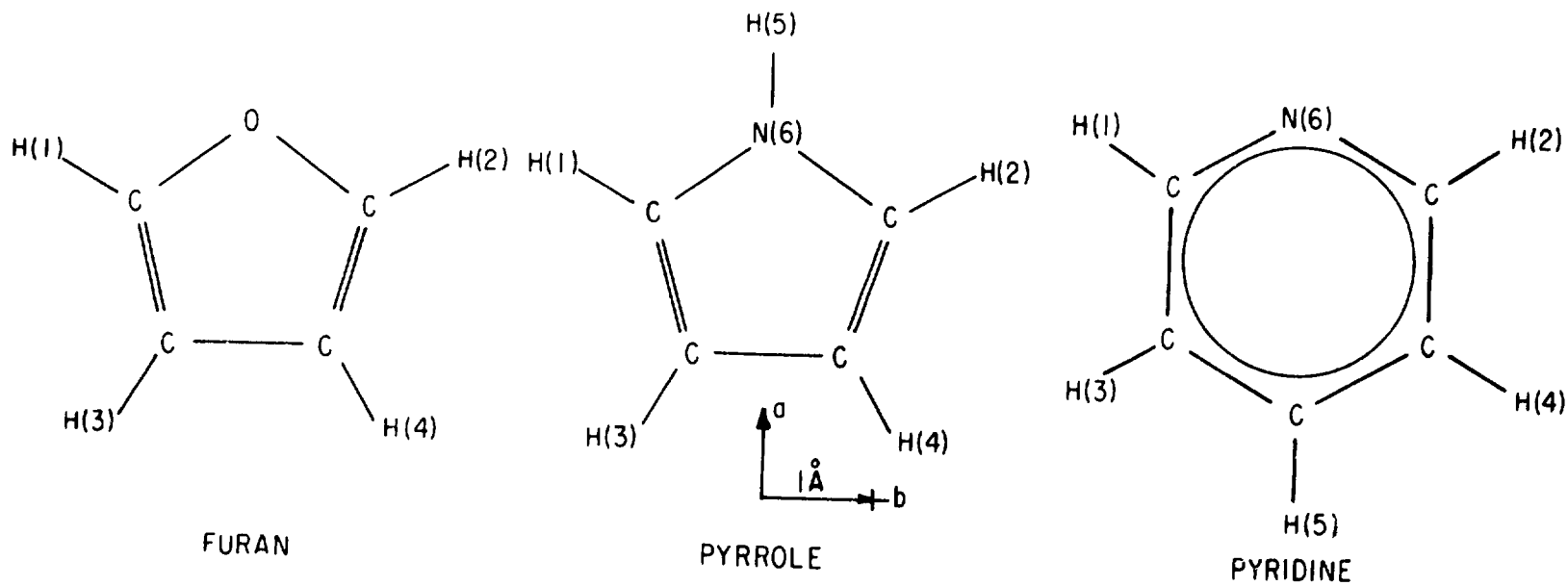above prediction from pyrrole constants.

Fig. 38.   Molecular structures of furan, pyrrole, and pyridine.

for representative spectra).

The nitrogen quadrupole interaction dominates the hyperfine structure for pyrrole and splits the spectra into widely spaced manifolds which can be labeled by the quantum numbers $F_N = I_N + J$. Since it is so large, the quadrupole interaction is fitted separately. The spin-spin interaction determines the width of each manifold ($\sim$20kHz) with the spin-rotation tensor elements (three for each type of proton) which determine the pyrrole hfs. The results of a 14-parameter least-squares fit are shown in Table XI.

We can compare the pyrrole results to those for the similar ring molecule furan, C_4H_4O, which was previously studied in this laboratory. The similarity in spin-rotation tensor elements for the corresponding protons in the two molecules is striking. This implies that the molecular electron distribution at these sites is barely changed by the substitution of N for the O in the ring. We are now studying another similar ring, pyridine, C_5H_5N, to further understand the effects of small changes in ring atoms on the hfs. (See Fig. 38 for a comparison of molecular structures.) Table XII below gives our measured values for the transition frequencies.

TABLE XII. Observed pyridine transition frequencies.

$J = 3$ ($3_{30} \rightarrow 3_{31}$)	ν (KHz)
$F_N = 3 \rightarrow 3$	2320047 ± 1
$4 \rightarrow 4$	2320636 ± 1
$2 \rightarrow 2$	2320844 ± 1

$J = 10$ ($10_{9,1} \rightarrow 10_{9,2}$)	
$F_N = 9 \rightarrow 9$	3524251.4 ± 0.5
$11 \rightarrow 11$	3524191.6 ± 0.5
$10 \rightarrow 10$	3523584.7 ± 0.5

We are also attempting to study the hyperfine structures of $H_2C^{17}O$, which has recently been observed in the interstellar medium.
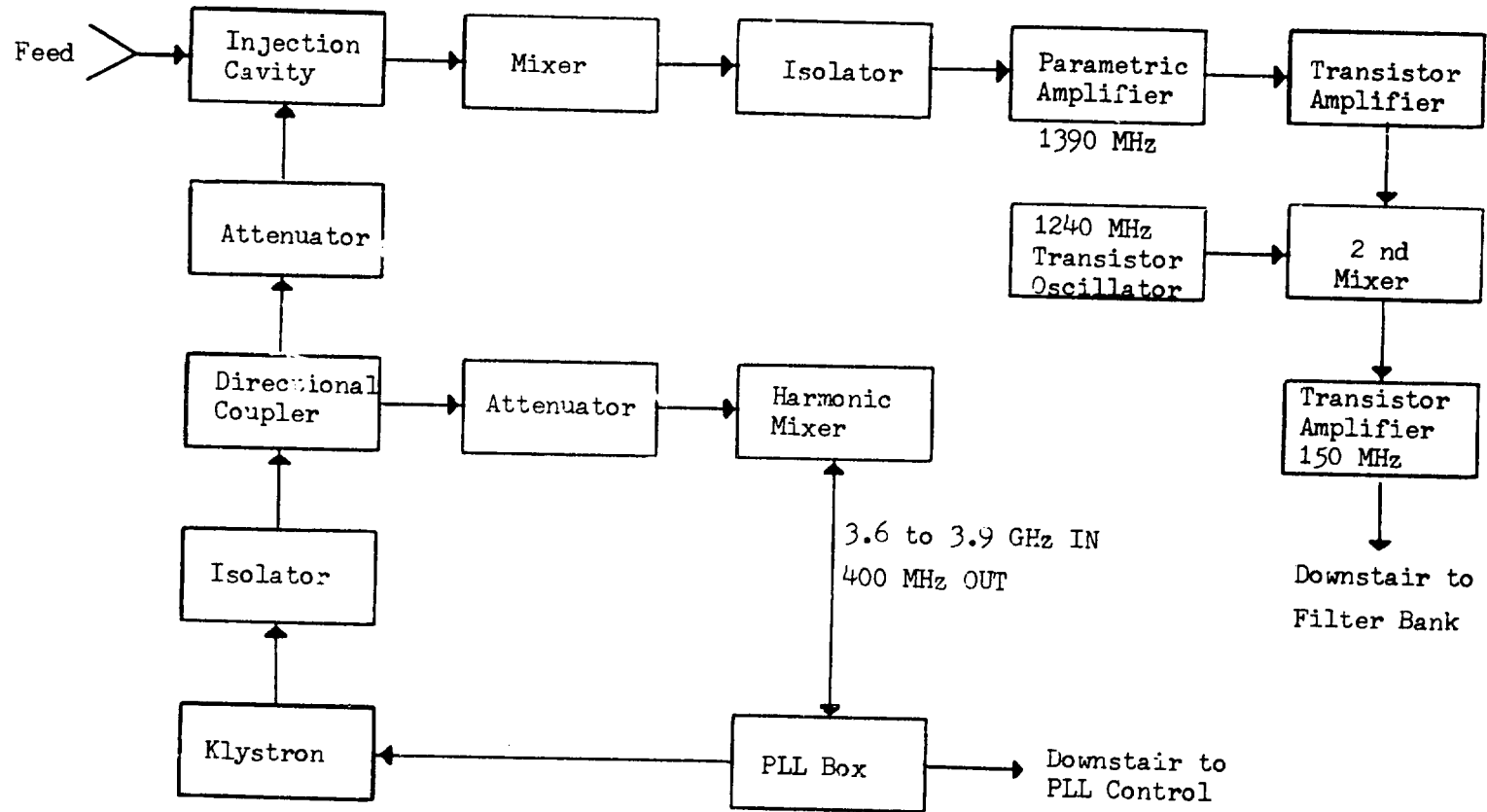
Fig. 39.   Front-end box block diagram.

C. CARBON MONOXIDE SKY SURVEY*

(G. Chin, H. Cong, P. Thaddeus)

One of the most exciting projects in molecular astronomy today is a Galactic survey in the CO region of the microwave spectrum (2.6 mm, 115 GHz). The 21-cm survey of atomic hydrogen has heretofore provided the only information we have of detailed Galactic structure. A small 4-ft radio telescope operating in the millimeter region will have the same angular resolution as the largest 21-cm telescope. The CO sky survey will not only complement the 21-cm survey but will provide greater information on the denser region of the Galaxy which the 21-cm telescope cannot give.

Construction of the millimeter-wave telescope is essentially completed. The 48-in aperture Cassegrain with a primary focal ratio of 0.375 has been delivered and mated to an alt-azimuth fork mount. The primary parabolic reflector was numerically machined out of a lightweight aluminum casting to an rms accuracy of 0.001 in. The receiver, which consists of a Schottky-barrier mixer, followed by an IF parametric amplifier at 1400 MHz and then a conventional 1400-MHz receiver, is also essentially completed (see Fig. 39). The 40-channel filter bank with 2.5-km/sec (1-MHz) spectral resolution and the analog-signal multiplexer has been built and tested satisfactorily.

The Nova minicomputer which controls the telescope pointing as well as the data acquisition with its complement of peripheral equipment and interfaces is operating satisfactorily (see Fig. 40). The telescope position is sent to the computer by digital shaft-encoders, and position errors are corrected by the computer pulsing digital stepping motors. The computer can control the tracking of the telescope within the shaft-encoder resolution, which is 40 arc-sec. The angular resolution of the telescope at 2.6 mm is about 8 arc-min. The Nova computer is operating in a multiprogram mode in which every 50 msec the computer is interrupted in its keyboard task
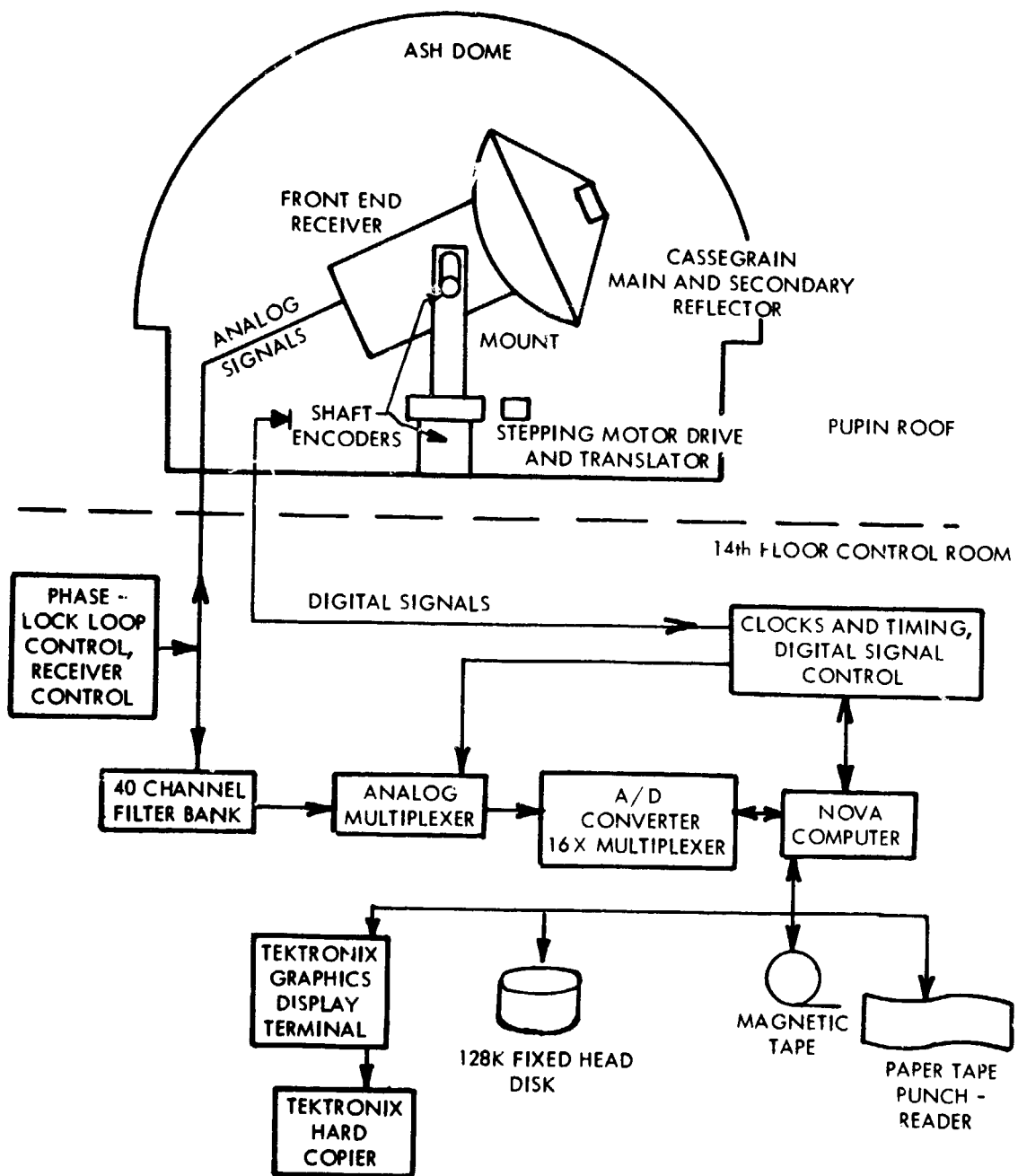
Fig. 40. Block diagram for telescope system.

to strip 40 channels of data and update the telescope position. A Clocks and Timing Unit (CTU) routes the digital and analog signals to the computer and provides the local siderial time for position updating. For the Nova computer a powerful interactive programming language has been written which allows for flexible modes of telescope operation as well as for powerful calculations using a hardwired Floating Point Unit.

A 12-ft astrodome has been built on the roof of Pupin Hall to house the millimeter telescope. The dome is equipped with heaters and an air conditioner to provide a thermally stable operating environment. Observations are made through a thin nylon radome. The control room, containing the circuitry, is inside Pupin.

The telescope has been assembled in the Laboratory and is operating as designed. Assembly of the entire system at Pupin will take place in mid-June, 1974, after a final noise test on the receiver.

III. RESONANCE PHYSICS

A. PHOTON ECHOES IN NEODYMIUM^{3+}*

(S. Chandra, Y. Chen, S. R. Hartmann)

Last year we reported the first observation of photon echoes for the $^4I_{9/2} \rightarrow {}^4F_{3/2}$ transition of Nd^{3+} in $CaWO_4$. We described the temperature dependence and magnetic field behavior of the echo. Since then we have succeeded in detecting echoes for the same transition in two other crystals: LaF_3:Nd^{3+} and YAG:Nd^{3+}. Below we present a comparative study of the echo behavior in the three crystals.

In all three crystals, the ground state, $^4I_{9/2}$, is split into five Kramer's doublets ($Z_1 - Z_5$), and the $F_{3/2}$ state into two doublets (R_1 and R_2) as shown in Fig. 41. The echoes were excited between the Z_1 and R_1 levels. Our samples were: LaF_3Nd^{3+} (0.1 atom %), with transition frequencies corresponding to 8626 Å, 8767 Å, and 8749 Å, respectively. The experimental arrangement was similar to that described in last year's Progress Report,[1] except that the excitation-laser pulses were collinear, and consequently the echoes were also emitted collinearly. A three-stage Kerr-cell optical shutter prevented the photomultiplier detector from saturating. The laser $\underline{E}$-field was vertical. The LaF_4 and $CaWO_4$ samples were oriented with the c-axis perpendicular to both the $\underline{E}$-vector and the direction of propagation to maximize the echo signal. The sample temperature was varied between 3° and 20° K, and a magnetic field variable up to 3 kG was applied along the c-axis. The shot-to-shot signal fluctuation was typically a factor of two.

The photon-echo amplitude in each crystal depended on both magnetic field and sample temperature. The echoes were larger in $CaWO_4$. They were typically two orders of magnitude smaller in LaF_3 and three
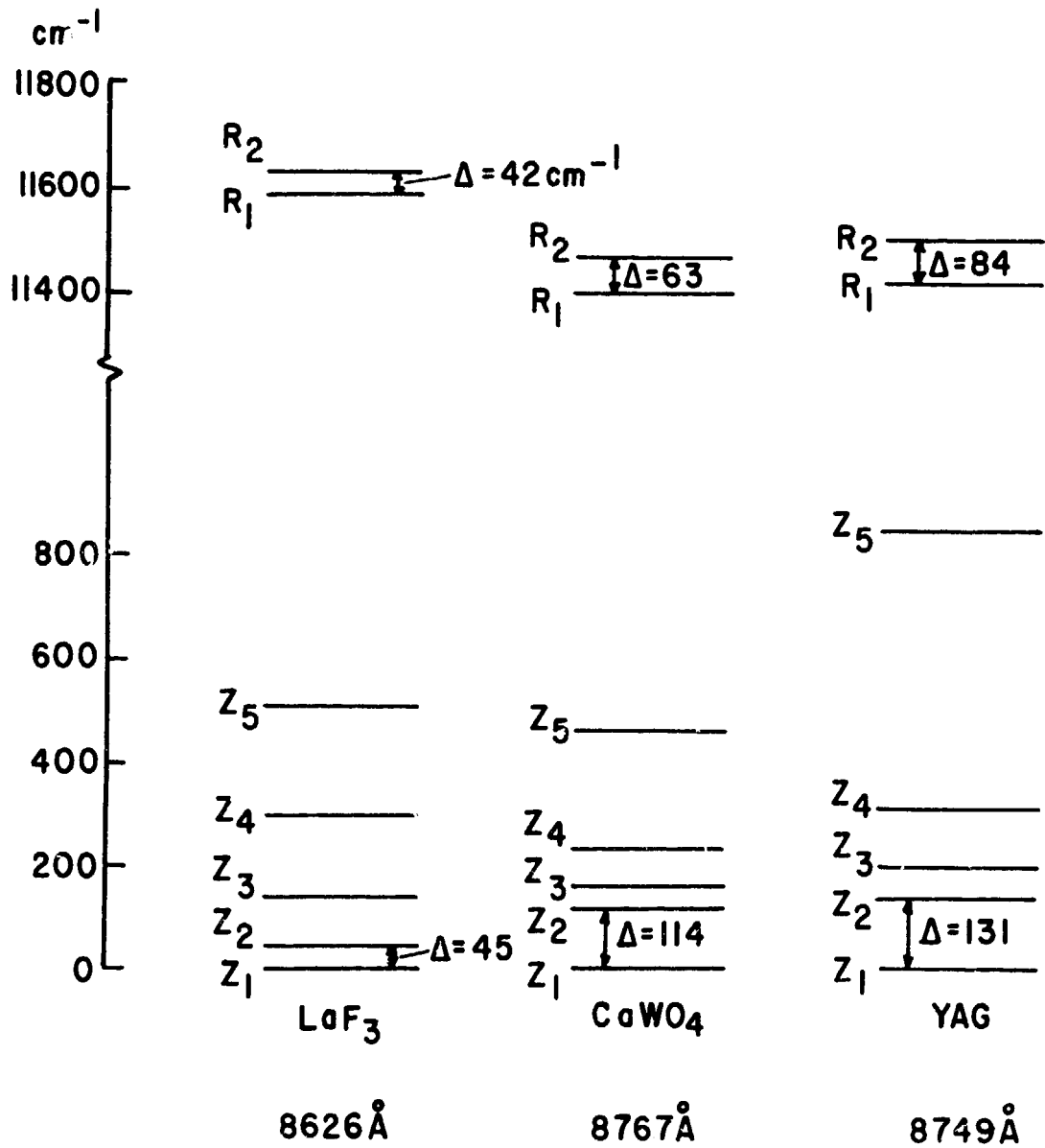
Fig. 41. The $^4I_{9/2}$ and $^4F_{3/2}$ energy levels of Nd^{3+} in the three crystals.
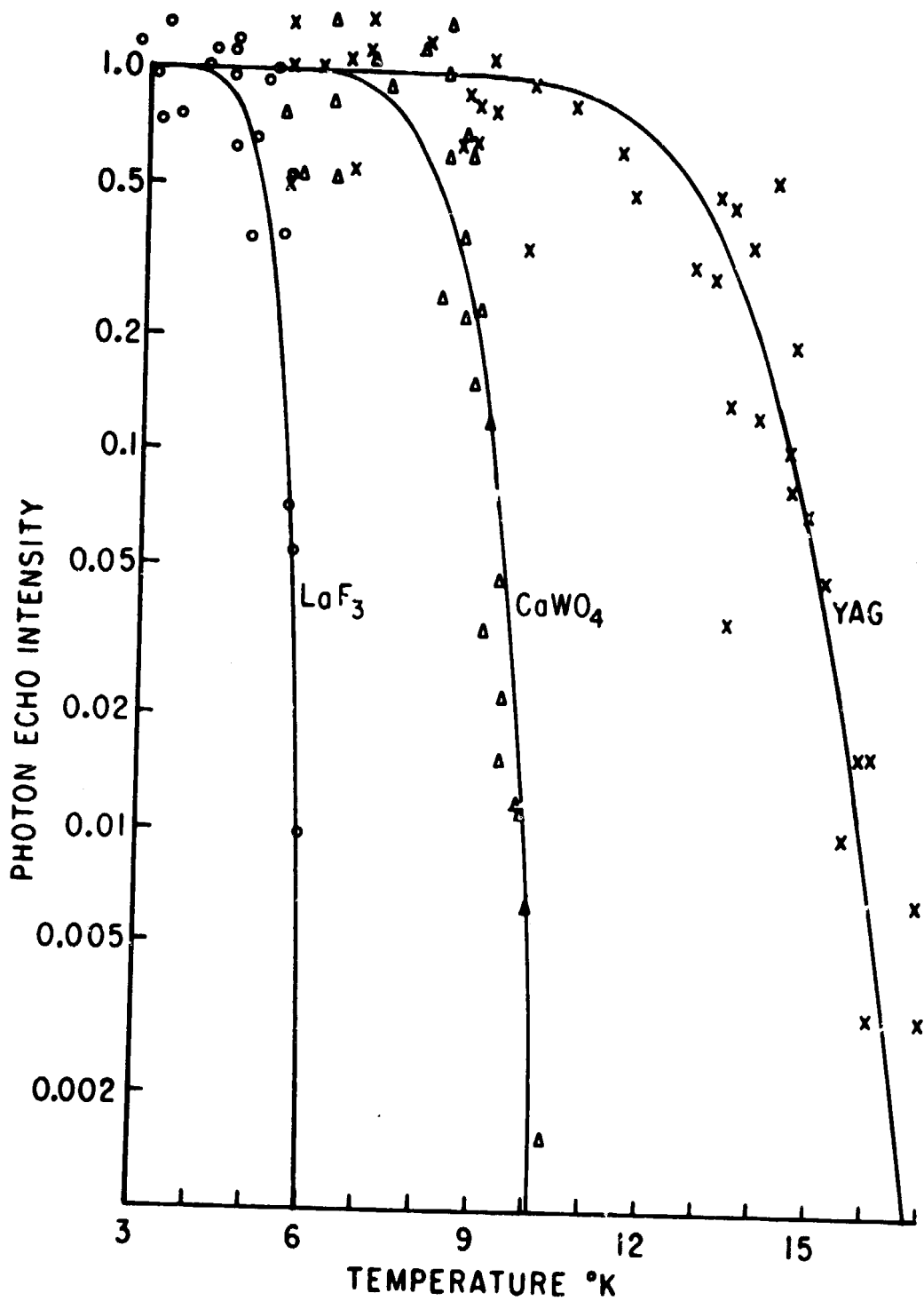
91

Fig. 42. Temperature dependence of photon echoes in Nd^{3+} in the three crystals.

orders smaller in YAG. Photon echoes in YAG, although considerably more difficult to observe than in the other two crystals, were still easily observed. There is a threshold temperature above which the echo amplitude at fixed excitation-pulse separation decreases rapidly (Fig. 42). This behavior was unaffected by the magnitude of the applied magnetic field. The threshold temperature for an excitation-pulse separation of 64 nsec was $\sim 5°K$ for LaF_3, $\sim 8°K$ for $CaWO_4$, and $\sim 13°K$ for YAG. We attribute this sharp decay to phonon-induced relaxations of the Orbach and Raman type. For either mechanism the most important contribution comes from levels closest to the echo levels Z_1 and R_1, viz. Z_2 and/or R_2. The Orbach relaxation rate behaves as $\sim \Delta^3 \exp(-\Delta/kT)$, while the Raman relaxation rate follows $\sim \Delta^{-4}T^9$, where Δ is the energy separation between R_1 and R_2 or between Z_1 and Z_2. We note that the ordering of the observed threshold temperatures follows that of Δ (see Fig. 41 for values of Δ). Our experimental data do not allow us to determine which of the two relaxation mechanisms is responsible for the echo decay. We think that it is probably the Orbach-type process that dominates the relaxation. We arrived at this conclusion by some theoretical considerations based on spin-lattice relaxation data of electron-spin-resonance experiments.

The solid lines in Fig. 42 are drawn for the following relaxation-time constants:

$LaF_3:Nd^{3+}$: $\tau_{10} = 1.5 \times 10^{12} [\exp(-65/T) + \exp(-60.5/T)]^{-1}$ sec;

$CaWO_4:Nd^{3+}$: $\tau_{10} = 3 \times 10^{-12} \exp(91/T)$ sec;

$YAG:Nd^{3+}$: $\tau_{10} = 14 \times 10^{-12} \exp(121/T)$ sec.

The dashed curve is a fit for YAG with a Raman process.

The magnetic field dependence of photon echoes was studied for fields up to 3 kG. For pulse separations up to 300 nsec in $CaWO_4:Nd^{3+}$, the echo signal increased monotonically with the applied field for the initial few hundred gauss and thereafter became constant. Figure 43 shows the echo behavior in $LaF_3:Nd^{3+}$ for various pulse separations. Figure 44 gives a comparison of the echo behavior in the three crystals
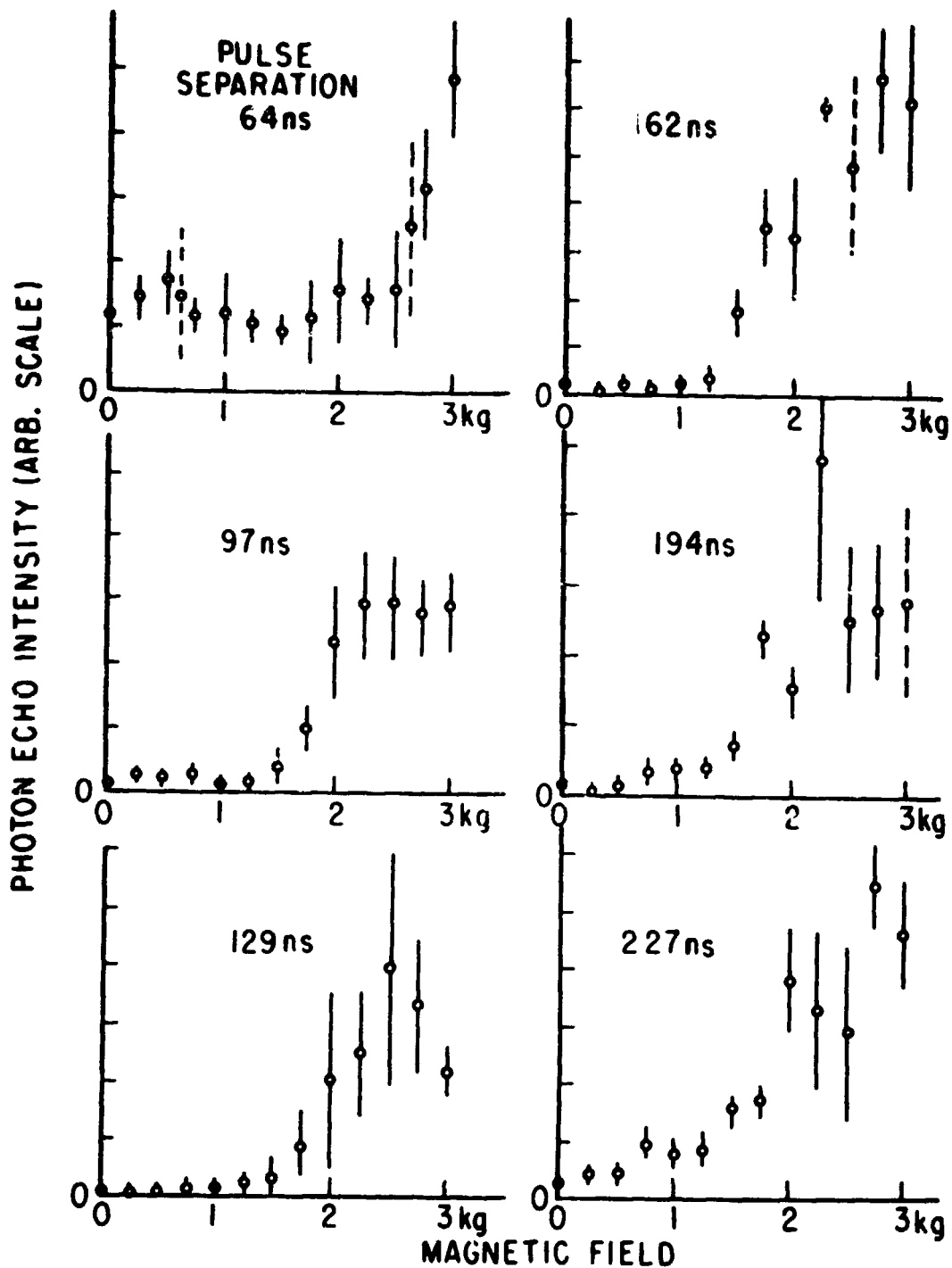
Fig. 43. Photon-echo signal in $LaF_3:Nd^{3+}$ (0.1 atom %) as a function of applied magnetic field for indicated fixed pulse separations. The solid error bars represent standard deviations. Dashed vertical bars are drawn for single shots.
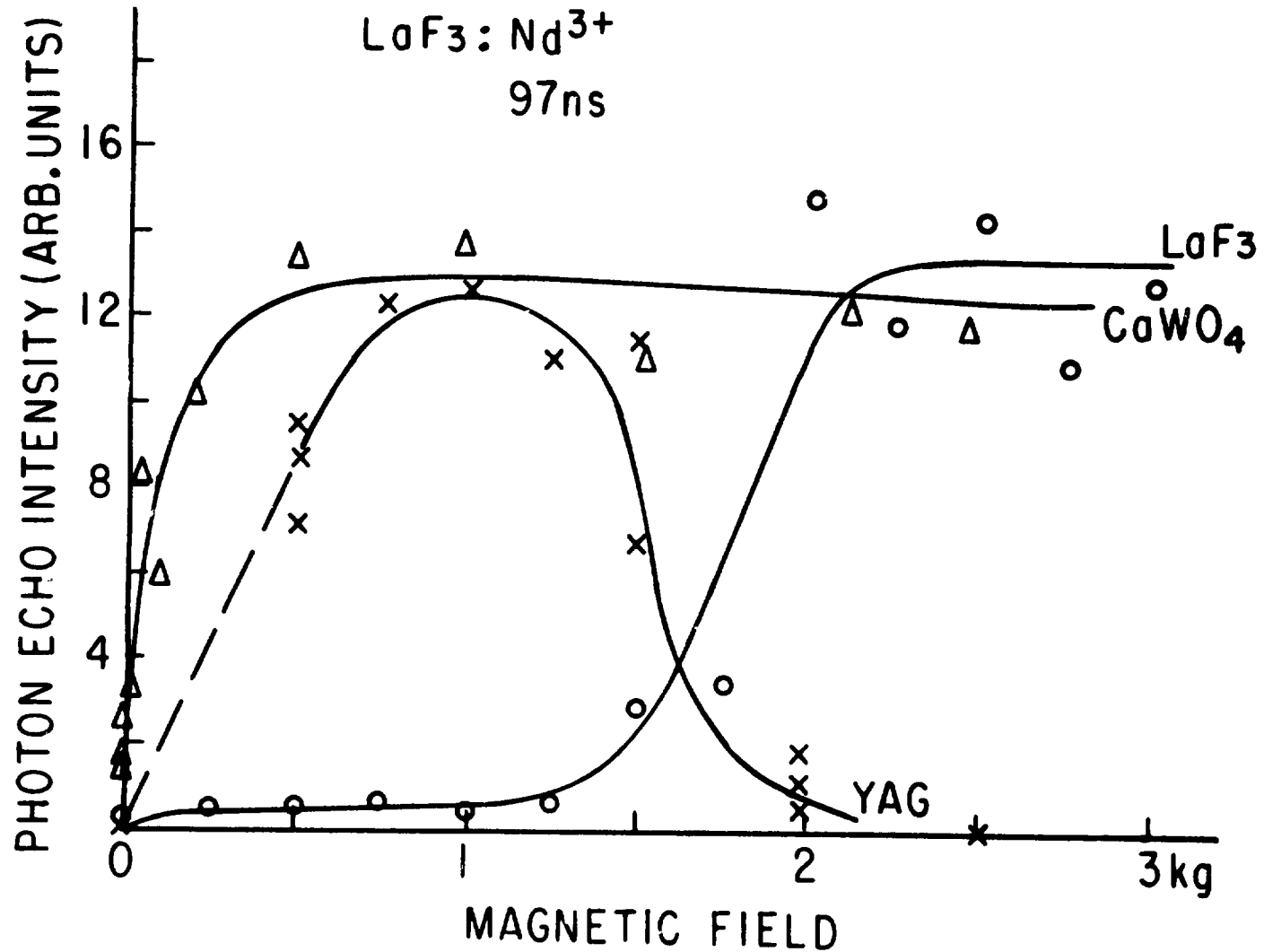
94

Fig. 44. Contrasting magnetic field behavior of photon echoes in the three host crystals. Nuclear magnetic superhyperfine interactions are believed responsible for the modulations.

for a fixed pulse separation of 97 nsec. We attribute the difference in the magnetic behavior of the echo to the difference in the magnetic interaction of the Nd^{3+} atoms with neighboring paramagnetic nuclei present in the crystals.[2] In $CaWO_4$ only 14% of the tungsten nuclei are magnetic and only weakly so ($\gamma_n/2\pi = 0.175$ MHz/kG). We therefore do not expect any modulation of the echo since we have $\gamma_n Ht \ll \pi$ (where H = 3 kG and t = 97 nsec pulse separation). This is in agreement with our observation. For both $LaF_3:Nd^{3+}$ and $YAG:Nd^{3+}$ we expect and observe modulation effects. In LaF_3 there are eleven F nuclei ($\gamma_n/4\pi = 4.0$ MHz/kG) within 3 Å of the Nd^{3+} ion. In YAG the ten nearest Al nuclei ($\gamma_n/2\pi = 1.1$ MHz/kG) are within 4 Å of the Nd^{3+} ion.

(1)   CRL Progress Report, June 30, 1973, p. 68.

(2)   D. Grischkowsky and S. R. Hartmann, Phys. Rev. B <u>2</u>, 60 (1970).

B.   PHOTON-ECHO RESONANCE IN RUBY*

(S. R. Hartmann, P. Liao, S. Meth)

We are continuing our investigation of photon echoes in ruby using the gated cw system described in the previous Progress Report.[1] We are using the more powerful laser pump, and are presently mounting the entire experiment on a vibration-isolation system to reduce vibrations and increase the echo signal.

1.   Modifications in Equipment

The gated cw system is shown in Fig. 45. The Spectra Physics Model 170 Argon-Ion Laser is capable of producing 6 W at 5145 Å; however, we have been able to generate as much as 9 W for short periods. The remaining optical apparatus has not been changed from that described in the previous Report.

We have completely automated the photon-echo experiment by using a unique echo multipulser designed and built in the CRL electronics shop. When triggered, this device produces a series of clock pulses whose time separation is controlled by a 10-turn potentiometer. The
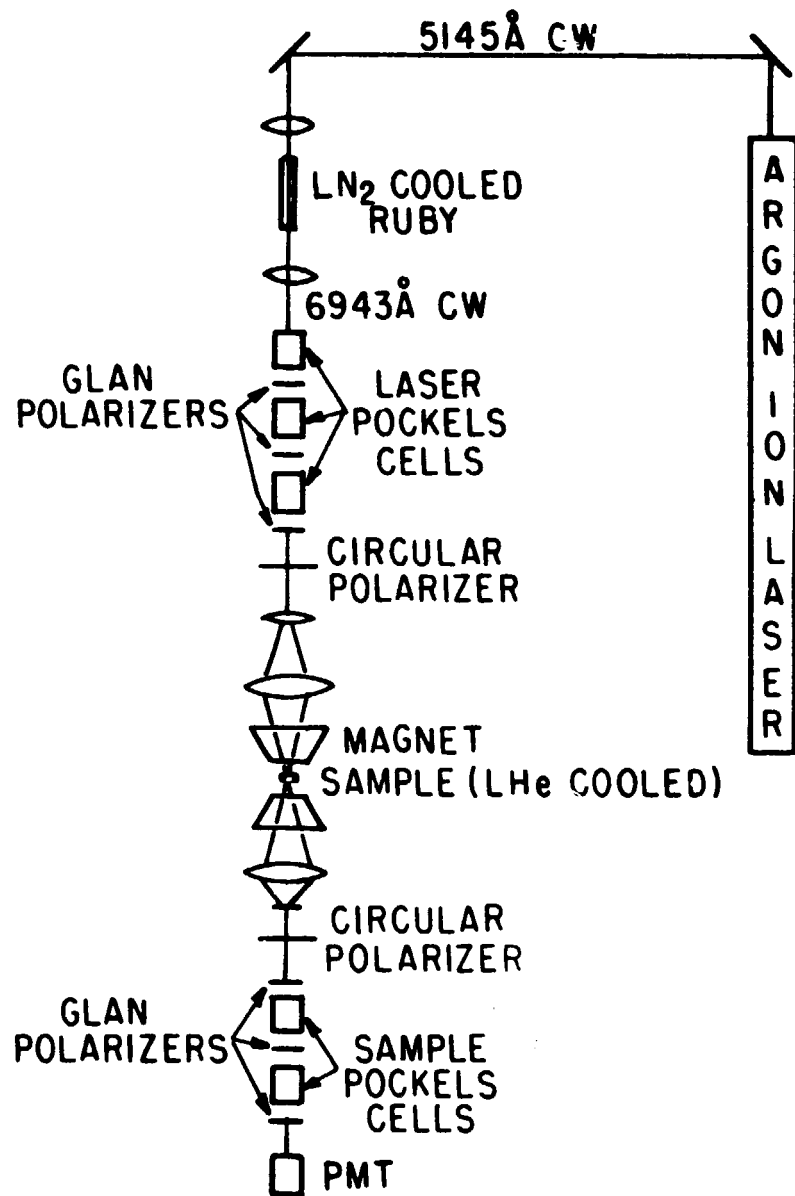
Fig. 45. Optical arrangement of photon-echo experiment.

experimental timing sequence is triggered by these clock pulses, with the first and second pulses triggering the first and second laser pulses, respectively. The sample Pockel's cells are closed during the laser pulses to prevent saturation of the photomultiplier tube, and the third clock pulse triggers the e cells to open just prior to the arrival of the echo. This clock pulse also initiates the timing sequence for the data-acquisition electronics. We have replaced the box-car integrator with an integrated circuit Analog Devices SHA-5 sample-and-hold.

When the experiment is operating, the PDP-8/e computer controls the multipulser potentiometer, varying the pulse separation in a manner programmed by the experimenter. Thus, in about 30 min we can acquire data corresponding to a sweep of pulse separation from 200 nsec to 6 μsec, in increments of 100 nsec. This corresponds to a decrease in data-taking time by a factor of at least five over manual operation.

We had been able to produce a fairly stable, nonspiking cw ruby beam with argon pumping power as high as 4.2 W. At higher power, we were unable to eliminate the ruby spiking due to vibrations of the ruby-laser rod with respect to the argon beam. We also had an extremely small laser spot size (~100-μ diameter) at the sample. If, between the two laser pulses, the beam moves with respect to the sample, the two spots will not overlap completely, resulting in a decrease of the echo signal. To reduce these problems, we have used a 4-ft by 10-ft, 3600-lb cast iron, ribbed optical table, mounted on a Jodon Engineering Vibration-Isolation System. This system of pneumatic legs reduces by a factor of 50 the transmission of floor vibrations to the table at 10 Hz, the resonant frequency of the laboratory floor. We are in the process of mounting the entire experiment on the table. We have already mounted the ruby laser and pump and have obtained a nonspiking cw ruby beam at 6-W pump power. No spiking was observed to 8-W pump power, but the 170 Laser cannot sustain such high powers for very long periods. This should increase the ruby output over that of the old system by 50%. We hope with the new system to be able to measure photon echoes across at least three orders of magnitude in pulse separation, and

six orders of magnitude in echo intensity.

2. Photon-Echo Modulation

The photon echo is the optical analog of Hahn's spin echo.[2] Two resonant pulses of light, separated by a time τ, pass through the sample. These pulses act as the 90° and 180° pulses of the spin-echo pulse sequence, so that at a time τ after the second pulse, the sample radiates the photon echo. As in the case of spin echoes, the formation of the photon echo is sensitive to changes in the local field at the echo-atom site and hence to interactions with other atoms and nuclei. The interaction of the chromium atoms in ruby with neighboring aluminum nuclei causes a marked modulation of echo intensity with respect to pulse separation similar to that observed in electron-spin echoes.[3]

Recent photon-echo nuclear double-resonance (PENDOR) studies have allowed the determination of Cr-Al interaction parameters associated with the excited state.[4] These parameters, together with those determined for the ground state from spin-echo ENDOR experiments,[5] allow the calculation of photon-echo behavior in a manner similar to that used for spin-echo behavior.[6] The results of these calculations are shown in Figs. 46 and 47, along with corresponding experimental data taken with the automated, gated cw system.

The data of Fig. 46 correspond to conditions that were measured previously: the magnetic field is applied at a slight angle with respect to the optic axis of the crystal. Our data agree with the data published earlier in the short time regime[7] but extend also to longer pulse separations. The solid curve, which corresponds to the theory, does not include the overall exponential decay of the photon-echo envelope. The comparison of theory with experiment appears to be excellent. We expect to extend the pulse separation as far out as 20 μsec or longer in the near future and thereby study the interesting oscillatory behavior exhibited by the echo.

Figure 47 shows the photon-echo modulation for the magnetic field applied parallel to the optic axis for the $\bar{E}(^2E)(1/2) \to {}^4A_2(1/2)$ transition. The theoretical calculations were multiplied by an exponential
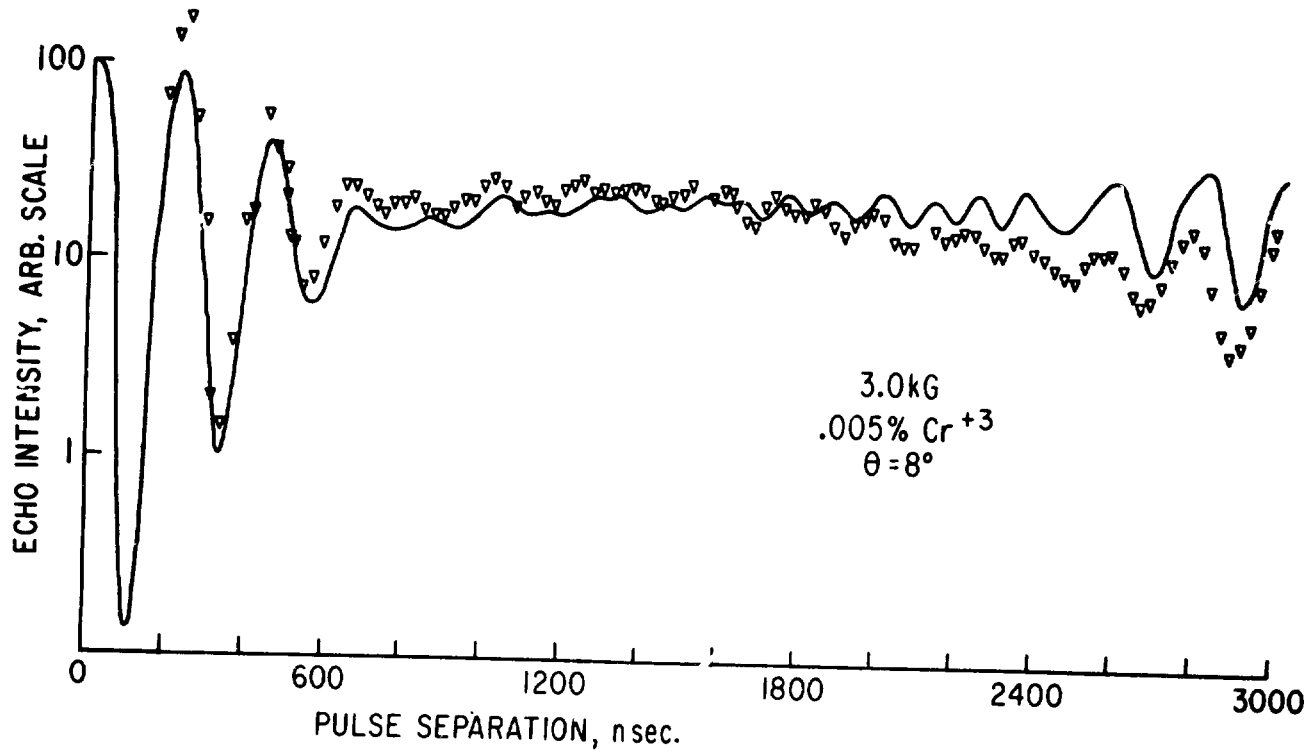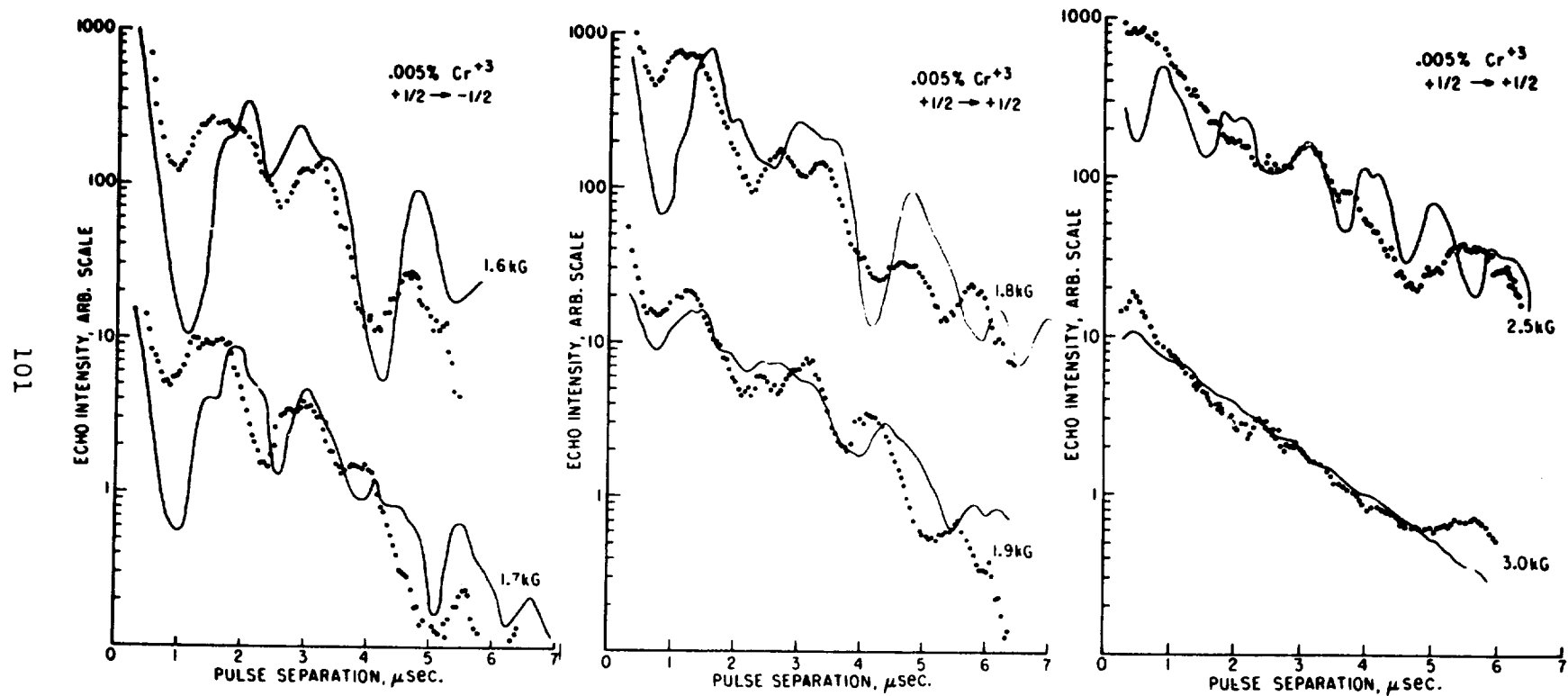
Fig. 46.   Off-axis photon-echo modulation.

Fig. 47.   On-axis photon-echo modulation.

a) figure with axes "ECHO INTENSITY, ARB. UNITS" (vertical, log scale 0.1 to 1000) and "PULSE SEPARATION, μsec." (horizontal, 5 to 30), labeled:

5kG
$-1/2 \rightarrow -1/2$
.005% Cr^{+3}

b) figure with axes "ECHO INTENSITY, ARB. SCALE" (vertical, log scale 1 to 1000) and "$t^{1/2}$, μsec.$^{1/2}$" (horizontal, 0 to 6), labeled:

5kG
$-1/2 \rightarrow -1/2$
.005% Cr^{+3}
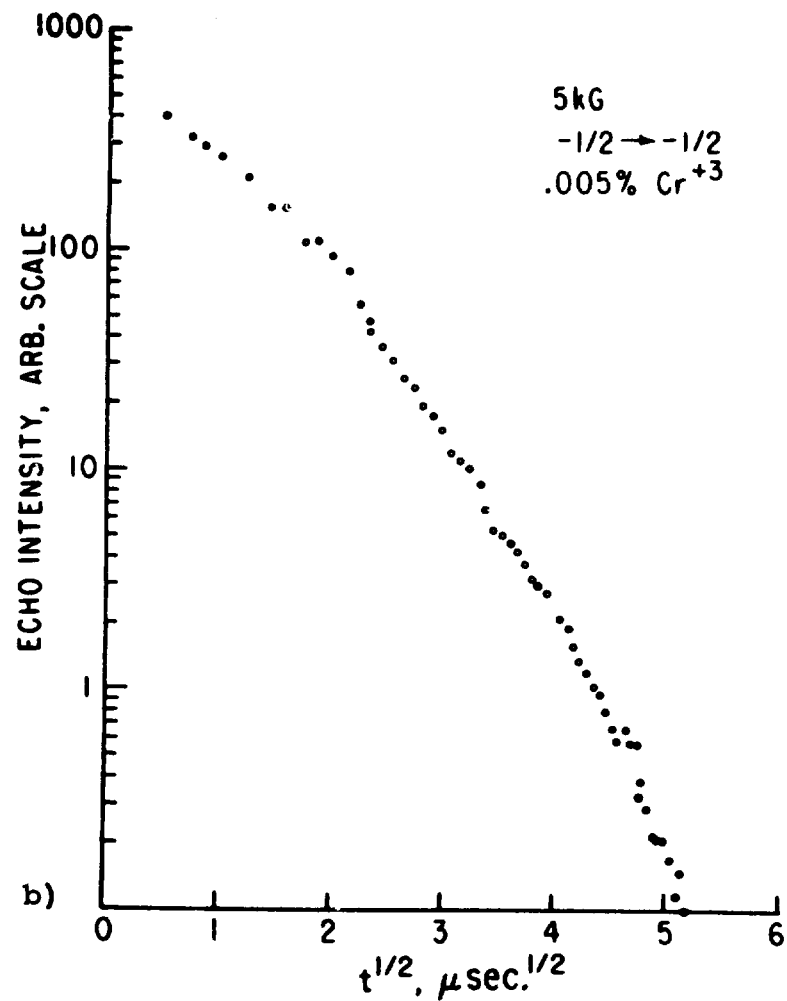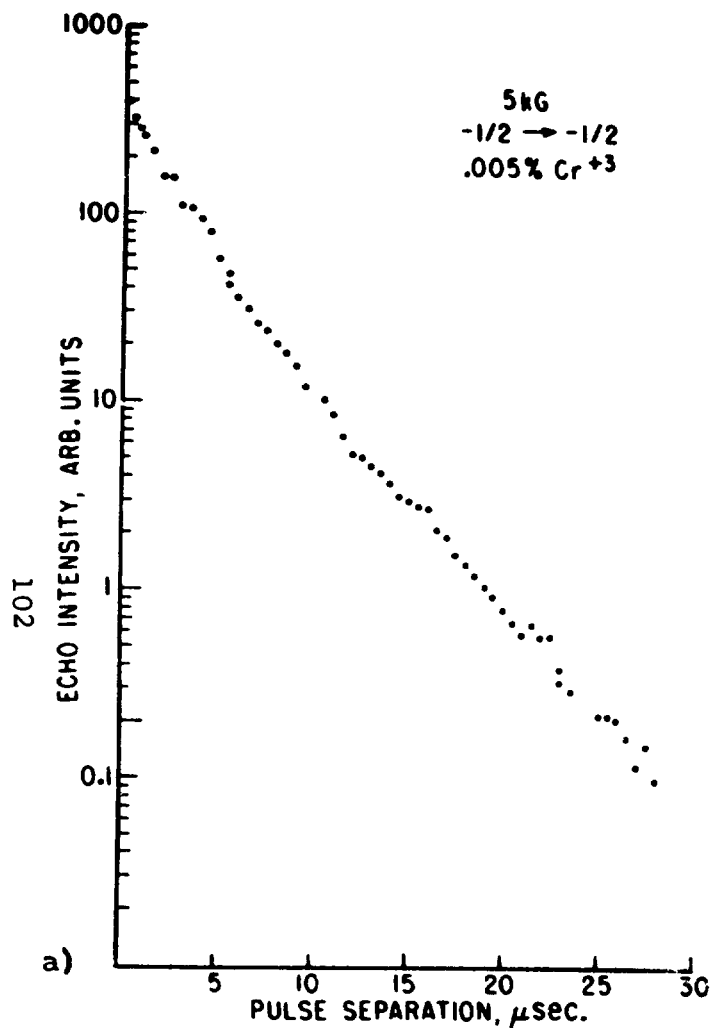
102 (vertical page number)

102

Fig. 48. a) Typical photon-echo exponential decay. b) Same data plotted vs $t^{1/2}$.

TABLE XIII. Results of least-squares fit to the function $S = A \exp(B\tau^N)$ of photon-echo exponential decay.

Cr^{+3}(%)	Date of Experiment	H(kG)	N	Error($\pm$)
0.037	3/27/73	5.0	0.95	0.65
0.02	7/26/73	3.0	0.97	0.32
0.17	7/30/73	3.0	1.34	2.21
0.17	7/31/73	3.0	1.40	0.75
0.02	7/26/73	5.0	0.82	0.26
0.037	3/26/73	0.75	1.80	1.75
0.037	3/26/73	0.75	1.43	1.17
0.037	3/27/73	0.5	1.66	1.86
0.037	3/27/73	1.0	0.65	0.76
0.02	7/26/73	0.5	0.74	0.67
0.02	7/26/73	0.75	0.31	0.55
0.02	7/26/73	1.0	0.77	0.39
0.005	9/6/73	5.0	0.81	0.12
0.035	6/6/73	1.95	0.86	0.37

decay factor, whose decay time was estimated from the data. At lower fields, the depth of the modulation is quite substantial. The agreement between theory and experiment is generally fair, bu'·' poor when compared to spin-echo modulation results.

3. Concentration-Dependent Relaxation

We have measured the concentration and field dependence of the exponential decay of the photon echo for a large number of concentrations and fields, and all the decays appear as a simple exponential. In Fig. 48a we plot the echo intensity versus τ for a 0.005% Cr^{+3} sample at 5 kG. The decay appears to be a simple exponential when compared to Fig. 48b which is a plot of the same data against $\tau^{1/2}$. One should note the difficulty in distinguishing between $\exp(-a\tau^{1/2})$, which is the decay observed by Compaan,[8] and $\exp(-bn\tau)$ as we have observed in the limit of high fields.

To indicate the difficulties involved, we performed a least-squares fit to the function $S = A \exp(-B\tau^{N})$ for approximately 20 different decays. The data in Fig. 48 show the most points and would be expected to yield the most accurate result. The numerical analysis yielded the result $N = 0.81 \pm 0.12$, which seems to favor the simple exponential decay. Some of the other results are given in Table XIII. It appears that the standard deviations are sufficiently large to admit either $N = 1/2$ or $N = 1$ as possible solutions. We hope to alleviate this ambiguity with the new experimental setup, when we extend pulse separations beyond the present two decades. We should then obtain more data points per curve and more accurate results.

A description of recent photon-echo experiments is being prepared for publication, and experiments will continue in photon-echo exponential decay and photon-echo modulation.

(1) CRL Progress Report, June 30, 1973, p. 72.

(2) E. L. Hahn, Phys. Rev. 80, 580 (1950).

(3) P. F. Liao and S. R. Hartmann, Solid State Comm. 10, 1089 (1972).

(4) P. F. Liao, R. W. Leigh, P. Hu, and S. R. Hartmann, Phys. Letters 41A, 285 (1972).

(5) P. F. Liao and S. R. Hartmann, Phys. Rev. B 8, 69 (1973).

(6) D. Grischkowsky and S. R. Hartmann, Phys. Rev. B 2, 60 (1970).

(7) L. Q. Lambert, Phys. Rev. B 7, 1834 (1973).

(8) A. Compaan, Phys. Rev. B 5, 4450 (1973).

C. ECHO BEHAVIOR IN RUBY*

(P. Fu, S. R. Hartmann)

We have extended the range of pulse separation for which electron-spin echoes at 9.31 GHz in the $^4A_2$ ground state of ruby can be observed. We have measured echoes of +1/2 and -1/2 Zeeman levels in a magnetic field of approximately 3.3 kG, and +3/2 and +1/2 Zeeman levels in a field of approximately 7.5 kG. Echoes of the Zeeman +1/2 → +3/2 transition in a magnetic field of about 0.785 kG have not been observed because of the very weak echo amplitude, which is a factor of ~10^3 smaller than that associated with the +1/2 → -1/2 Zeeman transition. The range of pulse separation is 0.5 to 7.0 μsec for the +1/2 → -1/2 transition and 0.5 to 16.4 μsec for the +3/2 → +1/2 transition. Because the echo amplitude decays as the time separation between the exciting microwave pulses is increased, we observed the echoes by signal averaging. The echo was fed to an analog-to-digital converter whose digital output was interfaced into a PDP8/e computer. The time separation between the microwave pulses was controlled by computer and measured by a frequency counter. The optical axis of the ruby crystal was aligned parallel to the dc magnetic field. The Cr_2O_3 concentration was 0.005% by weight. We pumped the helium to increase the signal-to-noise ratio and measured the echoes at a temperature of ~2°K.

Using the following spin Hamiltonian, we calculate the spin-echo amplitude as a function of pulse separation:[1]

$$\mathcal{H} = g\beta HS_z + D[S_z^2 - \tfrac{1}{3}S(S+1)] + \sum_j \{-\hbar\gamma HI_z^j + S_z[(A+B_z)^j I_z^j\}$$
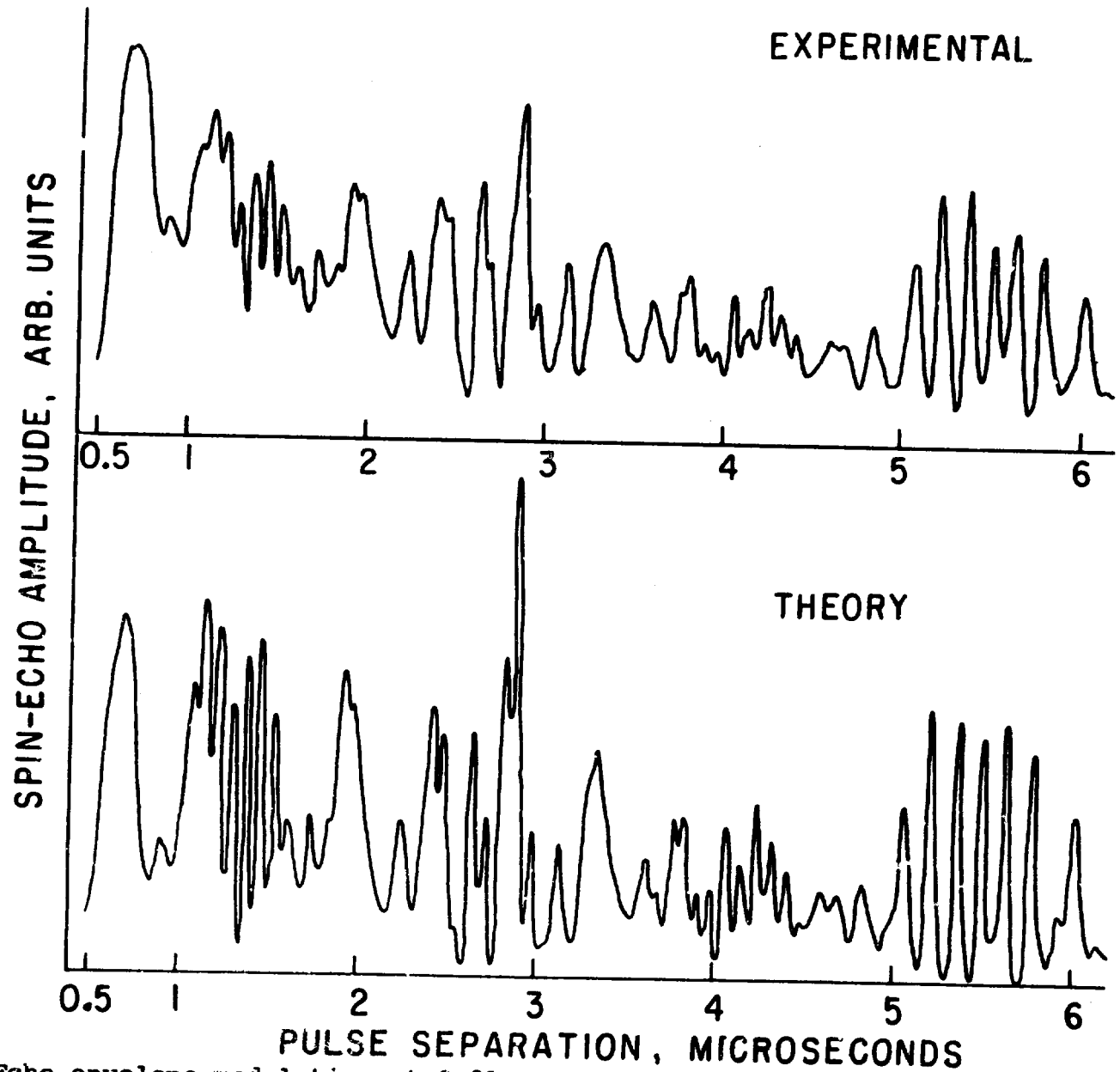
105

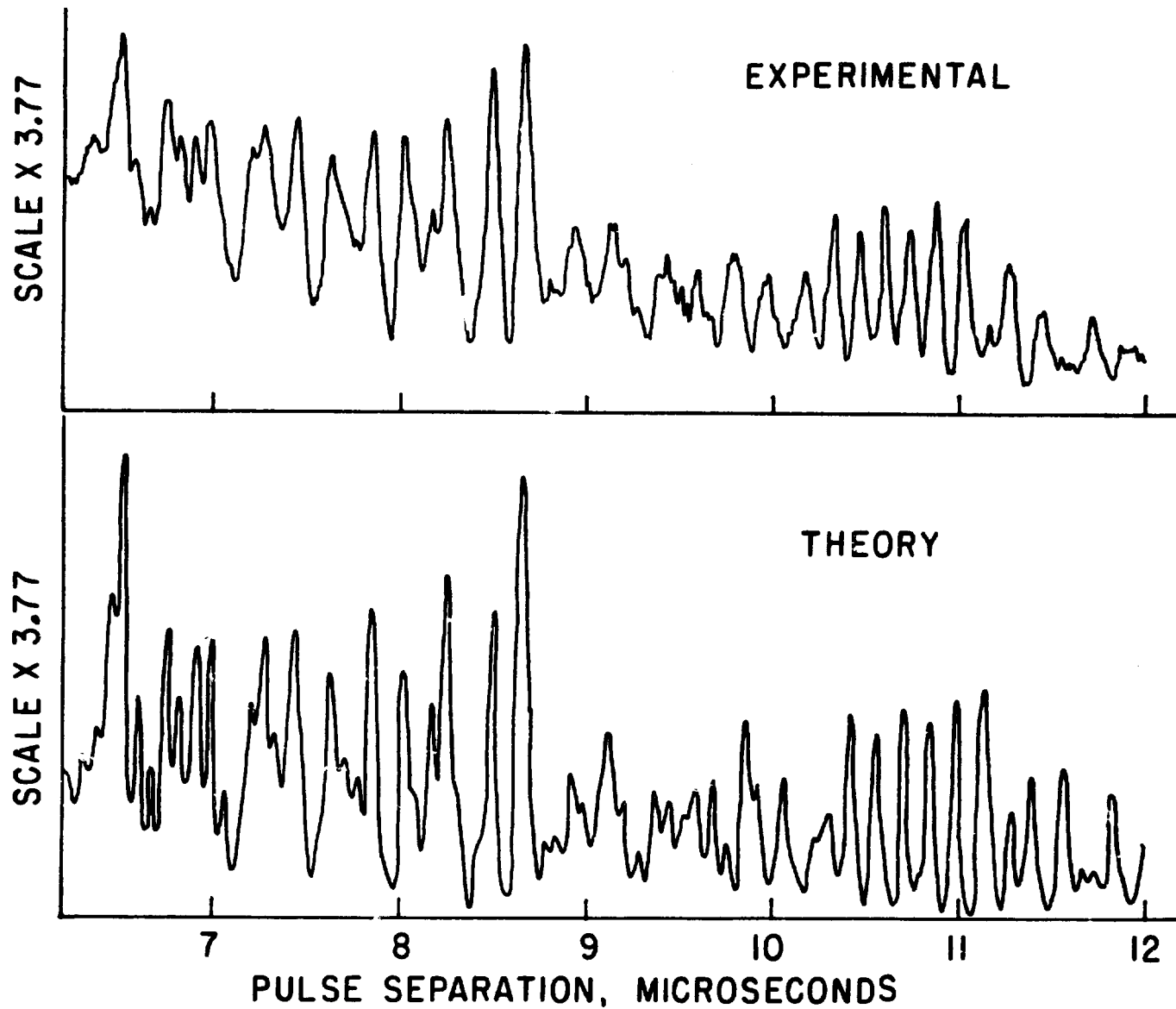Fig. 49. Echo-envelope modulation at 9.31 GHz, 7.5 kG, for a pulse-separation range of 0.5 to 6 μsec.

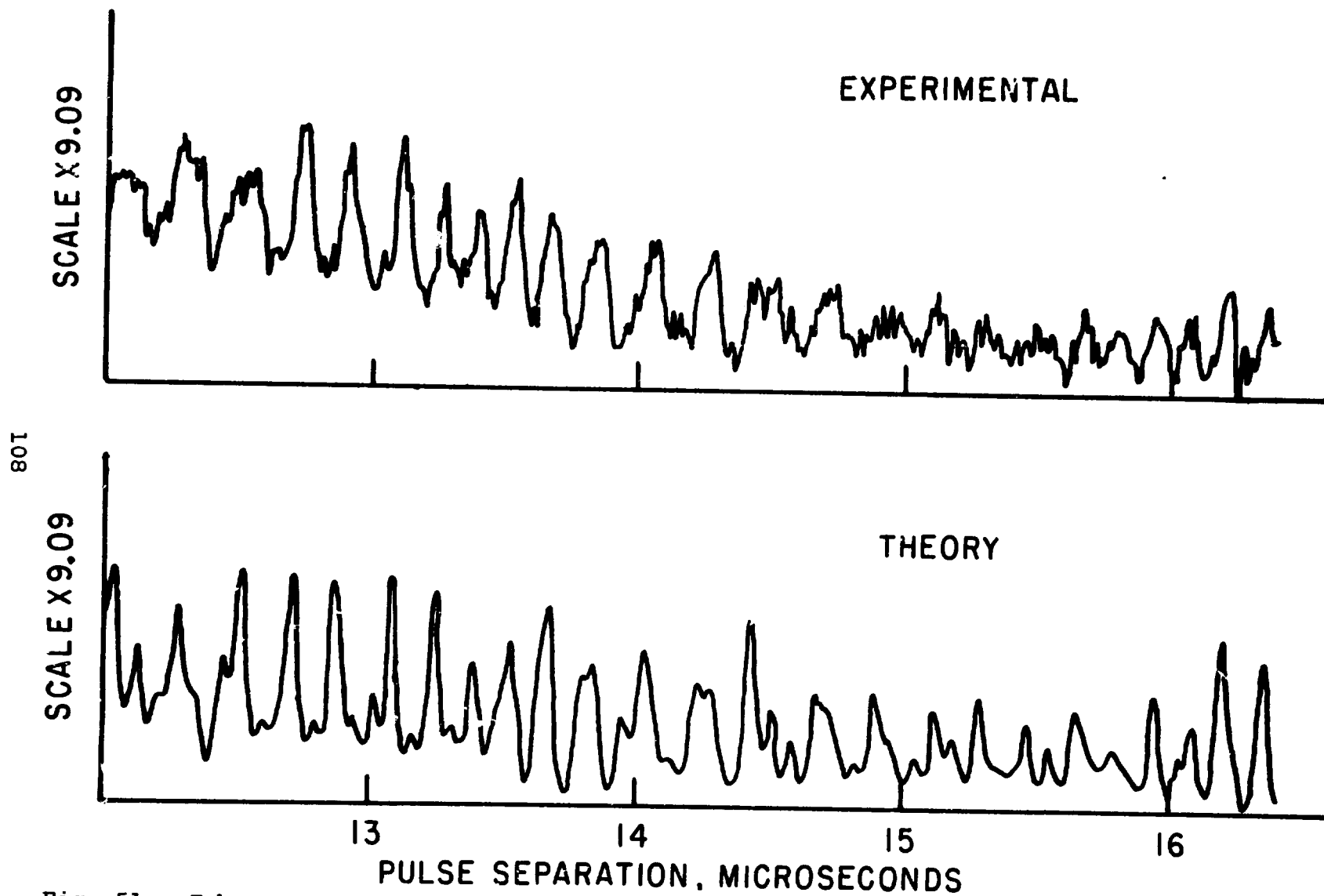Fig. 50. Echo-envelope modulation at 9.31 GHz, 7.5 kG, for a pulse-separation range of 6 to 12 μsec.

Fig. 51.   Echo-envelope modulation at 9.31 GHz, 7.5 kG, for a pulse-separation range of 12 to >16 μsec.

$$+ B_t{}^j I_1{}^j] + \theta^j \exp(-i\theta_1 I_2{}^j) \exp(-i\theta_2 I_1{}^j) \exp(-i\theta_3 I_z)$$

$$\times [I_z{}^{j2} + \frac{\eta}{3} (I_1{}^{j2} - I_2{}^{j2})] \exp(i\theta_3 I_z{}^j) \exp(i\theta_2 I_1{}^j)$$

$$\times \exp(i\theta_1 I_2{}^j)\}$$

where A^j, $B_z{}^j$, $B_t{}^j$, θ^j, θ_1, θ_2, θ_3, and η are the hyperfine inter-action constants of neighboring aluminum neighbors. These parameters were measured using the technique of echo ENDOR.[2] The subscripts 1 and 2 refer to the direction in the transverse plane parallel to and perpendicular to the transverse component of the local field at the aluminum neighbor site, respectively.

The results of the $+1/2 \rightarrow -1/2$ transition at 3.3 kG are the same as our previous measurements.[3] The experimental curves of transition $+3/2 \rightarrow +1/2$ at 7.5 kG are shown as the upper curves in Figs. 49, 50 and 51. The lower curves in the figures are the theoretical calculations, for which we assume an exponential decay with decay constant $1/T \simeq 0.25$ μsec^{-1} in order to approximate the effect of dephasing interactions not included in the Hamiltonian. Although the relative magnitudes of the peaks are not correct, the general features of the echo behavior agree extremely well.

Program for the next interval: We will measure the spin-echo modulation of ruby for the $-1/2 \rightarrow -3/2$ and $+1/2 \rightarrow -1/2$ transitions at 16.2 GHz. We will also set up the apparatus for the spectral-diffusion experiment.[4]

(1)   D. Grischkowsky and S. R. Hartmann, Phys. Rev. B 2, 60 (1970).

(2)   P. Liao, Ph.D. thesis, Columbia University, 1973 (unpublished).

(3)   CRL Progress Report, June 30, 1973, p. 102.

(4)   P. Hu and S. R. Hartmann, Phys. Rev. B 9, 1 (1974).

D. RAMAN ECHOES*

(A. Flusberg, S. R. Hartmann, R. A. Weingarten)

Using an improved apparatus, we have studied several nonlinear processes in atomic thallium vapor. We are seeking to optimize parameters for the generation and detection of Raman echoes. Consequently, we have examined stimulated Raman scattering (SRS) and four-wave parametric mixing (FWM) in the thallium vapor.

Stimulated Raman scattering in thallium vapor is usually accompanied by self-focusing of the incident ruby-laser pulse.[1] To overcome this, a 1/16-in aperture was placed in the oscillator of the ruby laser to restrict possible transverse laser-cavity modes. We measured the far field laser-intensity distribution of the system using a pinhole in the focal plane of a lens and a photodetector. The intensity distribution was approximately Gaussian with a half-width (at $1/e^2$) divergence of 0.66 mrad. Because of the small aperture in the laser oscillator, total laser power was reduced to 5 to 15 MW. Therefore, we used a 1-m focal length lens to focus the laser beam at the center of the thallium-vapor zone of the heat-pipe oven.[2] In the presence of SRS, we measured the divergence of the laser beam leaving the oven and found that it had increased to 1.23 mrad. No evidence of self-focusing was observed.

The generated Stokes light was detected with fast and slow photodetectors. A typical Stokes pulseshape is shown in Fig. 52. The exciting laser pulse was basically smooth, although there was some modulation corresponding to the interference of different longitudinal modes of the laser oscillator. Fabry-Perot analysis of the laser pulse indicated that most of its energy was concentrated in one or two modes approximately 1 GHz apart. Stokes pulseshape modulations do not appear to correspond to any laser modulations.

Despite the presence of the modulations, the Stokes energy followed a fairly regular pattern as a function of thallium vapor pressure (see Fig. 53). The high density points correspond to a
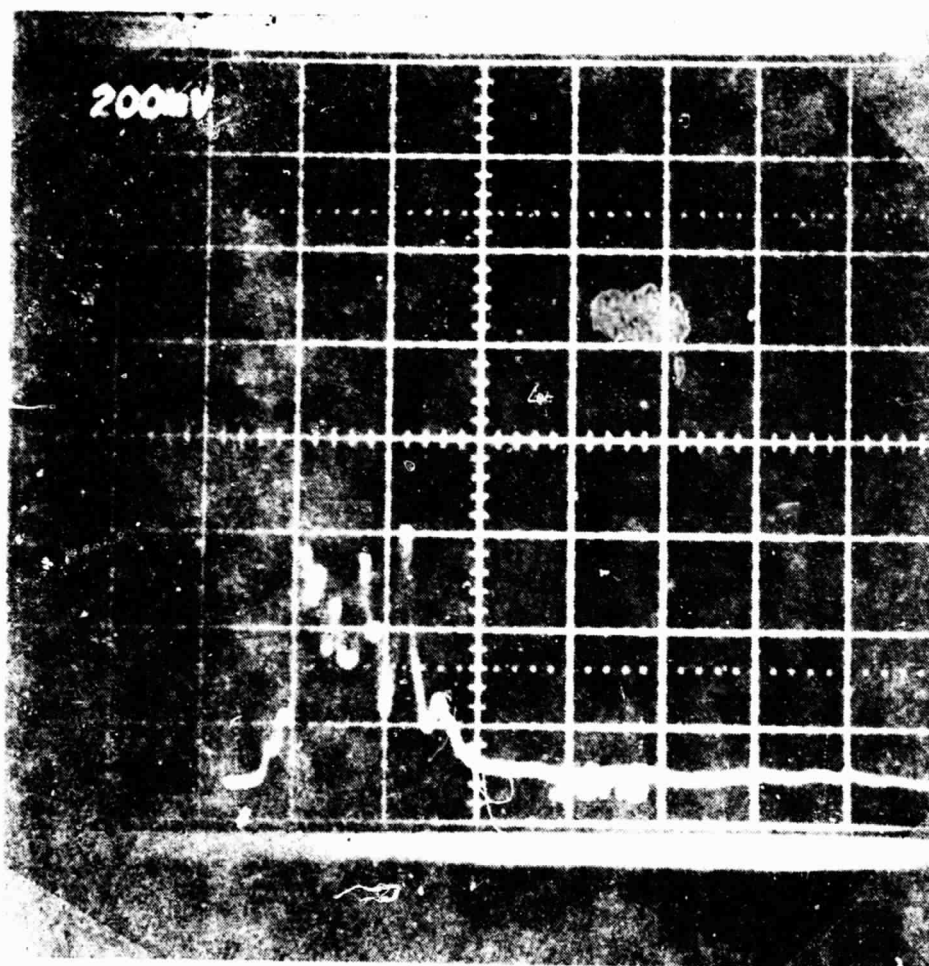
Fig. 52. Stokes pulseshape at 90 torr thallium vapor
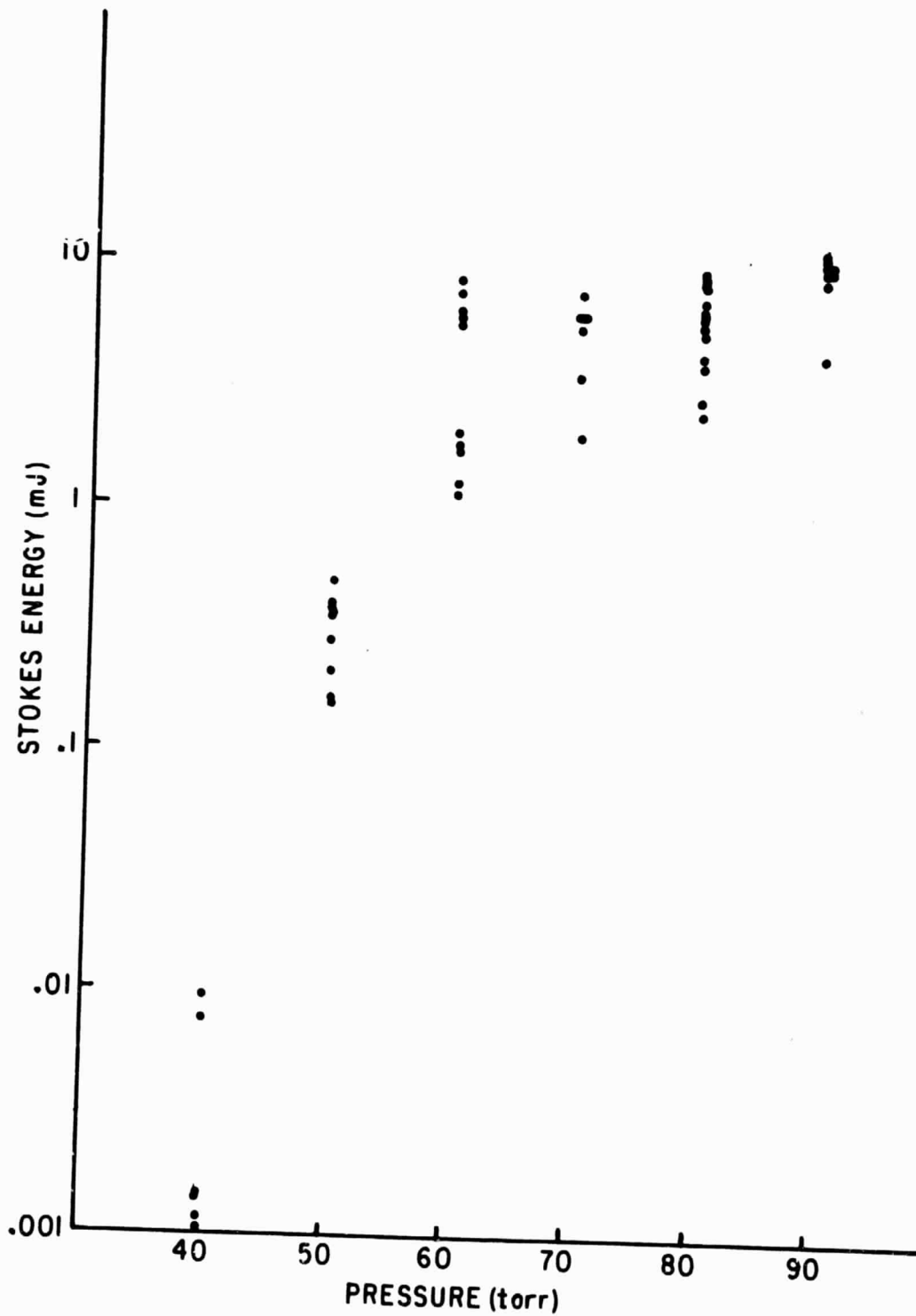pressure. Stokes energy = 1.2 mJ.

111

Fig. 53.   Stokes energy output as a function of thallium
vapor pressure at constant laser-pulse power.

112

saturation of the medium wherein an appreciable fraction of the thallium atoms are being excited by the SRS. The threshold near 40 torr is very sharp, as indicated in the figure.

The Raman-echo effect arises from the rephasing of a macroscopic excitation of the thallium atoms following their interaction with two laser-Stokes pulses. Each atom is driven into a superposition of the two lowest lying states, the $6^2P_{1/2}$ ground state and the $6^2P_{3/2}$ metastable state. Because these two states are not coupled by an electric dipole transition (as they are in the photon-echo experiment) the rephased excitation can be detected only by use of a third frequency, at the time of the echo, to induce dipole moments in the atomic ensemble. As a prelude to this, we examined the effect of the third frequency pulse, from a tunable dye laser, simultaneously incident on the vapor with a laser-Stokes pulse. In form, this interaction is very similar to four-wave mixing with the fourth wave, generated in the vapor, being the Stokes or anti-Stokes frequency of the dye-laser frequency.

The thallium vapor was contained in a 15-cm long quartz cell. The dye-laser anti-Stokes frequency was detected using a IP28 photomultiplier tube (see Fig. 54). Some integration in the detector and electronics can be assumed. Using a gated pulse stretcher to integrate the photomultiplier pulse, we obtain a measure of the energy contained in the dye-laser anti-Stokes pulse. In Fig. 55, we have plotted this value, normalized by the dye-laser energy, as a function of the product of the laser and Stokes energies. Although there are point-to-point fluctuations, the data fall very close to a straight line. A least-squares fit of the points yields for the slope a value of 0.96 ± 0.02 without consideration for experimental uncertainties.

The dye laser was tuned to be near the $6^2P_{3/2} \to 7^2S_{1/2}$ (5350-Å) transition to enhance the FWM process. The effect of varying the thallium vapor density in the quartz cell on the scattering is indicated in Fig. 56. The lowest density points indicate an N^2-dependence of the scattering, whereas a least-squares fit of all the points except the highest density point indicates a slope of 1.58. It is clear that the scattering as a function of density is turning over. This is an effect attributable to phase mismatch among the four waves inter-
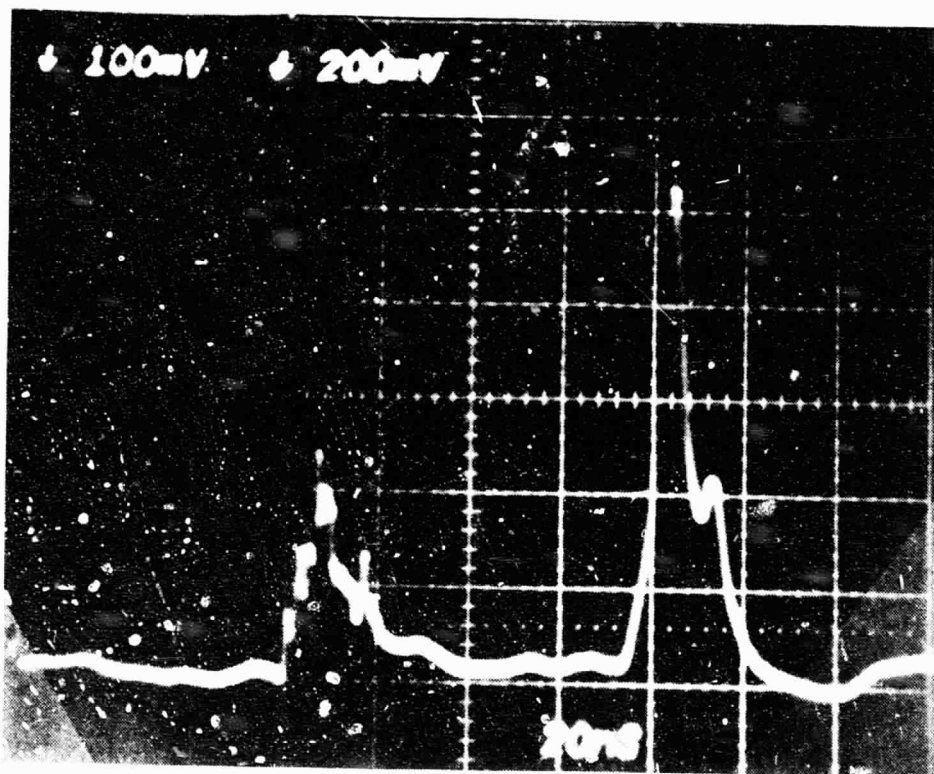
SP   PM

Fig. 54.   Dye-laser anti-Stokes pulse as detected by
           photomultiplier (PM) and corresponding
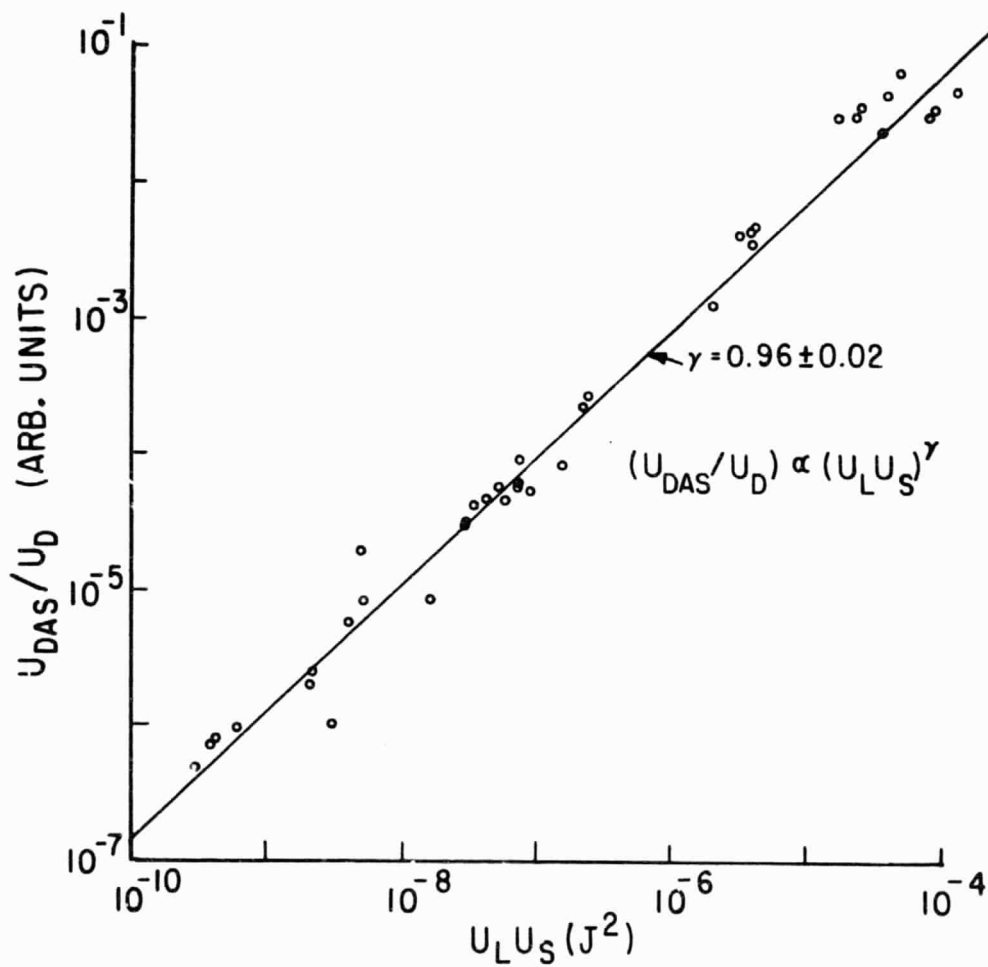   Stokes pulseshape (SP).

114

Fig. 55. Normalized dye-laser anti-Stokes signal as a
function of the product of the laser and Stokes
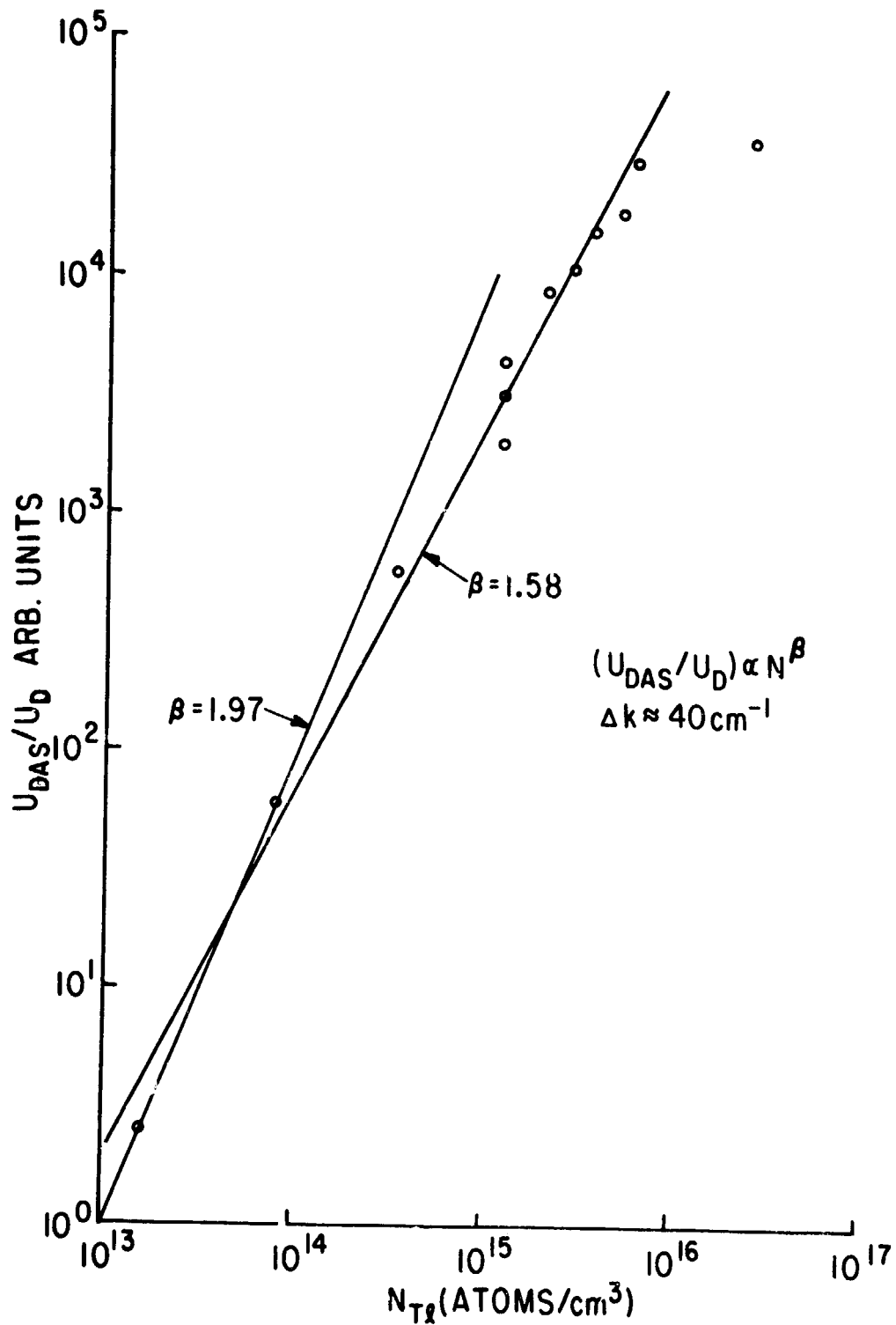energies at constant vapor density.

115

Fig. 56. Normalized dye-laser anti-Stokes signal as a function of thallium vapor density.

acting in the FWM process.

Program for the next interval: We believe that a better under-
standing of SRS in thallium vapor is essential. We are examining
this process experimentally and theoretically to determine the opti-
mum conditions in which to observe the Raman echo.

(1) R. A. Weingarten, L. Levin, A. Flusberg, and S. R. Hartmann,
Phys. Letters 39A, 38 (1972).

(2) C. R. Vidal and J. Cooper, J. Appl. Phys. 40, 3370 (1969).

E. COHERENCE EFFECTS IN TWO-PHOTON ABSORPTION

(Z. Friedlander, S. R. Hartmann)

We have increased by more than a factor of four the power-output
capability of our temperature-tuned ruby laser and have carefully
studied the dependence of the fluorescence from cesium gas excited
by a two-photon absorption on the incident laser intensity over this
extended power-output range. We have investigated two of the casca-
ding single-photon fluorescences, namely the $9^2D_{5/2} \rightarrow 6^2P_{3/2}$ and
the $7^2P_{3/2} \rightarrow 6^2S_{1/2}$ decays, following the $6^2S_{1/2} \rightarrow 9^2D_{5/2}$ two-photon
excitation.

We obtain Q-switched laser pulses that are 8 nsec long and up
to 100 MW/cm^2 in intensity. The output wavelength can be tuned over
the range 6934 Å to 6943 Å in steps of 0.05 Å to 0.01 Å by changing
the temperature of the ruby. A given ruby temperature can be re-
produced from shot to shot to within 0.05°C; this indicates a wave-
length stability of better than 0.01 Å. We have previously deter-
mined that maximum fluorescent yield for the above transitions is
obtained at a ruby temperature of -116.2 ± 1.3°C, corresponding to
a laser-output wavelength of 6935.76 ± 0.4 Å. This photon energy
corresponds to one-half the $6S_{1/2} \rightarrow 9D_{5/2}$ energy interval in cesium,
and we note that there is no level that can be reached from the
ground $6S_{1/2}$ state with the absorption of a single photon of this

energy. Most of the experiments described below were performed with the ruby at a temperature of -116.4°C.

Fabry-Perot pictures taken at 15- to 20-MW/cm^2 laser-output intensity show several longitudinal modes lasing, with the average width of the laser line being 0.075 cm^{-1}. The natural width of the R_1 line in ruby at this temperature is 1.5 cm^{-1}. At higher power levels more modes lase, with a corresponding increase in the frequency width of the laser line.

As in previous experiments, the unfocused laser light, filtered by a long-pass #2-58 Corning glass filter, is incident on the 15-cm Pyrex cell containing the cesium. The cell is kept in a temperature-regulated oven at 200 ± 1.5°C, corresponding to a gas pressure of 0.1 torr and a density of 2.21 × 10^{15} atoms/cm^3. The laser power incident on the cesium cell is varied by means of neutral density filters placed before the oven. The fluorescence is observed by means of a 1P28V1 RCA photomultiplier tube, preceded by a copper sulfate filter to eliminate the laser light, and an interference filter appropriate for the wavelength being observed. Part of the laser beam is split off before reaching the cesium cell and, appropriately filtered, is incident on a Monsanto MD 1 diode. The photomultiplier tube and diode outputs are simultaneously displayed on a dual-beam 555 Tektronix oscilloscope operating in the "add" mode. Thus the laser pulse and the fluorescence pulse were photographed together for every shot.

We have seen the 5846.58-Å $9D_{5/2} \rightarrow 6P_{7/2}$ and the 4555.20-Å, $7P_{3/2} \rightarrow 6S_{1/2}$ decays following the two-photon $6S_{1/2} \rightarrow 9D_{5/2}$ absorption and have studied the dependence of the fluorescent intensity and pulsewidth in both transitions on the incident laser intensity and pulsewidth and on the density of the cesium. The radiative lifetimes of the $9D_{5/2}$ and $7P_{3/2}$ levels in cesium are calculated to be 200 nsec and 120 nsec respectively. The calculated mean life-time between collisions for an ideal gas at 200°C and 0.1 torr is

1.27×10^{-6} sec, or about two orders of magnitude longer than our expected radiative lifetimes.

The 5846-Å fluorescence was studied at incident laser powers in the range 0 to 90 MW/cm^2. The laser pulsewidth (FWHM) varied between 9 and 10 nsec in this experiment. At 4-MW/cm^2 incident laser power we obtain fluorescent pulses 29 nsec long. In the 4- to 24-MW/cm^2 range we observe a dramatic decrease in the fluorescent pulsewidth from 29 to ~8 nsec, with most of the decrease occurring below 16-MW/cm^2 incident laser power. The fluorescent pulsewidth stays at 7 - 8 nsec for 24 - 90 MW/cm^2 incident laser power. The fluorescent pulsewidth is thus two to four times that of the laser at low incident power levels.

The fluorescent light intensity at 5846 Å varies linearly as the square of the input laser intensity, as we would expect for a second-order process; but its behavior divides itself into two regions, depending on the laser intensity. In the 0- to 42-MW/cm^2 incident laser-power range, which we shall call Region 1, the fluorescent intensity increases linearly as the square of the laser intensity with a slope of 1.7×10^{-40} flr. photons/(laser photons)^2. This represents data taken over a range of ruby temperatures from -116.4°C to -117.9°C, and the results were consistently reproducible in experiments performed many months apart. Region 2 corresponds to high, never before attained, incident laser power levels that range from 42 to 90 MW/cm^2. The fluorescent intensity also varies linearly as the square of the incident laser intensity, but with a slope of only 3.7×10^{-41} flr. photons/(laser photons)^2. Thus there is a leveling off of the fluorescent intensity yield at higher incident laser powers, as unusually short lifetimes are obtained.

The 4555-Å fluorescence corresponding to the $7P_{3/2} \rightarrow 6S_{1/2}$ transition, or lower leg of the cascading single-photon transitions back to the ground state, was studied in a similar way for incident laser power in the range 0 to 72 MW/cm^2. Its behavior is different from

119

that of the 5846-Å fluorescence. The fluorescent pulsewidth increases only slightly, rather than decreasing at higher incident laser intensities. The duration of the fluorescent pulse for this transition is also an order of magnitude shorter than the calculated incoherent radiative lifetime. The fluorescent intensity vs laser-intensity-squared dependence also has two distinct regions of linear dependence, but the fluorescent intensity rises sharply, rather than leveling off, at high incident laser-power.

The incident laser intensity was varied between 0 and 7 MW/cm^2. The duration of the laser pulse was 7.5 to 9 nsec throughout this power range. We obtained fluorescent pulses 3 to 4 nsec in duration in the range of 0- to 14-MW/cm^2 incident laser power, with the pulsewidth increasing slightly to 4 to 5 nsec for incident laser power in the range 14 to 72 MW/cm^2. In the region of 0- to 12.2-MW/cm^2 incident laser power, the fluorescent intensity varies directly as the square of the laser intensity, with a slope of 1.6×10^{-40} flr. photons/(laser photons)^2. At a threshold of 22.8-MW/cm^2 incident laser power the fluorescent yield increases by three orders of magnitude to a slope of 1.5×10^{-37} flr. photons/(laser photons)^2. This linear dependence with the higher slope holds for the entire region 22.8- to 72-MW/cm^2 incident laser power. Note that the laser power threshold for the high yield of 4555-Å fluorescence is roughly the same as that for the production of the very short-lived, 8-nsec, 5846-Å fluorescence.

As previously reported, no fluorescence can be obtained when the ruby temperature is tuned above -114°C or below -121°C, or when the cesium cell is at room temperature. (The melting point of cesium is 28.5°C.) The fluorescent intensity drops sharply as the cesium temperature is decreased. The number density of the cesium atoms in the cell drops by about an order of magnitude for every 50°C decrease in temperature. Experiments are in progress to determine the exact nature of the dependence of the fluorescent intensity on the density

cf the cesium vapor. Theoretical study of the above experimental results is in progress, as are further experiments to study coherent effects in two-photon absorption.

F. FREQUENCY SHIFTS IN RESONANT SYSTEMS*
(R. Friedberg, M. Friedlander, S. R. Hartmann)

We have completed construction of the experiment to measure the predicted shift in the resonance-transition frequency of atomic cesium. The tungsten-ribbon lamp housing is fitted with two collimator assemblies in order to use the light coming from both sides of the tungsten ribbon.

Each of the two cell-reservoir assemblies is housed in a two-section oven that will bake out the cell-reservoir assemblies prior to filling and control their temperatures during the experiment. Since the density of cesium in the absorption cell is the variable we wish to control, we must control separately the temperature of the absorption cell and that of the reservoir. We maintain the temperature of the reservoir lower than that of the cell so that the reservoir temperature determines the vapor pressure in the cell-reservoir assembly. We can then control the density in the cell by controlling the cell temperature. The temperature in the cell-reservoir assemblies is monitored by high output thermocouples and regulated by a four-channel proportional temperature controller with a stability of 0.005%.

We have obtained beam-splitting and beam-recombining optics which allow us to use for stabilization whichever of the cesium-resonance transitions is not being used for the experiment. Using an rf excited cesium lamp with this optical system, we are able to monitor the alignment and stability of both Fabry-Perot interferometers

simultaneously during the experiment. We use a PDP-8/e computer interfaced to an analog-to-digital converter and to eight stepping motors (which rotate 10-turn potentiometers to control the parallelism and separation of the plates in the two Fabry-Perots) to lock the Fabry-Perots onto the cesium-resonance line.

We have aligned the exit-slit prism and have used it to separate the high and low frequency sides of the resonance lamp profile. Some initial parasitic light problems caused by the accidental equality of the prism apex angle and the bevel angle of the exit slit have been overcome.

The outputs of the two RCA 31034 photomultiplier tubes are clipped, using fast hot carrier diodes, to eliminate large noise spikes of unknown origin which are characteristic of this photomultiplier tube. This precaution prevents overloading of the lock-in amplifiers in their more sensitive ranges. The total power through-put of the system agrees with calculations based on the brightness of the tungsten lamp and the transmittance of the optical components.

The four signals of interest from the four lock-in amplifiers are monitored by the eight-channel analog-to-digital converter of the PDP-8/e computer (the same one used for Fabry-Perot stabilization). Fabry-Perot stabilization and signal averaging proceed simultaneously. We will measure the frequency shift in the near future.

G. FREE-INDUCTION TWO- AND THREE-PULSE ECHO DEGRADATION DUE TO SPECTRAL DIFFUSION USING AN UNCORRELATED RANDOM-JUMP MODEL*
(P. Fu, S. R. Hartmann, P. Hu)

As stated in last year's Progress Report,[1] we have calculated the behavior of the free-induction, two-pulse echo, and three-pulse

echo signals using a sudden-jump model of spectral diffusion decay.[2] We have worked in the time domain, and our results, which are expressed in closed form, are equally valid for short, intermediate, and long times. Our model assumes that the monitored resonance signal arises from a set of spins, labeled A, which are isolated from each other; the A-spin signal is relaxed by the fluctuating dipolar field of spins, labeled B, which are flipping randomly between two quantum states at an average rate W. The A and B spins can be treated as spin 1/2 systems, and spin placement is random. This is the model, and it is solved exactly. Klauder and Anderson[3] and Mims[4] have also worked with a sudden-jump model (or its equivalent). Our formulas for the signal behavior reduce to theirs for the two-pulse and three-pulse echo for short times[5] and for the two-pulse echo for long times.[6]

The experimental situation has been unclear. Mims has measured the behavior of two-pulse and three-pulse echoes in $CaWO_4$ crystals doped with either Ce and Er or with Mn and Er. In both samples it is the flipping of the Er spins due to spin-lattice interactions (T_1 processes) which causes the spectral diffusion. His analysis of experimental results did not favor a sudden-jump model; however, he did not rule it out completely. He noted major discrepancies between his experimental and his calculated values of T_M (the time it takes the signal to decay to 1/e of its original value) that make it impossible to decide conclusively in favor of any particular model.

We have reanalyzed the experimental data of Mims[7] using our formulas, and we find rather good agreement with the sudden-jump model for those of his experiments in which either the Mn- or the Ce-echo signal is studied. On the other hand, we are unable to explain his experiment in which the Er-echo signal is studied.

For the two-pulse echo we found the echo amplitude to be given by

$$E(2\tau) = \exp\left[-(\Delta\omega_{1/2}/W)K(2W\tau)\right], \tag{1}$$

with

$$K = z\left[\exp(-z)\right]\{I_1(z) + (\pi/2)\left[I_1(z)L_0(z) - L_1(z)I_0(z)\right]\}. \tag{2}$$

In Eq. (1) the linewidth is given by

$$\Delta\omega_{1/2} = \left[16\pi^2/9(3)^{1/2}\right]n\mu_a\mu_b\hbar^{-1},$$

where τ is the pulse separation time of the B spins, and n is their number density. The terms $I_\nu(z)$ and $L_\nu(z)$ are the modified Bessel and Struve functions of order ν. In the limit $W\tau \ll 1$, $E(2\tau)$ is given by

$$E(2\tau) = \exp(-2W\Delta\omega_{1/2}\tau^2),$$

while for $W\tau \gg 1$, it is expressed as

$$E(2\tau) = \exp\left[-2(1/\pi)^{1/2}W^{-1/2}\Delta\omega_{1/2}\tau^{1/2}\right].$$

We plot in Fig. 57 the echo amplitude as a function of $\Delta\omega_{1/2}\tau$ for several values of the parameter $\eta = \Delta\omega_{1/2}/W$. Each curve in Fig. 57 starts out as a Gaussian. However, on the scale chosen, the initial Gaussian character for the curves with $\eta = 2 \times 10^0$, 2×10^{-1} is not readily apparent, as it is confined to a small region near the origin. In fact the curve with $\eta = 2 \times 10^0$ approximates a simple exponential, whereas the curve with $\eta = 2 \times 10^{-1}$ first drops precipitately and exhibits approximately an $\exp(-\tau^{1/2})$ behavior. One should note also that for a given value of $\Delta\omega_{1/2}\tau$, the value of $E(2\tau)$ is unity in the limit of very large or very small values of η. It follows that the time $T_M = 2\tau$, at which $E(2\tau)/E(0) = 1/e$, has a minimum. This minimum occurs at $\eta \simeq 1$, i.e. $W \simeq \Delta\omega_{1/2}$. (8)

For the three-pulse echo we found

$$E(2\tau + T) = \exp\{-(1/2)(\Delta\omega_{1/2}/W)\left[(1 - \exp -2WT)G(2W\tau)\right.$$

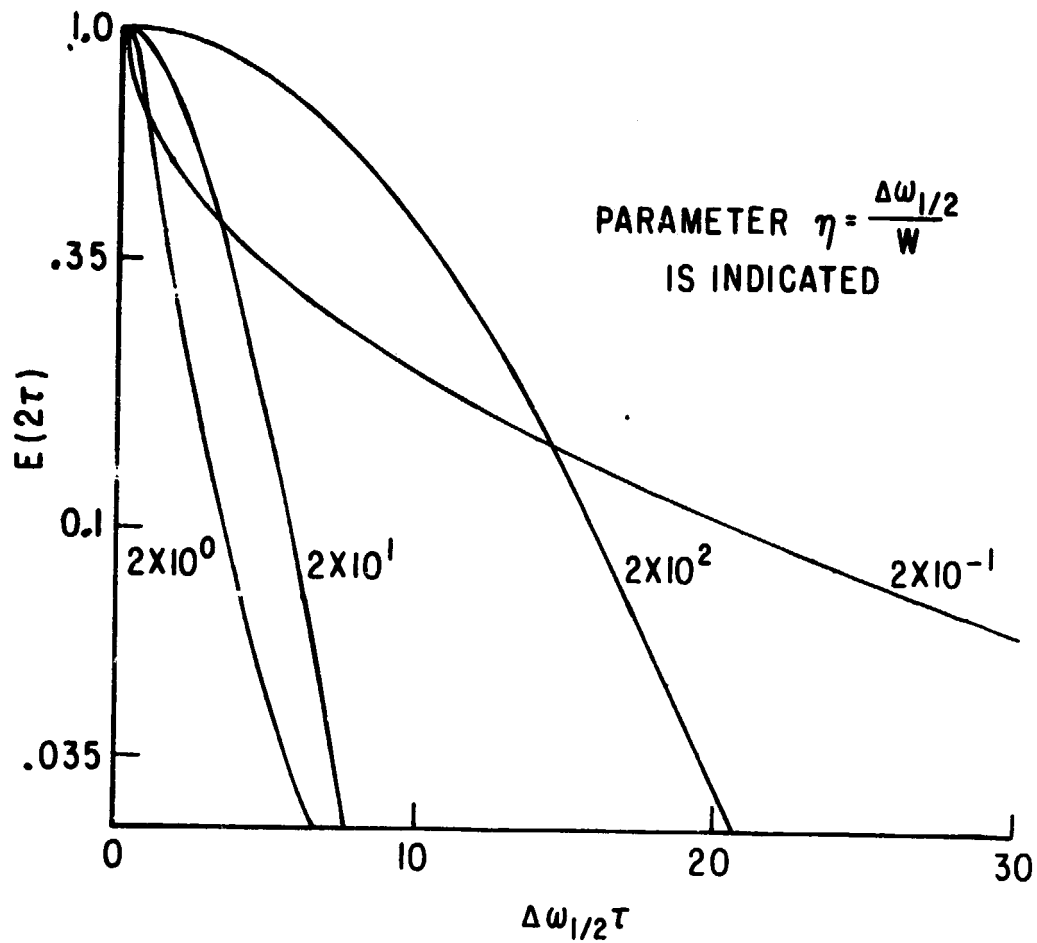$$\left. + (1 + \exp -2WT)K(2W\tau)\right]\}, \tag{3}$$

124

Fig. 57. The echo amplitude $E(2\tau)$ plotted as a function of $\Delta \omega_{1/2}\tau$ for several values of η,

with

$$G(z) = z \exp(-z) [I_0(z) + I_1(z)].$$ (4)

The function $G(z)$ may be evaluated from the formula

$$G(z) = zG'(z),$$

where $G'(z)$ is plotted and tabulated in Ref. (2).

Mims has measured the two-pulse and three-pulse echo envelope for Ce in a $CaWO_4$ sample doped with Er at 9.4 GHz and at several different temperatures.[9] Only the data taken at 2.2°K is published, and these we have fit with our formulas, Eqs. (1) and (3), to obtain the results shown in Figs. 58 and 59. Since both two-pulse and three-pulse echo experiments were performed on the same sample at the same temperature, we have used the same values of $\Delta\omega_{1/2}$ and W in fitting all the data. The fit is reasonably good.

The concentrations of the Ce and Er were 2×10^{18} spins/cm^3 and 2.5×10^{18} spins/cm^3, respectively. This leads to a value of $\Delta\omega_{1/2} = 6.1 \times 10^6$ sec^{-1}, which is only a factor of two larger than that used in our fit. This is probably within the experimental error of the measured Er concentration.

The value of W can be obtained from T_1 by the relation $W = 1/2T_1$. Since the echo amplitude decay of the Ce spins was measured with the applied magnetic field normal to the c-axis, we have not used the value $W = 6.3 \times 10^1$ as would be obtained from Mims' measurement of T_1 for Er^{3+} in $CaWO_4$. Instead we have used the data of Antipin et al.,[10] who measured T_1 in Er-doped $CaWO_4$ with H normal to the c-axis. Their measurements were made at 9.3 GHz and 36 GHz. Extrapolating their measurements to the 54.5-GHz measurement corresponding to the Er^{3+} splitting at which the Ce measurements were made, we find a value of $W = 2.1 \times 10^3$, which is close to the value $W = 3.5 \times 10^3$ used in our fit. We summarize the above data on $\Delta\omega_{1/2}$ and W in Table XIV.

The only echo-envelope data shown for the $CaWO_4$ sample doped with Mn and Er are for the two-pulse echo. Here we have obtained the

126

TABLE XIV. Values of $\Delta\omega_{1/2}$ and W relevant to analysis of Ce-echo data in $CaWO_4$:Ce, Er.

	Mims[a]	Antipin et al.[b]	Our data
$\Delta\omega_{1/2}$	6.1×10^6		3×10^6
W	6.3×10^1 (H $\parallel$ to c-axis)	2.1×10^3 (H $\perp$ to c-axis)	3.5×10^3 (H $\perp$ to c-axis)

(a) W. B. Mims, Phys. Rev. 168, 370 (1968).

(b) A. A. Antipin, A. N. Datyshev, I. N. Kurkin, and L. Ya. Shekun, Soviet Phys. - Solid State 10, 468 (1968).

TABLE XV. Values of $\Delta\omega_{1/2}$ and W relevant to analysis of Mn-echo data in $CaWO_4$:Mn, Er.

	Mims[a]	Our data
$\Delta\omega_{1/2}$	0.55×10^6	0.55×10^6
W	2.5×10^6	2.3×10^6

(a) W. B. Mims, Phys. Rev. 168, 370 (1968).

127

The figure shows a plot with y-axis labeled $E(2\tau)$ (values marked 1.0, .35, 0.1, .035) and x-axis labeled $\tau(\mu sec)$ (values 0, 2.5, 5, 7.5, 10, 10.5). Annotations in the figure: $\Delta\omega_{1/2} = 3 \times 10^6$ and $W = 3.5 \times 10^3$.
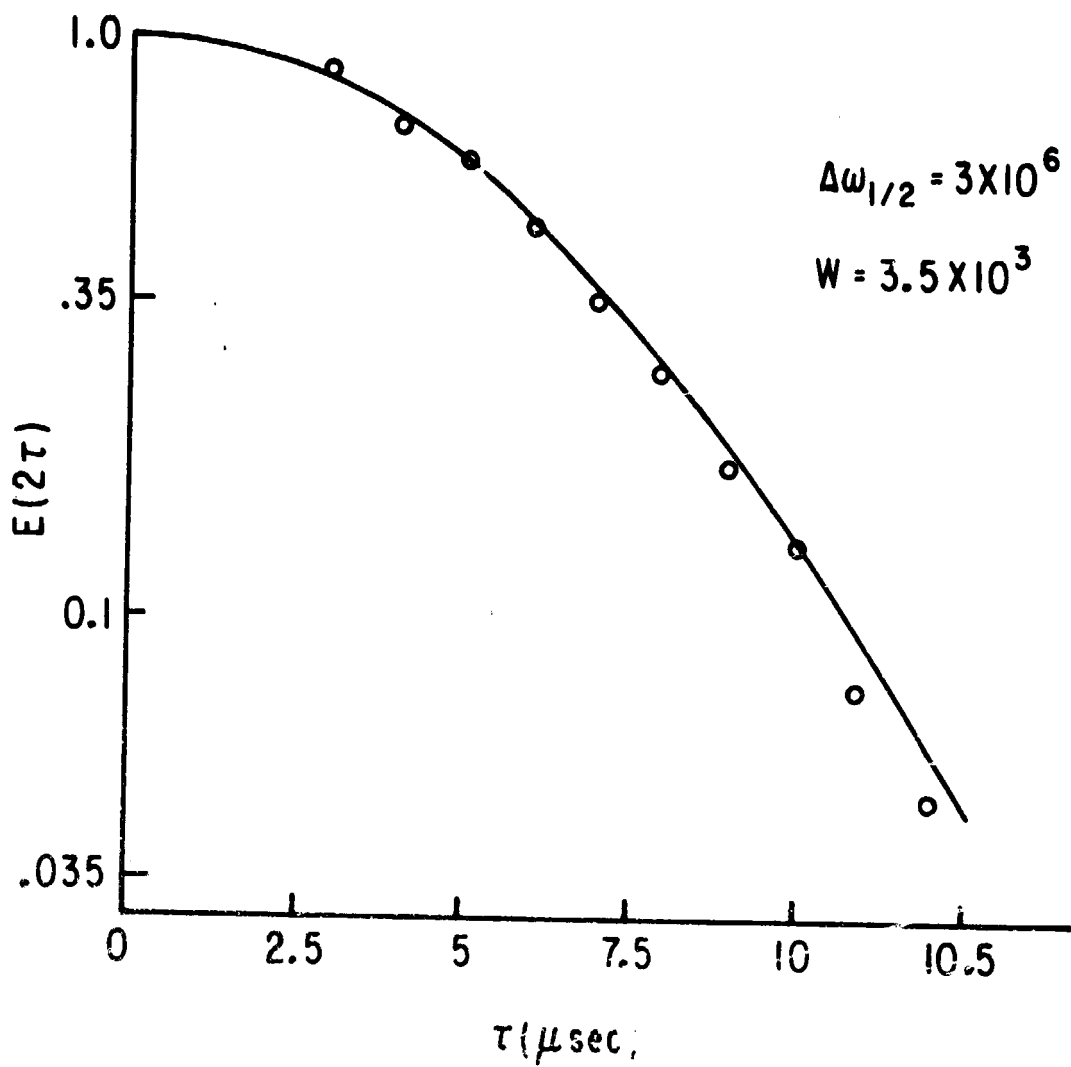
Fig. 58. Two-pulse echo amplitude $E(2_\tau)$ for Ce in (Ca, Ce, Er) WO_4 sample. The solid line is the theoretical fit using Eq. (1) with the parameters W and $\Delta\omega_{1/2}$ shown in the figure. The data are those from Fig. 6, Ref. (3) renormalized for best fit.
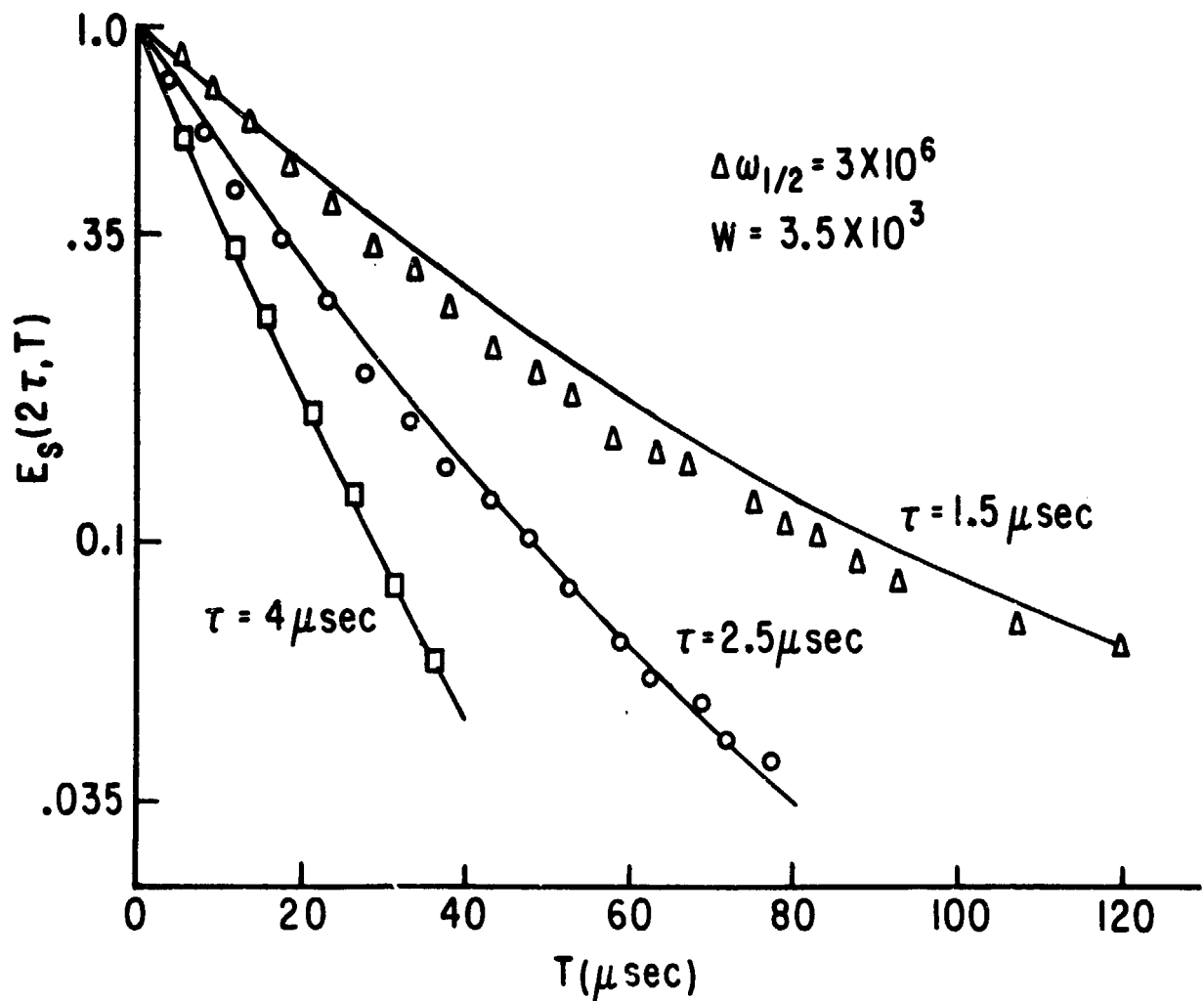
128

Fig. 59. Three-pulse echo amplitude $E_s(2\tau \div T)$ for Ce in the (Ca, Ce, Er) WO_4 sample for different values of τ. The solid lines are the theoretical fits using our calculations with the parameters W and $\Delta\omega_{1/2}$ shown in the figure. The data are those from Fig. 7, Ref. (3) renormalized for best fit.

129

fit with our Eq. (1) shown in Fig. 60. The concentrations of Mn and Er correspond to 3.0×10^{16} spins/cm^3 and 1.1×10^{18} spins/cm^3, respectively. This yields a value of $\Delta\omega_{1/2}$ of 0.55×10^6 sec^{-1}, which is exactly what we have used in our fit. For W we have used the value 2.3×10^6 sec^{-1}, which is close to the value of 2.5×10^6 sec^{-1} which we would obtain from the T_1 measurement of Mims. In this case the echo measurements were made with H parallel to the c-axis so that Mims' measurements apply. Our value of W is well within experimental error as it corresponds to a region of temperature T where one must extrapolate measured data. We summarize the $\Delta\omega_{1/2}$ in Table XV.

If we had drawn Figs. 58 and 59 with respect to $\Delta\omega_{1/2}\tau$, rather than with respect to τ, and if we had then chosen the scale of Fig. 57, the curves would have been modified only slightly. This follows because for Fig. 58 we have a value of $\Delta\omega_{1/2}\tau = 31.5 \simeq 30$ at $\tau = 10.5$ μsec, whereas for Fig. 60 this value is $\Delta\omega\tau = 33 \simeq 30$ at the corresponding endpoint $\tau = 60$ μsec. For Figs. 58 and 60 the values of η are 8.6×10^2 and 2.4×10^{-1}, respectively, which places them in the context of Fig. 57. From Eq. (1) we can calculate

$$E(2\tau) = \exp\left(-2W\Delta\omega_{1/2}\tau^2\right), \quad W\tau \ll 1$$

and

$$E(2\tau) = \exp\left[-2(1/\pi)W^{-1/2}\Delta\omega_{1/2}\tau^{1/2}\right], \quad W\tau \gg 1.$$

The above values of η do not quite correspond to the extreme limits characterized by these equations. In fact, Mims obtains a good fit using $E(2\tau) = \exp\left[(-2\tau/T_M)^x\right]$, with $x = 1.9$ and $x = 0.7$ for the data we have plotted in Figs. 58 and 60, respectively.[11] In the extreme limits these values would be $x = 2.0$ and $x = 0.5$.

It is important to note that in order to obtain the correct value of T_M it is necessary to obtain data points for sufficiently small τ. This is brought out dramatically in Fig. 60, where a simple extrapolation of the data points leads to a value of T_M which is approximately a factor of three larger than it should be on the basis of the solid curve drawn in Fig. 60. Some of the T_M values of
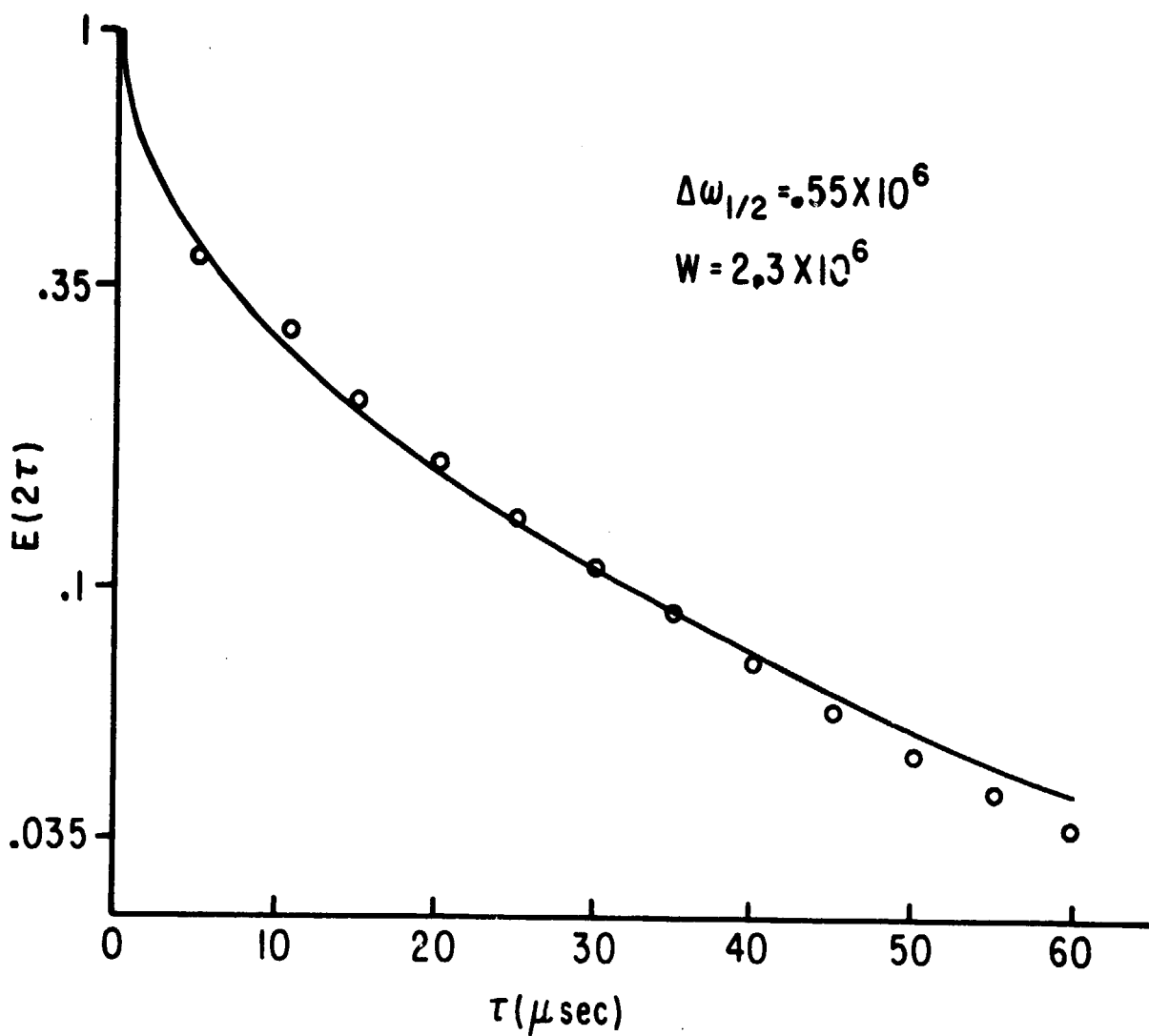
130

Fig. 60. Two-pulse echo amplitude for Mn^{2+} in the (Ca, Mn, Er) WO_4 sample. The solid line is the theoretical fit using Eq. (1) with the parameters W and $\Delta\omega_{1/2}$ shown in the figure. The data are those from Fig. 8, Ref. (3) renormalized for best fit.

131

Ref. (4) are therefore considerably different from what we would estimate on the basis of our formulas. In particular we would expect that the plot of T_M as a function T given in Fig. 5 of Ref. (4) should be modified. A major effect on this plot would be to shift the minimum of T_M [at $T \simeq 4.5°K$ according to Fig. 5, Ref. (4)] in the direction of higher temperatures. From the data of Antipin et al.[12], which enable us to estimate W as a function of T, and from our formulas, we infer that T_M should be a minimum at ~ 6.5°K. This may correspond to a bigger shift than we can expect by reinterpreting T_M.

In contrast to the success we have had in fitting the Ce- and Mn-echo signal data, we have not been able to fit Mims' measurement of the two-pulse decay envelope corresponding to the Er-spin signal [Fig. 9, Ref. (4)]. These experiments were performed with the same $CaWO_4$ crystals used in the Ce-echo measurements. In order to obtain a fit we have had to use values of W about two orders of magnitude larger than could be inferred by T_1 measurements. The problem is that the echo amplitude decays too fast. Mims has also noted the anomalously fast decay and has discussed several possible explanations for it.

From the rather good agreement between the echo data and our formulas using parameters whose value is close to that derived by independent considerations, we conclude that the sudden-jump model may very well be appropriate for resonance experiments applied to this material. More experimental work is clearly necessary. We have obtained a $CaWO_4$ crystal doped with Nd^{3+} and will investigate the spectral diffusion behavior experimentally.

(1) CRL Progress Report, June 30, 1973, p. 115.
(2) P. Hu and S. R. Hartmann, Phys. Rev. B 9, 1 (1974).
(3) J. R. Klauder and P. W. Anderson, Phys. Rev. 125, 912 (1962).

(4) W. B. Mims, Phys. Rev. 168, 370 (1968).

(5) J. R. Klauder and P. W. Anderson, op. cit., p. 912.

(6) W. B. Mims, op. cit., p. 370.

(7) Ibid., p. 370.

(8) P. Hu and S. R. Hartmann, op. cit., p. 1.

(9) W. B. Mims, op. cit., p. 370.

(10) A. A. Antipin, A. N. Datyshev, I. N. Kurkin, and L. Ya. Shekun, Soviet Phys. - Solid State 10, 468 (1968).

(11) W. B. Mims, op. cit., p. 370.

(12) A. A. Antipin et al., op. cit., p. 468.

H. SUPERRADIANCE*

(R. Friedberg, S. R. Hartmann)

We have extended our work on superradiant stability [1,2] to pinpoint the conditions under which the superradiant condition is unstable.

The field of an oscillating dipole can be resolved into a real part (in phase with the dipole) and an imaginary part (90° behind). The reaction of the real part shifts the frequency, while that of the imaginary part damps the radiation.

For coherent spontaneous emission by a small sample into free space, Dicke and others have derived the equation $d\theta/dt = (1/2)N\tau_o^{-1} \sin \theta$ for the tipping angle θ, but the derivation assumes that the field is uniform throughout the sample. Since this is not true of the real component, which far exceeds the imaginary, we ask whether there is any system which should exhibit "Dicke decay."

It may be thought that nmr experiments have verified Dicke's equation for the small sample, but these experiments have not been done in free space. A tuned coil surrounds the sample and absorbs its energy before it has time to radiate. The sample is damped not by the imaginary component of its own field but by the real component, which the coil amplifies with a lag of 90°. We do not consider this an example of Dicke decay.

133

Certain ringlike arrangements of atoms in single file will produce reaction fields that are the same for all atoms because of circular symmetry. Such a system will exhibit true Dicke decay, but the arrangement seems unrealistic.

In a large sample, the real field can be neglected but the imaginary part is not uniform. Certain authors have nevertheless assumed that the atomic excitation density is uniform and have derived Dicke's equation for the large sample. Such derivations are incorrect, since a ray emitted coherently in a favored direction must gain intensity as it nears the exit face. The experiment performed at MIT indicated secondary peaks (ringing) in the emission intensity, in contradiction to Dicke's equation but in agreement with a one-dimensional Maxwell-Bloch analysis.

There remains the possibility that in small samples of particular shape, the nonuniformity of the real field, though large, does not destroy the coherence among parts of the sample because of subtle restoring effects. We have studied the sphere in detail. We expect it, starting from complete inversion, to follow Dicke's equation down to the Bloch equator and suddenly dephase.

Our analysis uses a linear approximation for the small departures from uniformity in the Bloch vector. The linearized equations admit proper solutions that predict oscillations of frequency $\sim (kR)^{-3} \cos\theta$ and amplitude $\sim (kR)^2 \sin\theta$, with characteristic spatial distribution. Near the equator certain modes become unstable because of the role played by the third Bloch component.

We have also divided the sphere into annular regions and followed their development by computer, taking no account of the foregoing concepts. This calculation has verified the existence of oscillations, the dependence of frequency and amplitude on θ and kR, and the dramatic loss of coherence at the equator.

(1)   R. Friedberg, S. R. Hartmann, and J. T. Manassah, Phys. Letters <u>40A</u>, 395 (1972).

(2)   R. Friedberg, S. R. Hartmann, and J. T. Manassah, <u>Coherence and Quantum Optics</u>, L. Mandel and E. Wolf, eds. (Plenum Publishing Corporation, New York, 1972), p. 183.

IV. MACROSCOPIC QUANTUM PHYSICS

A.   QUANTIZED ROTATION AND VISCOSITY OF SUPERFLUID HELIUM
(R. Biskeborn, R. Guernsey)

An analysis of the data from an experiment in which we measured
the temperature dependence of the viscosity of liquid He^4 near the
superfluid transition is in progress. The apparatus was similar to
that described previously[1] with the following modifications: We
replaced the linenized Bakelite (Micarta) chamber with a copper sample
chamber (a hollow cylinder 4.62 cm in diameter and 0.77 cm high) in
order to simplify the geometry by eliminating the capillary fill tube,
to increase the thermal contact between the helium boundary layer and
the resistance thermometer, and to increase the strength of the cell.
This permitted operation at higher differential pressures between the
cell and the surrounding vacuum can (see Fig. 61). The new torsion
pendulum was sufficiently sensitive to refine considerably the earlier
work of Webeler and Allen,[2] who measured the damping on a piezo-
electric crystal driven in a torsional mode. In this latter work,
in order to provide reliable thermometry, the He^4 sample was doped
with He^3 (0.5%) to supress its lambda point relative to that of the
superfluid bath. In the present work the good thermal contact between
the resistance thermometer, which was mounted in a copper housing on
the bottom of the cell and the helium sample, contained in the oscil-
lating cell, resulted in reliable thermometry both above and below T_λ.
All of the lambda-point data were taken with the main bath (out-
side the vacuum can) either warming or cooling to produce drift rates
of typically $80°\mu K/min$ to $10°\mu K/min$ in the cell via exchange gas con-
tact through the can (at a pressure of typically 200-μ Hg). The ampli-
tude of oscillation of the pendulum, which is driven on resonance in

TOP VIEW

BRASS RESERVOIR

STAINLESS STEEL
TORSION MEMBER

COPPER CELL

MU METAL SHIELD
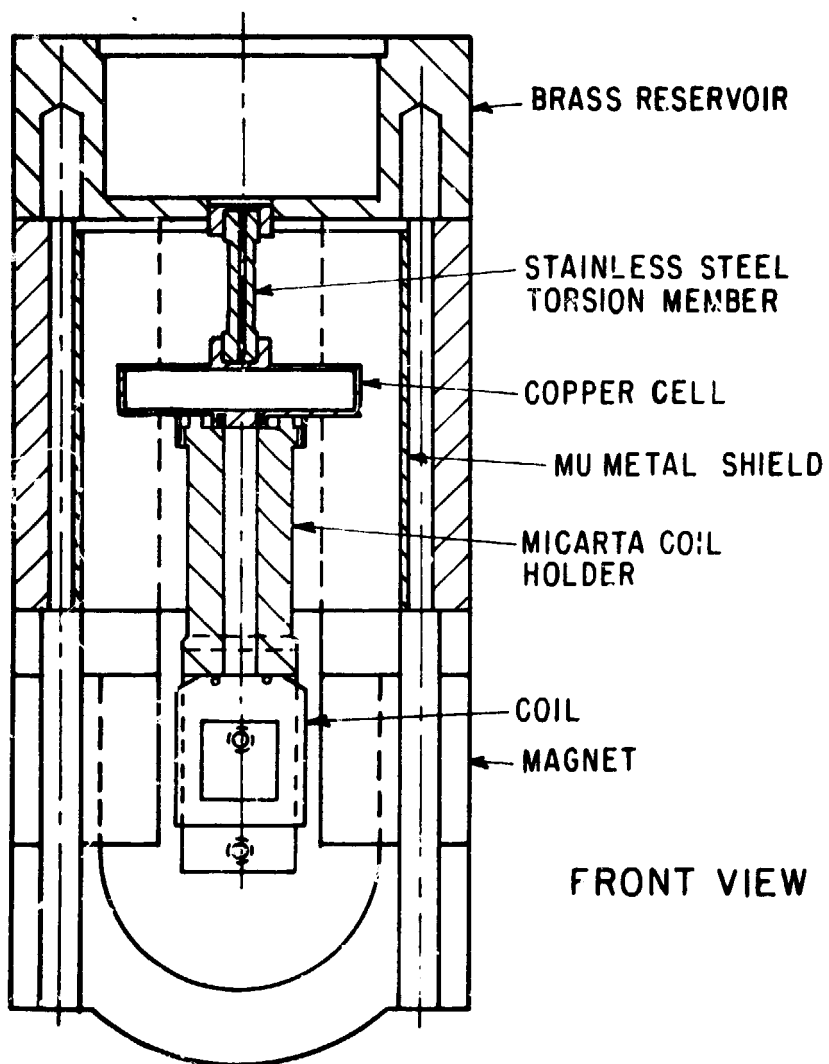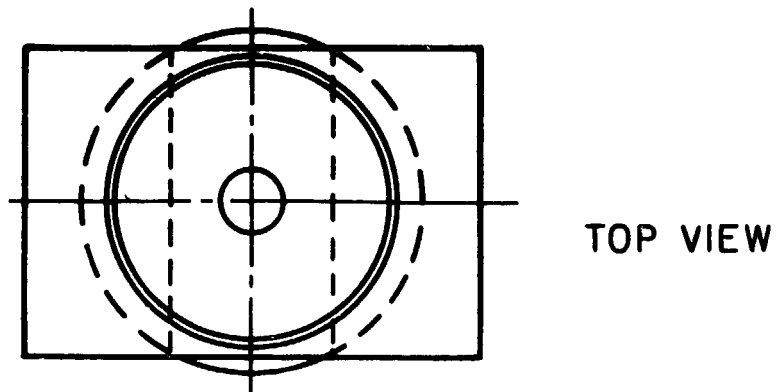
MICARTA COIL
HOLDER

COIL

MAGNET

FRONT VIEW

Fig. 61. Probe.

137

an electronic feedback loop described earlier,[3] is proportional to the voltage on the coil [now attached to the bottom of the cell (see Fig. 61)]. Since the impedance of the coil on resonance is purely resistive and inversely proportional to the exponential decay constant of the pendulum, it is sufficient to monitor the (constant) coil voltage and (changing) current as a function of temperature to determine this constant, which is proportional to the square root of normal fluid density times the viscosity (after the background has been subtracted out).

In order to compute viscosity, the normal fluid density must be known. Taking the most recent work available[4] we find from a preliminary analysis (see Figs. 62 and 63) that the formula

$$\frac{\eta - \eta_\lambda}{\eta_\lambda} = A \left(\frac{T - T_\lambda}{T_\lambda}\right)^x$$

gives $x \simeq 0.67$ and a value for A not in agreement with previous measurements[5] (see Fig. 63). It is interesting to note that the superfluid fraction also varies as $[(T - T_\lambda)/T_\lambda]^{2/3}$ as a first approximation.[6] The resolution is such that it is possible to resolve changes in viscosity of the order of 0.025% corresponding to temperature intervals of ~5° μK. The lambda point is identified by the abrupt change in slope in the damping itself to better than 5° μK. For small (<~100°μK/min) rates the damping-temperature slope is essentially indepent of drift rate.

Data have been taken over two decades in amplitude at 732.5-Hz oscillation frequency. The lowest of these results gives a peak angular velocity equal to one-half of the critical angular velocity (ω_c = 552 μrad/sec) for the creation of one vortex in a steadily rotating cylinder of the same dimensions. No amplitude dependence was found. It is not yet known if the largest peak angular velocity is as large as any previously studied.

In order to make a direct comparison to the data of Ref. (4) we used a 0.5% mixture of He^3 in He^4. We found that the lambda point of the mixture was suppressed by 7.75° mK, but that the viscosity was the
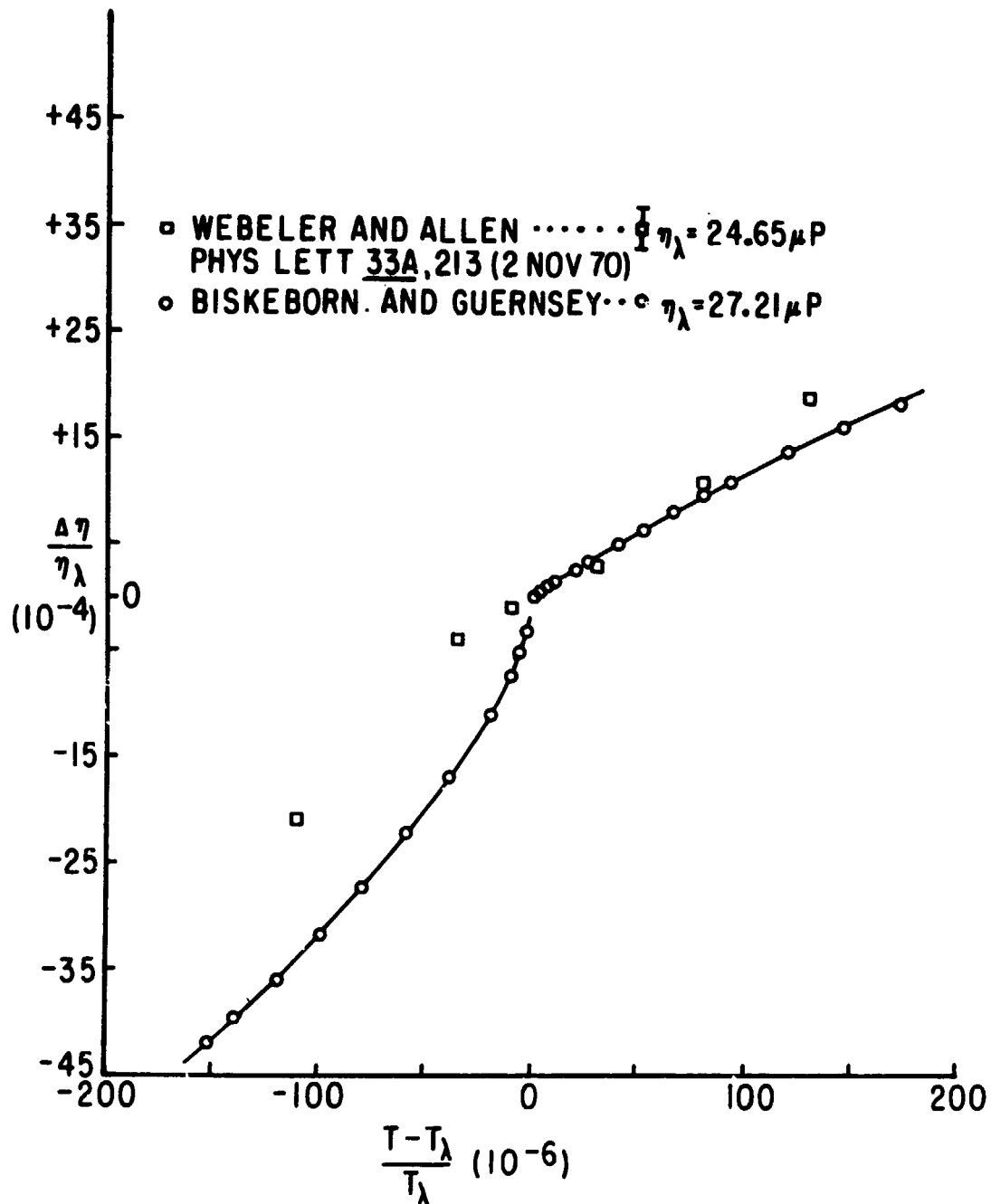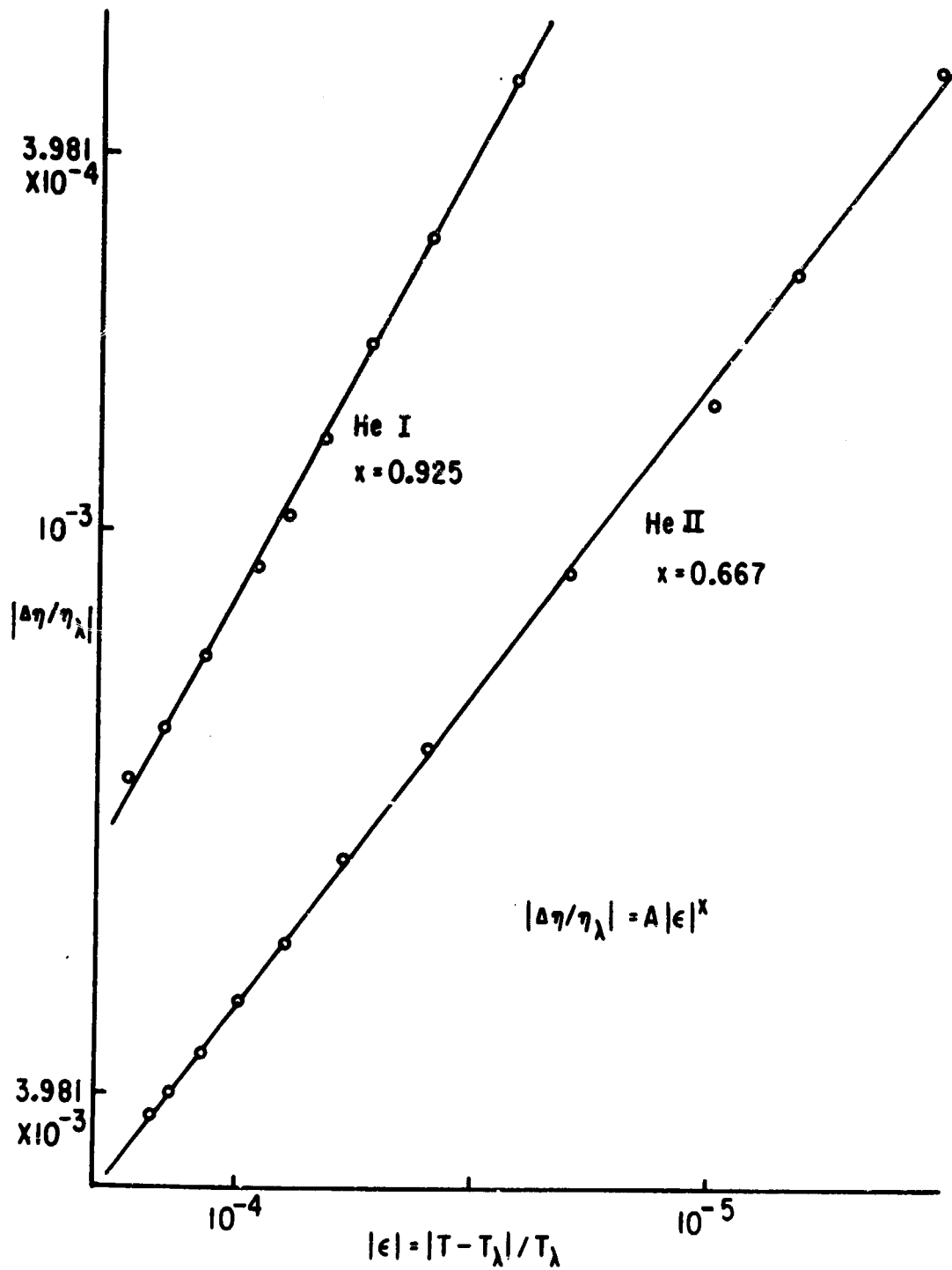
138

Fig. 62. Viscosity of He^4 near T_λ.

Fig. 63. Critical exponents for the viscosity near T_{λ}.

same. While in qualitative agreement with Ref. (2), our data give an exponent which is 26% lower.[7]

It has also been possible to record data over the temperature range from 1.2°K to 4.2°K. These data are now being analyzed. Previous measurements have indicated a discrepancy between oscillating and steady rotation measurements of viscosity between 1.2° and 1.5°K. We expect that the present research may help clarify this problem.

Program for the next interval: After completing the current analysis, we will attempt to understand the structure in the damping which we found with the Micarta cell.[8] We then hope to study the pressure dependence (up to perhaps 15 atm) of the exponent x cited above.

(1) CRL Progress Report, June 30, 1973, p. 129.
(2) R. W. H. Webeler and G. Allen, Phys. Rev. A 5, 1820 (1974).
(3) CRL Progress Report, op. cit., p. 129.
(4) D. S. Greywall and G. Ahlers, Phys. Rev. A 7, 2145 (1973).
(5) G. Ahlers, Phys. Letters 37A, 151 (1971).
(6) J. A. Tyson and D. H. Douglass, Jr., Phys. Rev. Letters 17, 472 (1966).
(7) G. Ahlers, op. cit., p. 151.
(8) CRL Progress Report, op. cit. p. 129.

B.   FACTORS DETERMINING THE FRACTION OF He-II IN THE SUPERFLUID STATE
     (R. Guernsey, J. Kaplan)

In the last Progress Report[1] an experiment was described in which relative motion of the superfluid and its container might be sensed by thermal modulation of the sample. We have completed construction of the apparatus and have made the first trial run.

The results are encouraging: The random noise was reduced to less than 1 nV in a pendulum with a Q of 2000, and the heater could be run at more than 1/4 W in the steady state. The precision in measuring angular velocity of the superfluid should therefore be about 5×10^{-7} rad/sec. The rotation quantum interval for the superfluid

141

in this sample container should be about 400×10^{-7} rad/sec.

In this first run, however, we were unable to study the superfluid motion because of a large additional coupling between the oscillating heat input and the pendulum. We have investigated this signal and suspect that it originates in the generation of sound or thermal expansion and contraction of the wires leading to the pendulum coil.

In the coming months we will attempt to eliminate the stray coupling and then proceed to study the quantized rotation of the superfluid.

(1) CRL Progress Report, June 30, 1973, p. 134.

C. EXPERIMENTS ON THE NEW PHASES OF LIQUID He^3
(A. Becker, R. Guernsey, R. J. McCoy, M. Steinback, C. S. Wu)

We are continuing an experimental program to measure both mechanical properties and the interaction of magnetic and mechanical properties in the anomalous phases, A and B, of liquid He^3. Our approach utilizes a high-Q torsion pendulum as described in last year's Progress Report.[1]

Our first experimental apparatus, an Andronikashvili-type cell to measure the superfluid fraction of He^3, is now almost finished. We have completed construction and pressure testing at 60 atm of the cell, which consists of 93 five-mil disks spaced three mils apart, the pressurization system and a capacitative pressure gauge; and the thermal parts, which include a vibration isolation link to the dilution refrigerator, a superconducting thermal link, and a CMN demagnetization refreigerator. We have completed and tested the electronics for the system, primarily a sensing and feedback apparatus which drives the pendulum and monitors its motion. We are in the final steps of incorporating this unit into the apparatus.

Program for the next interval: We will measure the superfluid density ρ_s and normal viscosity η_n of He^3 A and B, both with zero magnetic field and with applied axial and transverse magnetic fields.

(1) CRL Progress Report, June 30, 1973, p. 137.

PERSONNEL

FACULTY

H. M. Foley, Professor of Physics

R. Friedberg, Associate Professor of Physics

R. W. Guernsey, Assistant Professor of Physics

W. Happer, Associate Professor of Physics, Co-Director

S. R. Hartmann, Professor of Physics, Co-Director

J. M. Luttinger, Professor of Physics

I. I. Rabi, University Professor Emeritus

A. M. Sachs, Professor of Physics

P. Thaddeus, Adjunct Professor of Physics

C. S. Wu, Pupin Professor of Physics

RESEARCH ASSOCIATES AND PHYSICISTS

Dr. A. J. Becker

Mr. M. J. Bernstein

Dr. S. Chandra

Dr. R. Gupta

Dr. P. Hu

Dr. P. Liao

Dr. R. J. McCoy

Dr. G. Moe

Dr. S. Svanberg

Dr. H. Y. Tang

Dr. G. R. Tomasevich

Dr. K. D. Tucker

Dr. R. A. Weingarten

GRADUATE RESEARCH ASSISTANTS

R. Biskeborn

Y. Chen

G. Chin

R. Cohen

H. Cong

R. Dickman

J. Farley

A. Flusberg

M. Friedlander

Z. Friedlander

P. M. Fu

L. Gaines

J. Kaplan

M. Kutner

L. Lam

K. Liao

N. A. Lin

S. Meth

R. Nerf

M. Steinback

C. Tai

A. Tam

P. Tsekeris

143

TECHNICAL RESEARCH ASSISTANTS

I. Beller   J. Gorham

PHYSICS DEPARTMENT ELECTRONICS ENGINEERING AND CONSTRUCTION SHOP

V. Guiragossian

PHYSICS DEPARTMENT MACHINE SHOP

E. Jauch

The facilities are available for the Columbia Radiation Laboratory.

ADMINISTRATION

J. Gilbert

M. Friedman   R. Wagner

EDITOR

A. Owen